Aalto University
School of Engineering

Dagur Ingi Ólafsson

Friction Stir Welding of Aluminum - Copper

School of Engineering

Dissertation for the Degree of Master of Science in Mechanical Engineering

Espoo, 26.11.2017

Supervisor and Advisor: Professor Pedro Miguel dos Santos Vilaça da Silva

"Vinnan göfgar manninn." (Icelandic Proverb)

![Aalto University School of Engineering logo]

Aalto University, P.O. BOX 11000, 00076 AALTO
www.aalto.fi
Abstract of master's thesis

Author: Dagur Ingi Ólafsson

Title of thesis: Friction stir welding of aluminum - copper

Degree programme: Mechanical engineering

Major: Mechanical engineering   **Code** IA3027

Thesis supervisor: Prof. Pedro Vilaça

Thesis advisor: Prof. Pedro Vilaça

Date 26.11.2017   **Number of pages:** 114   **Language** English

Abstract

The joining of dissimilar metals is one major challenge for welding technology. There are not many feasible welding techniques able to overcome the different physical properties and deliver a sound structural joint. The application of solid-state welding techniques, although challenging, is one common solution. This work details the development of welding conditions, tools and parameters for the Friction Stir Welding (FSW) of Aluminum-Copper (Al-Cu) butt joint. The application of FSW to these dissimilar joints has proved in the past to be feasible, but several technological and joint performance features, still demand further investigation and development. The motivation and support of this project was a cooperation between Aalto University and Promeco Oy, with ABB Drives Oy as a strategic partner, aiming at providing Promeco Oy with the ability to manufacture high-value dissimilar components, such as, Al-Cu bus bars.

Multiple conventional FSW tools were designed and tested. Parameters were developed to optimize 6 mm thick AA1050-H14/24 – CU-OF-04 butt joints. After preliminary tests, FSW tool was selected for optimization of the process parameters. The tool has ØD3 concave shoulder and ØB threaded taper N/A long probe. The Taguchi method for design of experiments was used for the optimization of three process parameters: travel speed, weld position and offset position of the tool in relation to the joint line between the base materials. The weld was then thoroughly characterized. Tensile, bending and microhardness tests were used to establish the mechanical properties. Optical microscope and scanning electron microscope were used to investigate the microstructure. Joining mechanisms and intermetallic compounds in the weld were investigated using an X-ray diffraction analysis. The electrical resistance of the weld was assessed using a microhmmeter.

The optimized parameters were found to be N/A travel speed; N/A tool plunge and N/A offset into the aluminum. The properties of this optimized weld resulted in 84.8 % Global Efficiency to Tensile Strength (GETS) and 40.8 % Global Efficiency to Bending (GEB) compared to AA1050-H14/24, and 97.2 % electrical conductivity efficiency compared to an ideal bimetallic component made of the same materials with no contact resistance.

To understand the benefits of having an Al bus bar with Cu bolted end, compared with one made of monolithic Al material, a dedicated experimental test setup and protocol was designed and implemented. This experimental test enables to monitor the force relaxation of a pre-loaded bolt joint, under cyclic thermal loading, simulating real operational conditions. The test was applied to both Al base material and Cu base material components. The experimental results show that the force relaxation in the Cu bolted joint was about 50 % lower compared with the Al. Thus, bus bars with Cu ends are more stable and will need less maintenance while in operation than bus bars with Al ends.

An advanced Stationary Shoulder FSW tool was designed, produced and is ready for testing, envisaging a weld joint with improved top surface finishing and good overall engineering performance.

Keywords Friction Stir Welding, Dissimilar Joint, Aluminum, Copper, Tool Design, Stationary Shoulder, Design of Experiments, Bus Bar, Intermetallic Compounds; Metallographic Analysis, Mechanical Properties, Electrical Resistance.

Acknowledgement

Table of Content

Abbreviations and Acronyms

AA	*Aluminium Association (e.g. AA1050)*
Al	*Aluminum*
ANOVA	*Analysis of variance*
BM	*Base material*
BOM	*Bill of materials*
Cr	*Chromium*
Cu	*Copper*
DoE	*Design of experiment*
DoF	*Degree of freedom*
Fe	*Iron*
FS	*Friction stir*
FSW	*Friction stir welding*
GEB	*Global efficiency to bending*
GETS	*Global efficiency to tensile strength*
HAZ	*Heat affected zone*
HB	*Brinell hardness*
HV	*Vickers hardness*
IMC	*Intermetallic compound*
Mg	*Magnesium*
Mn	*Manganese*
Pb	*Lead*
PcBN	*Polycrystalline cubic boron nitrade*
RPM	*Rounds per minute*
SEM	*Scanning electron microscope*
Si	*Silicon*
SSFSW	*Stationary shoulder friction stir welding*
Ti	*Titanium*
TMAZ	*Thermo-mechanically affected zone*
WNZ	*Weld nugget zone*
Zn	*Zinc*
σ_{eff}	*Conductivity efficiency*

1   Introduction

As various industries constantly strive to improve their competitiveness, with higher performance products made with efficient processes with low environmental impact. Most of the developments are supported by material optimization demanding advanced solution for processing, namely joining. The research and engineering community works towards meeting these demands willing to transfer the innovative solutions and know-how into industry. Friction Stir Welding (FSW) is a solid-state material joining technology, which opens up possibilities in bimetallic joints of dissimilar materials that is almost impossible to do with conventional fusion welding methods. Welded joints such as aluminum to steel, aluminum to copper and steels to other highly dissimilar iron based components have become a possibility as the process joins materials without melting them. This has opened up new possibilities in the design optimization and manufacturing of various products. E.g. in electrical applications enables to combine cheaper and lighter material, such as aluminum, with copper that has low electrical resistance, with more stable properties and corrosion resistance in a wider temperature range.

1.1   Scope

This thesis details the development of the process conditions for the FSW of aluminum (Al) – copper (Cu) butt joints. It is a cooperation research project between Promeco Oy and Aalto University, named FALCU, which aims at providing Promeco Oy with the know-how for making high-value components based on these joints. The good quality of new high-value products will contribute to increase the competitiveness of Promeco Oy into new international markets. ABB Drives Oy is a strategical partner in this project and a potential customer for the new high-value products.

The solid-state FSW process has shown to be a feasible technological solution to weld dissimilar Al-Cu joints. Fusion welding processes, even advanced technologies such as electron beam welding or laser welding, are not recommended to join Al and Cu, as they tend to form large Intermetallic Compounds (IMCs) [1]. These IMCs are hard and brittle, which critically compromises the quality and applicability of the joints. Moreover, solidification and liquefaction cracking are commonly encountered problems associated with the fusion welding of these materials. FSW is a joining process that uses a non-consumable tool, The combined rotation of the tool while travelling along the joint stirs the visco-plasticized material, activating joining mechanisms between the components without melting and solidifying them. Because the process does not melt the based materials it is very useful for the joining of dissimilar materials with different melting temperatures and other thermal properties, such as, Al and Cu.

The FSW of joints encompassing dissimilar materials is quite sensitive to variations in the clamping, tools and parameters. The FSW of Al-Cu has been previously investigated by other authors, mainly focusing on the influence of basic process parameters, such as, tool travel speed, spindle rotational speed and vertical forging force or penetration depth. The development of key technological issues, like dedicated shoulder and probe dimensions and geometrical features, on the other hand are typically not considered. Advantages of advancements in the technology,

such as Stationary Shoulder Friction Stir Welding (SSFSW), for the FSW of Al-Cu have also not been found for this particular application. The work done in this thesis started by developing the welding conditions and tools, based on trial-and-error approach for FSW of Al-Cu components. The best conditions were then selected for base of optimization of key FSW parameters and implementation of a dedicated test setup and protocol to prove the advantages that bimetallic Al electric bus bars, with Cu ends, have over the common monolithic Al bus bars used today.

1.2 Work Plan and Objectives

In order to fulfill the purpose of the thesis the challenges were systematically addressed. A wide theoretical background was established, enabling the familiarization with the materials and FSW process. Existing research on the subject was covered in-depth and built upon in a literature review. Specific Al and Cu materials were selected with the manufacturing of bus bars in mind. The selected Al and Cu were then characterized and tools were designed specifically tailored to the process setup. Based on comprehensive testing of the different manufactured FSW tools with evaluation of the mechanical properties, the best one was selected for optimization of the process parameters. The performance parameters were the efficiency of tensile strength, efficiency on bending and efficiency of electrical conductivity. The optimized conditions were implemented and properties thoroughly evaluated including microscopic analysis and hardness field establishment. A dedicated experiment was designed and conducted to investigate the operational difference between Al bus bars and Al bus bars with Cu connection ends.

The objectives of this work are as follows:

- Review and detail the current state of the art for FSW of Al-Cu joints.
  - Establish a comprehensive literature review.
- Characterize the properties of selected base materials.
  - Evaluate the tensile strength under static loading, bending strength, electrical resistance, hardness and metallurgical features.
- Develop the technological conditions of the process for the selected materials and thicknesses.
  - Design, manufacture and test conventional tools for the production of Al-Cu joints.
  - Design and manufacture a SSFSW module.
- Optimize the FSW process parameters based on design of experiments.
  - Apply the best conditions in the production of test specimens for mechanical and metallurgical characterization.
  - Monitor the optimized process temperatures using strategically positioned thermocouples.
- Evaluate the properties of joints produced with optimized FSW process parameters. Establish the results in terms of efficiency relative to the base materials.
  - Investigate and establish the tensile strength, bending strength, electrical properties, hardness and metallurgical features of the joints.

- Design and conduct an experiment to assess the operational performance of bimetallic bus bars compared to conventional ones made of Al.
  - o Determine the different clamping force relaxation rates these parts experience while in operation.

1.3 Organization of the Thesis

Following the present introduction, the second chapter is the State of the Art. The fundamentals of FSW, Al and Cu are covered and a comprehensive literature review on the FSW of Al-Cu joints is established. Additionally the technologies for evaluating the quality of welds and the procedures to implement the Design of Experiments (DoE) methodology, used for the process optimization, are detailed.

Chapter 3 describes the selection and characterization of the Al and Cu base materials used in this work. Chapter 4 details the development of tooling for the FSW of Al-Cu joints, focusing on conventional and SSFSW tools. Chapter 5 covers the optimization of the FSW process parameters using DoE and Analysis of Variance (ANOVA) methods.

In chapter 6, the optimized weld condition is characterized and the tensile, bending, electrical, metallurgical and hardness properties established. For the optimized welding condition, the temperatures are monitored using thermocouples. The setup and implementation of the test protocol, of an experiment proving the advantages of bimetallic bus bars, is covered in chapter 7.

Chapter 8 summarizes the work and comprises recommendations for future work.

This document is a public version of the work. Sensitive details have been removed and replaced with "N/A" and important dimensions of designed tools have been replaced with letters. Sensitive information in figures has been blacked out.

2 State of the Art

2.1 Introduction

This chapter first covers the fundamentals of FSW, tool design and SSFSW. Then it details issues related to the FSW of Al-Cu with a comprehensive review of other work done in the research area as well as a general characterization of the base materials. The applications of Al-Cu parts is briefly covered. How weld quality is evaluated and the DoE methodology is also discussed.

2.2 Fundamentals of Friction Stir Welding

The process of FSW is one of the most important recent discoveries in the field of joining materials. Invented in 1991 by Wayne Thomas and his colleagues at the welding institute in the United Kingdom [2], it has opened up numerous new possibilities for making high quality welds and avoiding defects that are common in more conventional fusion welding techniques.

FSW is a solid-state welding process; it joins materials without melting them. The process welds by rotating a non-consumable tool inside the materials to be welded in order to soften them locally using heat generated by friction and plastic deformation. Once softened, the joint surfaces are stirred and joined, still in their solid state, as the materials do not reach their melting temperatures. This increases the weld quality compared to fusion welding as it avoids the many problems associated with fusion welding such as changes in volume, gas solubility, distortion and residual stress [3].

FSW has numerous other benefits unrelated to the quality of welds. It has been shown to nearly reduce the emission of hazardous fumes to zero as well as to reduce the energy used during welding, therefore having less environmental impact than other more traditional welding techniques. The process can be used in all orientations as gravity has negligible impact during FSW. Due to high forces the process is typically fully mechanized which increases the equipment cost while lowering the skill requirements and cost of operators [3].
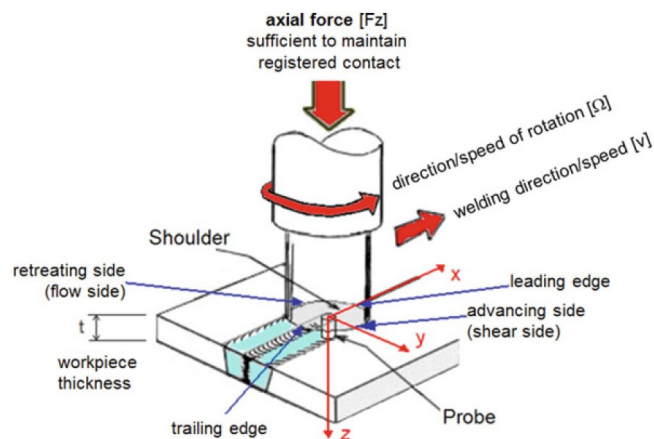

Figure 1 - A schematic of FSW [4]

Traditionally, the FSW tool consists of a shoulder, which sits on the surfaces of the materials being welded, and a smaller pin, usually called probe, that almost fully penetrates the materials. While the tool rotates and travels along the joint surfaces, the shoulder keeps the softened materials down, preventing them from escaping. When the materials are softened, deformed and plasticized they generate the majority of the heat input of the process. The friction between the rotating shoulder and the welded material also provides additional heat input into the weld. Inside the materials, the probe breaks up the original surfaces of the joint and mixes them together. In order to achieve a fully penetrated joint the probe must penetrate to at least 0.5 mm from the bottom surface of the materials. The probe is commonly threaded in order to provide a downward push to the material, which thwarts pores and voids from forming [3]. The design of the tool has been intensely researched and in some areas, conventional tools with flat shoulders and threaded pins have given way to other innovative shapes such as conical and scrolled shoulders and taper and plain probes [5].

It is possible to divide the FSW process into three parts: The plunge phase, the weld phase and the termination phase. During the plunge phase, the tool is plunged downwards, if the base materials are parallel to the ground, into the materials with a specific speed and force while rotating. Due to friction and pressure, the material is displaced and deforms around the pin as it is entering the base materials. The pin is usually plunged into the interface of the materials to be joined but sometimes, especially in FSW of dissimilar materials; it is plunged into either material at the side of the interface line and then moved towards it. During the weld phase, the rotating tool is moved along the joint. Plastic deformation and friction generate heat in order to soften the materials so it may flow around the pin. Once the tool has reached the end of the joint line, it is stopped and the tool is moved up out of the materials. This leaves a keyhole in the material at the end of the weld that can make it unfit for use. This is usually solved by using a run-off tab where the tool is withdrawn which is then cut off in order to avoid leaving the welded materials with a keyhole [3].

As the forces acting during the process are high this sets great requirements on the clamping system that keeps the materials fixed and prevents them from sliding, bending or separating. The backing plate has be very planar without any variations greater than 0.1 mm or otherwise the FSW machine has to be able to compensate for it in order to keep the constant bond of the pin. The most straightforward way to clamp sheets is using clamping claws. They provide a high clamping force while taking a long time to set up. In serial production, automatic clamping systems made of hydraulic or pneumatic fixtures are often used although they are quite expensive so their use can only be justified in industrial production situations [3].

In FSW, there exist two different material flow paths. These flow paths have an origin to the left and right of the movement of the tool. On one side, where the tangent of the tool's rotation is in the same direction as the tool's movement, the material is forced to flow forward along the tool. This side is called the advancing side, see Figure 1. The material on the other side is forced backwards along the tool and is thus called the retreating side [3]. This phenomena causes the

weld to be asymmetrical and becomes increasingly important in Friction Stir (FS) butt-welding of dissimilar materials.

FSW joints consist of four different regions; base material (BM), heat affected zone (HAZ), thermomechanically affected zone (TMAZ) and the weld nugget zone (WNZ), also called the stirred zone. The base material is remote from the weld, is unaffected by the process and has not been deformed. The heat affected zone is closer to the center of the weld and the zone has been through a change in microstructure and/or mechanical properties due to a thermal cycle which it has experienced. The thermomechanically-affected zone lies even closer to the weld center and has been both plastically deformed by the FSW tool and affected by the thermal cycle it has experienced. The weld nugget zone has, just like TMAZ been plastically deformed and heat affected but the difference between the two zones is that the material in the weld nugget zone has recrystallized [6].
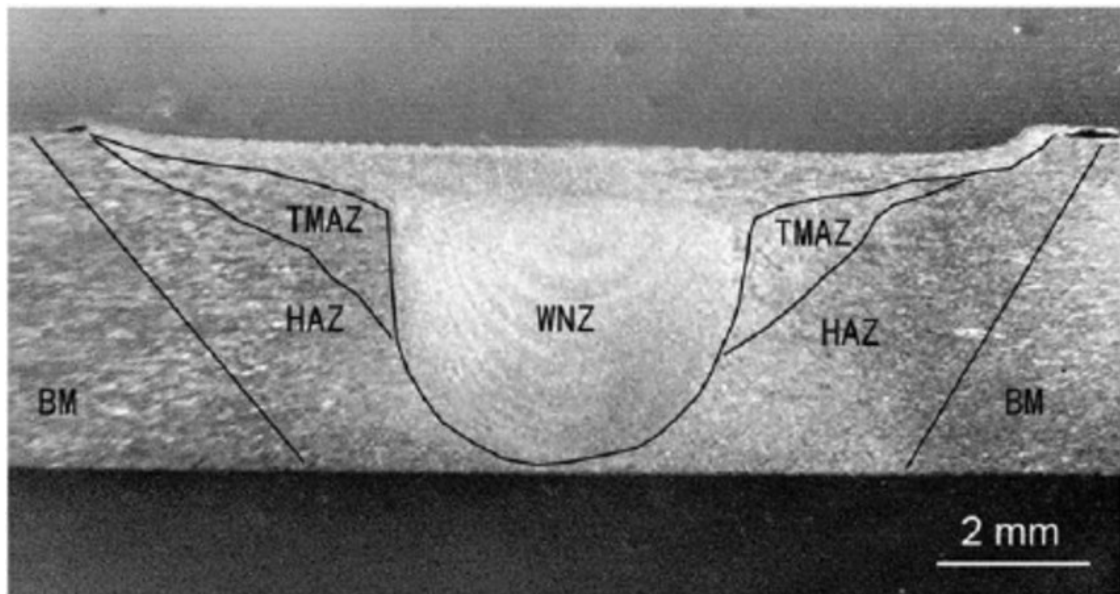
Figure 2 - A cross section of a FSW weld, showing the four different regions [7]

Many joint designs and geometries are possible to make with FSW. For FSW to be able to weld a certain joint design it is crucial to have: enough area for the shoulder path, the possibility to contain the softened weld material, enough clamping force to keep the welded materials from moving and to dissipate the heat of the process with a good enough heat sink. Common joint configurations like butt joints, lap joint, 90° joints and T-joints can all be welded using FSW. The joints themselves often need to be prepared to minimize contaminants and oxide layers that can result in poor fatigue strength, volumetric defects and low ductility locally [3]. The oxide layer can cause bonding problems and weak points within the weld. It is important that the rotating probe is able to break the layer up so that is not continuous inside the weld, which can drastically lower the weld's strength.

2.2.1 Conventional Friction Stir Tools

As stated before, a FSW tool traditionally consists of a round shoulder and a threaded cylindrical probe. The probe moves the softened material around and mixes it to form the joint while the shoulder keeps the material from escaping. During the process, the FSW tool is under severe stress and high temperatures, especially when welding hard materials such as Cu and steel. The geometry of the tool effects the heat generation rate, torque, traverse force and the thermomechanical environment that the tool and base materials experience. It is not only important to select a tool with geometry suitable for the materials and joint design but the tool needs to be manufactured from suitable materials and processed so that it can withstand the forces and the stress it experiences during the weld. Otherwise, the tool quickly wears out and fails. Most tools for welding Al are made out of steel. Tool steel, high-speed steel and other hardened steels are a popular choice and are also used for welding some dissimilar materials such as Al to magnesium and Al to Cu. For welding other, more demanding materials, tool materials like Polycrystalline cubic Boron Nitride (PcBN) and tungsten-based ones are a good choice. [5].
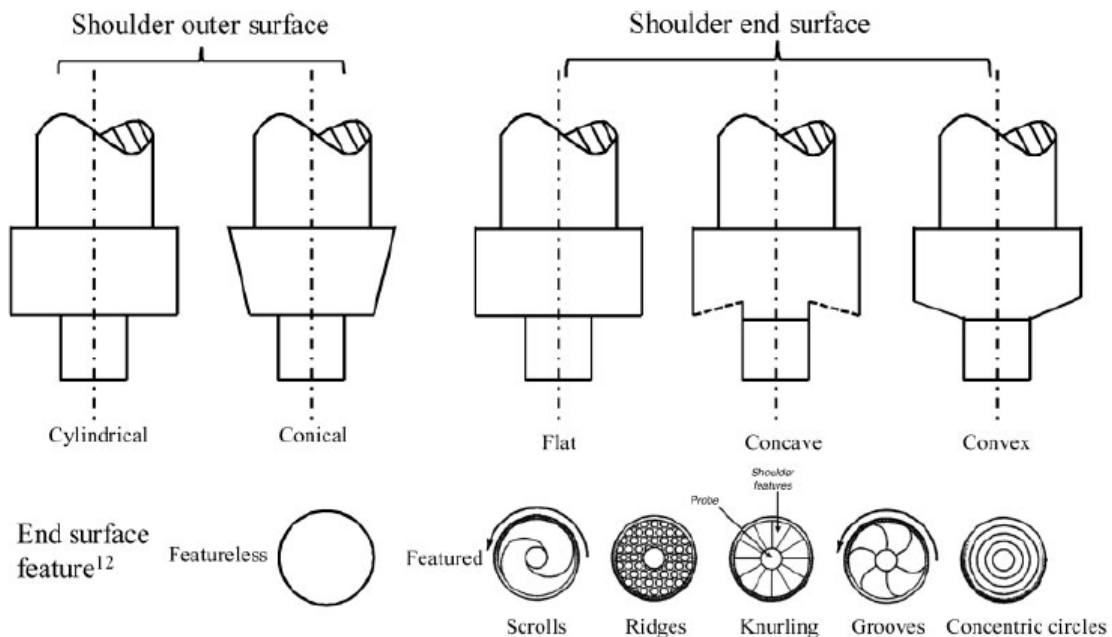
Figure 3 - Shoulder geometries [8]

The geometry of the FSW tool is a very important factor in the welding process, both the shoulder and pin geometry. The shoulder generates most of the frictional heat during FSW and the material flow is largely governed by the shoulders grip on the plasticized materials. The main influencing parts of the shoulder is the contact area between the shoulder and the welded material. The three most commonly used shoulder end surfaces are either flat, concave or convex. The simplest end surface is featureless but features such as scrolls and grooves are commonly used to influence and improve the material flow properties and the heat generated

during welding. Scrolled shoulders either, depending on the tool rotation, move material into or out from the weld center as the geometry guides the material into certain flow paths. Flat shoulders can pose a problem, especially when high forging loads are used as the flat surface does not efficiently keep the flowing material constrained under the shoulder, which can result in weld defects when the material escapes the weld. Concave shoulders do not have this problem. They are operated using a small tool tilt of 2-4°. When the tool moves inside the materials with an angle, the front end of the shoulder does not push through the material but is positioned a small distance above it. The surface material gathers inside the concave shoulder and is then deposited back into the weld from under the back end of the shoulder [8].

Probe geometries can also be quite variable; cylindrical threaded, triangular, threaded taper, square and flat cylindrical probes are commonly used in FSW. Flutes are also a common feature on probes, but threads and flutes increase the downward force from the pin onto the material [5]. Taper geometries lower the force acting on the bottom of the probe, thus extending the life of the tool. Flutes and scrolls on the probe increase turbulent flow in the weld, which promotes better mixing and the breakup of the oxides of the materials. This forces new chemically active surfaces of the two materials to form, which promotes the bonding of the materials.
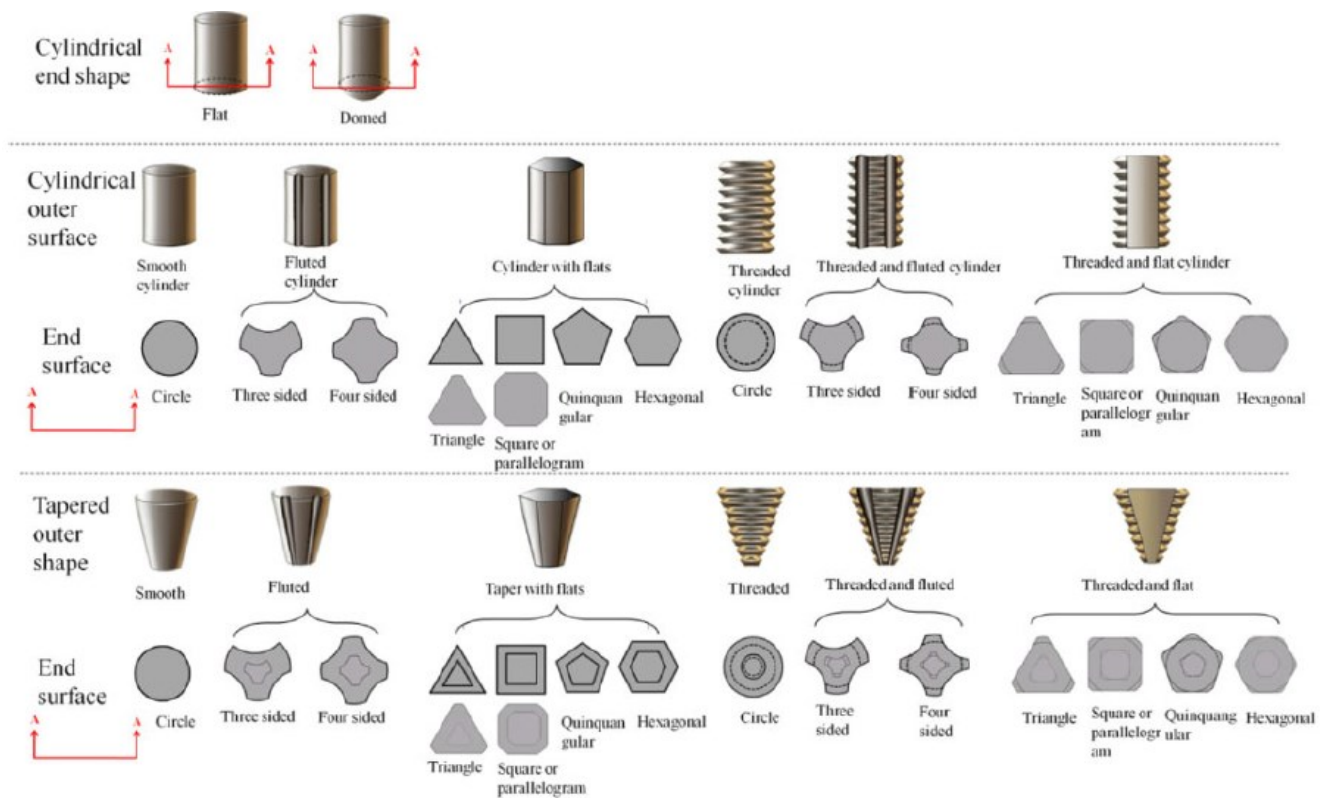

Figure 4 - Probe geometries [8]

As during welding the FSW tool, especially the probe, is under high stresses and forces while it rotates, which often results in heavy wearing of the tool. The tool can also plastically deform under elevated temperatures as the yield strength lowers. Therefore, tools are often liquid cooled

in order to keep the working temperature of the tool low to avoid plastic deformation. The tool wear mechanism during FSW is mostly diffusion and abrasion. Certain techniques have been used to reduce tool wear in FSW of dissimilar materials. In lap-welds, the softer material can be placed on top of the harder material so that the probe is mostly immersed in the softer one. This reduces the stress and forces on the probe resulting in less tool wear. Similar technique is often used when welding butt joints. There the tool is often offset towards the softer material, which reduces the contact with the harder material; reducing tool stress and tool wear [9].

2.2.2 Stationary Shoulder Friction Stir Welding

Stationary Shoulder Friction Stir Welding (SSFSW) is a variant technique of traditional FSW. As the name suggest the difference in technique is that in SSFSW the shoulder does not rotate. It was originally developed to weld titanium-based alloys, due to titanium's low thermal conductivity. SSFSW is also used for welding most other materials commonly welded by FSW as the variant offers numerous benefits over the traditional method [10]:

- Improved surface quality
- Reduced flash formation
- Less and more localized heat input
- More accurate control of the process is possible, which offers more stable welds
- Penetration of the probe into the base material can be adjusted during welding
- More flexibility as the stationary shoulder can be redesigned to fit different joint designs
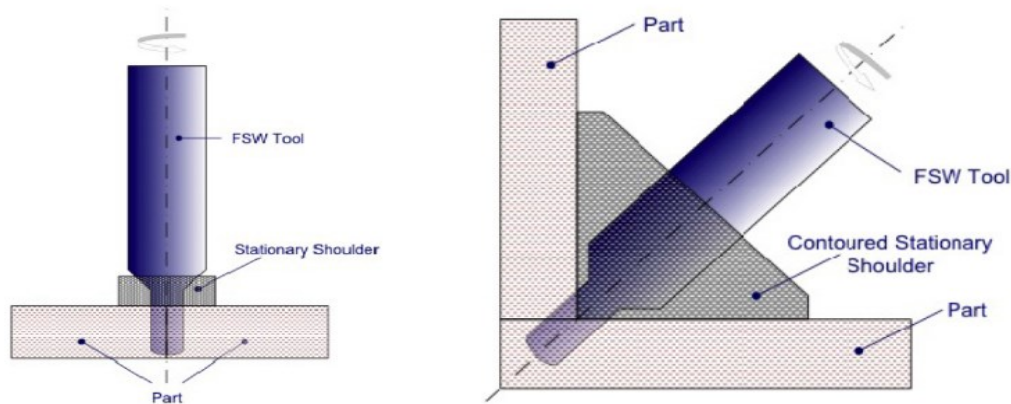
Figure 5 - Schematic view of a SSFSW tool [11]

The design and manufacturing of a SSFSW tool is quite demanding. High forces act on the system during welding and the probe spins inside the shoulder at considerably high speeds. Thus, the system needs to be structurally very rigid and have a good bearing between the shoulder and probe.

M.J. Russel *et al.*[12] developed a tool design for an SSFSW system meant for welding titanium. They publicized their conceptual design, which can be seen in Figure 6 below. Their design operates so that the probe rotates inside the stationary shoulder, which is kept from rotating

using a sled. As the system is designed for titanium, it includes an inert gas system to protect the welded metal. This is not needed in dissimilar Al-Cu FSW. In their presented design a support bearing is used between the rotating tool holder and surrounding stationary tool head while a sliding shoe is used between the rotating probe and the stationary shoulder.

1) Rotating spindle
2) Draw bar
3) ISO 50 Tool holder
4) Water cooling jackets
5) Argon input
6) Support bearing
7) Stationary tool head
8) Ti workpiece 9) Backing plate
10) Sliding shoe
11) Rotating pin
12) Sliding seal
13) Argon supply
14) Gas chamber
15) Inert gas input
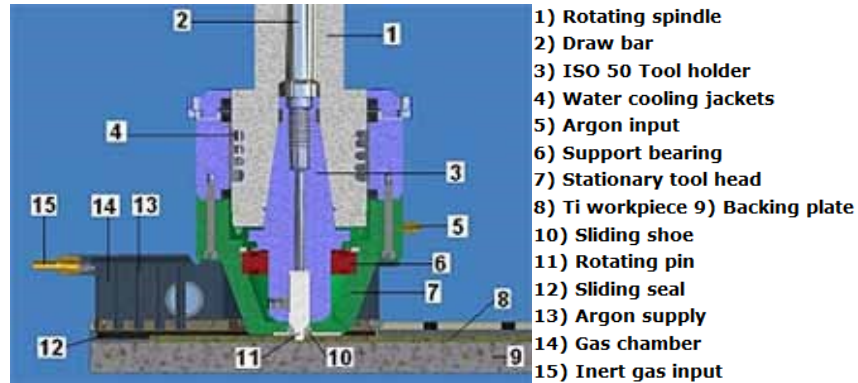
Figure 6 – TWI SSFSW concept design [12]

Beckman and Sundström [13] developed and designed a SSFSW tool module meant for the making of corner welds. Their work was done in co-operation with ESAB, a FSW machine manufacturer. The tool module was designed to be attached to a normal ESAB FSW machine so that it may be used for the welding of corner joints. Their final design concept can be seen in Figure 7.
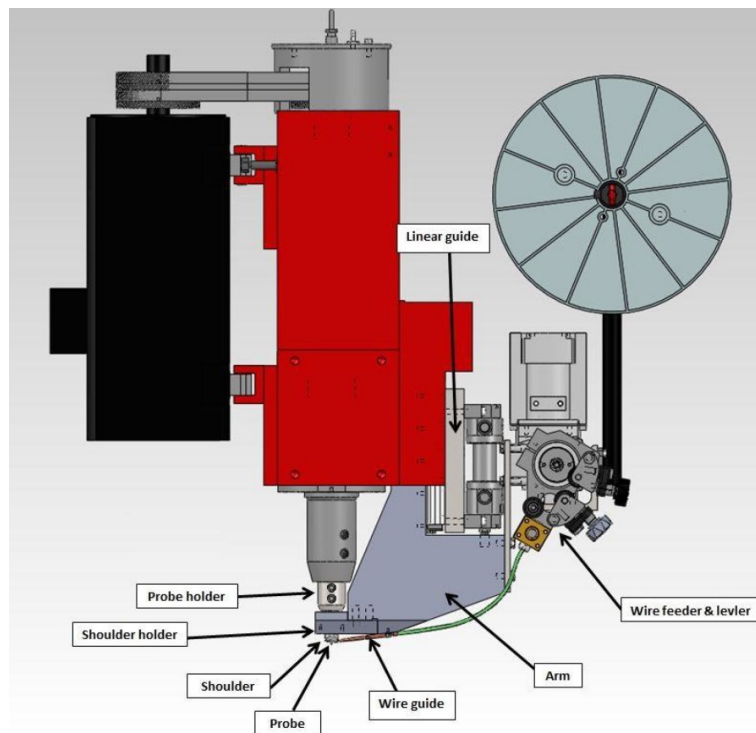
Figure 7 – Beckman and Sundström's concept[13]

Beckman and Sundström designed their system so that a sliding bearing is placed between the stationary shoulder holder and the rotating probe. Between the stationary shoulder itself and the probe they used a sliding fit. A sliding fit is a simple clearance between a stationary and a moving/turning part with H7/g6 hole tolerances and G7/h6 shaft tolerances [14]. A cross-section of the probe, shoulder, shoulder holder and bearing can be seen in Figure 8.
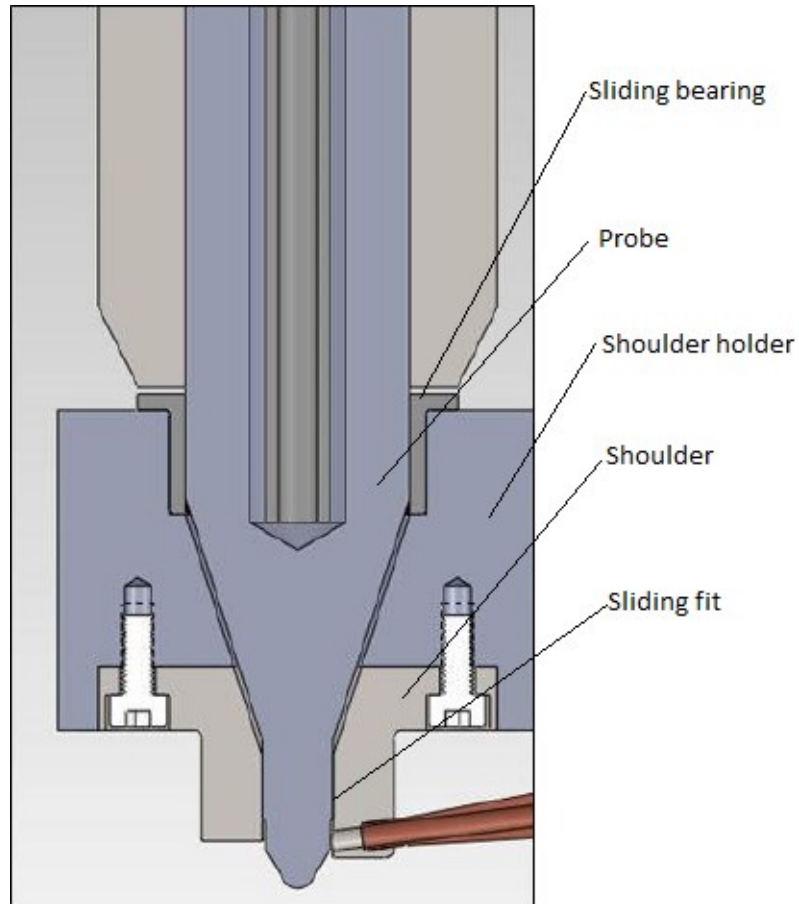
Figure 8 – Cross-section of Beckman and Sundström's design [13]

2.3   Friction Stir Welding of Aluminum-Copper

As a solid-state process, FSW operates under the fusion temperatures of the materials it is joining. It has therefore opened up possibilities to weld dissimilar materials with very different properties that normally create problems for fusion welding. Difference in fusion temperatures, as with Cu and Al make it near to impossible to acquire sound welds with fusion welding. Several issues like different deformation behaviors, formation of Intermetallic Compounds (IMCs) and differences in physical properties promote asymmetry in the flow of material and heat during dissimilar FSW and need to be taken into account [15].

Different flow mechanism on the advancing and retreating side need to be seriously considered when choosing material positioning when FSW of dissimilar butt joints. If the material on the retreating side does not soften enough during the process, it will restrict it from moving around the tool probe. Thus, it is important to place the harder and stronger material on the advancing side so that it can flow around the tool and result in stronger welds [3].

IMCs are defined as solid phases containing two or more metallic elements, with optionally one or more non-metallic elements, whose crystal structure differs from that of the other constituents [16]. They are generally very stable, brittle and with a high fusion temperature. They pose a problem in the welding of dissimilar materials, both in fusion and solid-state welding. In fusion welding they are generally formed during the solidification of the melted metals. In FSW, they form under high pressures and intense plastic deformation [17]. In fusion welding of dissimilar materials the amount of intermetallic compounds is so that it compromises the weld in almost every case and renders the welding method useless for many material combinations such as Al and Cu.

2.3.1 General Characterization of Copper and Aluminum

Cu is the metal that has been used by humanity for the longest. It can be found in its usable metallic form naturally and has been in use since 8000 BC. Cu was the first metal to be smelted from its ore, the first metal to be casted and the first metal to be alloyed with a different metal. In 3500 BC, humanity started alloying Cu with tin in order to create bronze, thus starting the Bronze Age [18]. Cu and its alloys have high thermal and electrical conductivity, good corrosion resistance, ductility and formability, which makes it ideal in numerous applications, especially as a transporter of electricity and heat. For a long time, Cu was the second most widely used commercial metal after iron. Due to its high cost, it has been replaced by other lower cost metals such as Al in some applications and is now the third most widely used commercial metal after iron and Al [19].

Figure 9 - Copper ore [20]

Pure Cu has a melting point of 1084.62°, atomic weight of 63.55 u, density of 8.96 g/cm^3 and is number 29 on the periodic table [21]. Pure Cu has a tensile strength from 172.5-345 MPa, depending on if it is casted, annealed or cold-worked. Cu is not only an important engineering material but it also has important antibacterial properties. Bacteria, yeasts and viruses die quickly on Cu surfaces, a phenomenon known since ancient times. Egyptians of old used it to sterilize chest wounds and drinking water; these methods were detailed in the Smith Papyrus, which was written between 2600 and 2200 B.C. [22].

The most known Cu alloys are Bronze and Brass. These names have been used for different alloy composition for over thousands of years. Bronze refers to numerous Cu-tin alloys while Brass is a Cu-zinc alloy. A list of Cu alloys and their typical applications can be seen from Table 1.

Table 1 – Common Cu alloys, their chemical composition and applications [23]

Alloy number	Chemical analysis [%]	Typical use
C11000	99.9 Cu	Architectural, electrical
C26800	65 Cu, 35 Zn	Plumbing, grill work
C61400	91 Cu, 7 Al, 2 Fe	Condenser, tubing
C71500	70 Cu, 30 Ni	Desalinization, tubing
C17200	98 Cu, 2 Be	Springs, tools
C81100	100 Cu	Electrical conductors
C83600	85 Cu, 5 Sn, 5 Zn, 5 Pb	Valves, bearings
C93700	80 Cu, 10 Sn, 10 Pb	Bearings, pumps
C96400	70 Cu, 30 Ni	Marine valves
C82400	98 Cu, 2 Be	Dies, tools
C90500	88 Cu, 10 Sn, 2 Ni	Gears
C95300	89 Cu, 10 Al, 1 Fe	Gears, bearings

As can see from Table 1, the alloys C11000 and C81100 are the ones mostly used in electrical applications. These alloys are both almost pure Cu and thus have electric conductivity superior to ones with a lower concentration of Cu. C81100 has an electrical conductivity of 92% IACS while C11000 has an electrical conductivity of around 100% IACS [24]. Cu and its alloys have excellent formability due to their face-centered cubic crystal structure. They are easily cast for hot or cold working into wire, plate, sheet, rod or tube by rolling, drawing, machining, forging, extrusion and joining methods [19].

Numerous different fusion and solid-state welding processes are able to weld Cu and Cu alloys. Common fusion processes such as oxy-fuel welding, resistance welding and arc welding processes are typically chosen to weld Cu and its alloys, while diffusion welding, friction welding, explosion welding and roll welding are common solid-state welding techniques used for the same task. In welding of Cu, its high thermal conductivity is a major factor affecting the weldability of the material. The thermal conductivities for the various alloys differ. Pure and nearly-pure Cu such as Oxygen-free Cu (C10200) and electrolytic tough pitch Cu (C11000) have a thermal conductivity of 391 W/m · K while heavily alloyed Cu such as Cu nickel (C71500) and nickel silver (C75200) have thermal conductivities as low as 29 W/m · K. Other Cu alloys have thermal conductivities somewhere in between. When arc welding Cu with high thermal conductivities it is important to adjust the welding parameters so that it maximizes the heat input of the process into the joint. Some volatile, toxic alloying chemicals are often existent in Cu and Cu alloys. This generally results in much more release of toxic fumes than when welding ferrous metals so that it requires a more effective ventilation system to protect the welding operator than normally. This is generally avoided in solid-state welding processes that operate under the fusion temperature of the material. Solid-state techniques are also much more suitable for welding dissimilar materials. Al-Cu joints are made by techniques such as diffusion welding, friction welding, cold welding, ultrasonic welding and recently FSW [24].

Al is the most abundant metal in the earth's crust, which consists of around 8% Al [25]. As a highly important consumer metal, Al and its alloys are used for foil, cans, kitchen tools, electrical applications and variety of structures. Due to its natural oxide layer, most Al alloys have a very high corrosion resistance in many different environments. Al is a great conductor of electricity and due to its low price and weight; it is often used to replace Cu in various electrical applications. As with most materials that are a good conductor of electricity, Al is also a good conductor of heat, which has led to its applications in radiators and cooking equipment. It is also widely used in transportation applications such as in aircrafts and train bodies due to the high strength relative to weight of certain alloys. The material is soft and ductile, which makes it one of the easiest metal to machine and form. Al and its alloys are not toxic to the environment and are among the most recycled materials as the energy required to recycle Al is only 5% of the energy needed to process new Al [19], [26].

Figure 10 – Pure aluminum [27]

Al has a low melting point for a metal, 655°C, although its oxide layer has a much higher melting point of 2072°C, which can make the material tricky to arc-weld. Al has a density of 2.70 g/cm³. It is easily formed and machined do to its face-centered cubic crystal structure and low work-hardening rate. Al and its alloys have a wide range of strength, depending on alloy composition and strengthening, from 69-607 MPa. Al alloys can be divided in two classes; cast alloys and wrought alloys. In the production and processing of Al, it is of vital importance to control the microstructure of the material. Coarse Intermetallic Compounds (IMCs) form by eutectic decomposition inside the material during the solidification of Al ingots. Some compounds, like $CuAl_2$ and $SiMg_2$, are soluble while others containing iron and silicon, like Al_2Fe and $\alpha Al(Fe,Mn,Si)$, are insoluble. The soluble compounds are dissolved into the material during ingot homogenization before the material is hot worked. The insoluble compounds are then broken up and aligned as stringers during hot working. These IMCs are very brittle and can damage the mechanical properties of the material [19]. They pose a considerable problem in the dissimilar welding of Al-Cu where they are formed under the process's heat and pressure.

Al alloys are divided into 9 categories depending on the major alloying element. The Aluminum Association registers and publishes specifications that describe the mechanical properties, chemical composition and nomenclature of Al alloys [28]. They developed a four-digit numerical designation, which is used to designate Al alloys and wrought Al. The first number defines the dominant alloying element in that series. The 1xxx series are composed of near-pure Al alloys. The two last digits in the 1xxx series dictate the presentence of Al, which is always between 99 and 100% while the second number indicates if one or more of the natural impurities were specially controlled. In the other series, the second number indicates the alloy modification and if it is zero, it indicates the original alloy. The last 2 digits are not as significant as in the 1xxx series as the only identify the different alloys existing in the series. The 9xxx series are only used in the designations for Al casting alloys. The numerical designation for Al casting alloys is different as it uses a decimal point within the number. In the 1xx.x, series the second

and third number are used to indicate the magnitude of Al in the alloy in the same way as in the 1xxx series. The last number in the casting series dictates the product form, 0 if it is a cast product and 1 if it is an ingot. The designations for both wrought and casted Al alloys can be found in Table 2.

Table 2 - Designation for Al alloys [19]

Designations for wrought aluminum alloys		Designations for aluminum casting alloys	
Series	Al content or main alloying element	Series	Al content or main alloying element
1xxx	99.00% minimum	1xxx	99.00% minimum
2xxx	Copper	2xxx	Copper
3xxx	Manganese	3xxx	Silicon + copper and/or magnesium
4xxx	Silicon	4xxx	Silicon
5xxx	Magnesium	5xxx	Magnesium
6xxx	Magnesium and silicon	6xxx	Unused
7xxx	Zinc	7xxx	Zinc
8xxx	Others	8xxx	Tin
9xxx	Unused	9xxx	Other

Al and its alloys can be joined by numerous joining method, as many or more than all other metals. Gas-shielded welding techniques are the most commonly used processes to join Al. Al has many chemical and physical properties that have to be taken into account when it is to be joined. Properties such as the solubility of hydrogen in liquid Al, the thermal, electrical and nonmagnetic properties, absence of color change once heated and wide differences between different alloys are important factors that should be considered in order to acquire sound welds. The thermal conductivity of pure Al, although not as high as Cu, is around 234 W/m · K, which makes it six times higher than of steel. It therefore needs, just as Cu, a high stable heat input in order to avoid alteration in fusion and penetration when being fusion welded. When Al is fusion welded to materials such as Cu, steel, magnesium, or titanium it causes the formation of very brittle IMCs, which severely deteriorates the properties of the joint. Other non-fusion welding processes are therefore used to join Al to other materials. The techniques commonly used are explosion welding, friction welding, flash welding, hot pressure welding and recently FSW [29].

2.3.2 Material Flow

The material flow during FSW of dissimilar materials is a complex mechanism. Not only is the material flow in normal FSW asymmetrical due to the rotation and movement of the tool but when the materials themselves have different properties which cause them to react differently to the forces from the tool it adds another layer of complexity on top. Quite a few researchers have mentioned how the materials have flowed in their research of dissimilar Al-Cu FSW.

Galvao et al. [30] researched the material flow in dissimilar FSW of thin Al and Cu sheets. They noted a great difference in the material flow depending on which material was placed on the advancing side. When the Al was placed on the advancing side, it underwent severe softening and was pushed away from under the shoulder by Cu, which entered the area with each revolution. This caused the Al to be expelled and gave rise to flash formation. In addition to this, no mixing of the base materials nor formation of IMCs occurred with the Al on the advancing side. When the Cu was on the advancing side, the shoulder drags the Al to the advancing side. There it is not able to push the Cu away from under the shoulder and thus becomes constrained inside a cavity under the shoulder and flows downwards from there. Then it is mechanically mixed inside the Cu that then gives rise to the formation of intermetallic structures. This material flow occurred in 1 mm thin sheets.

The flow mechanics are highly affected by the material positions; which material is on the advancing side and which one is on the retreating side. According to P. Carlone et al. [31] the material from the retreating side is moved to the advancing side behind the probe, where the formation of the weld bead takes place. When the softer material is placed at the retreating side, it is easier to force it towards the advancing side.

T.K. Bhattacharya et al. [32] studied the material flow in an Al-Cu Friction Stir (FS) butt-welded joint. They noted that a complicated macrostructural flow had occurred inside the nugget. A large amount of tiny Cu particles were scattered in the nugget along with streamline shaped continuous Al strips. On top of the nugget, the shoulder mainly influences the material flow. It makes the Al flow from the retreating side of the tool to the advancing side. This influence diminishes quickly lower into the weld, where bulk Cu flows from the advancing side to the lower area influenced by the probe. There it mixes with the Al and forms some IMCs. According to them, the classical FSW flow model is so that Al on the retreating side flows towards the advancing Cu which first flows downwards and then up again. This typically results in sound weld joints.

T. Saeid et al. [33] reported on the material flow of FS lap-weld of Al-Cu. According to them, the interface in the central region of the weld moves considerably into the bottom plate because of the circle-like vortex flow of the materials caused by the probe threads. Higher welding speeds reduced the vertical transport, especially on the retreating side. They attributed the reduction of vertical transport to fewer revolutions over the distance of the weld.

M. Guerra et al. [34] studied flow patterns during FSW with a threaded probe. They concluded by describing two processes by which the material is moved around the probe (nib) in FSW:

"Material on the advancing front side of a weld enters into a rotational zone that rotates and advances with the nib. This material is very highly deformed and sloughs off behind the nib in arc-shaped features. Material on the retreating front side of the nib is entrained and fills in material on the retreating side of the nib wake". The materials moved around by these two processes have very different properties according to them.

2.3.3 Weld Structure

Previous works have detailed the weld structure and Al-Cu interaction patterns in the FSW of Al-Cu. It is possible to divide these structures into three groups; lamellar intercalated features, homogeneous mixtures and composite-like structures [35]. In FS welded nuggets of Al and Cu it is typical to find more than one kind of interaction structure as is reported in most papers detailing the issue [36]-[38].

The lamellar intercalated morphology is swirl-like and vortex-shaped. It forms via intense solid-state plastic deformation and flow. The morphology usually consists of two or more IMC phases and the formation is deeply influenced by process parameters such as rotational speed and tool offset as reported by Galvao *et al.* [17] and Liu *et al.* [39].
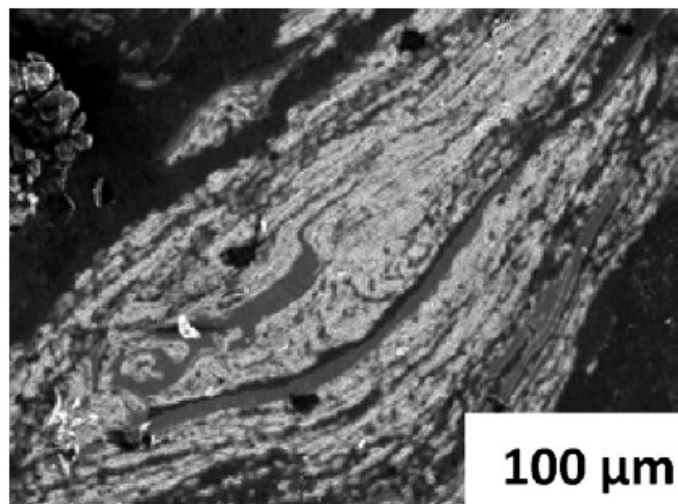

Figure 11 - Intercalated lamae (adapted from Muthu and Jayabalan [36])

The homogeneous mixtures have been characterized by Galvao *et al.*[1], [17] and they seem to be the rarest morphology that forms in the weld. According to them, the homogeneous mixtures form when intense stirring and heat-input is imposed on a shear layer which is very rich in either Al or Cu [35].
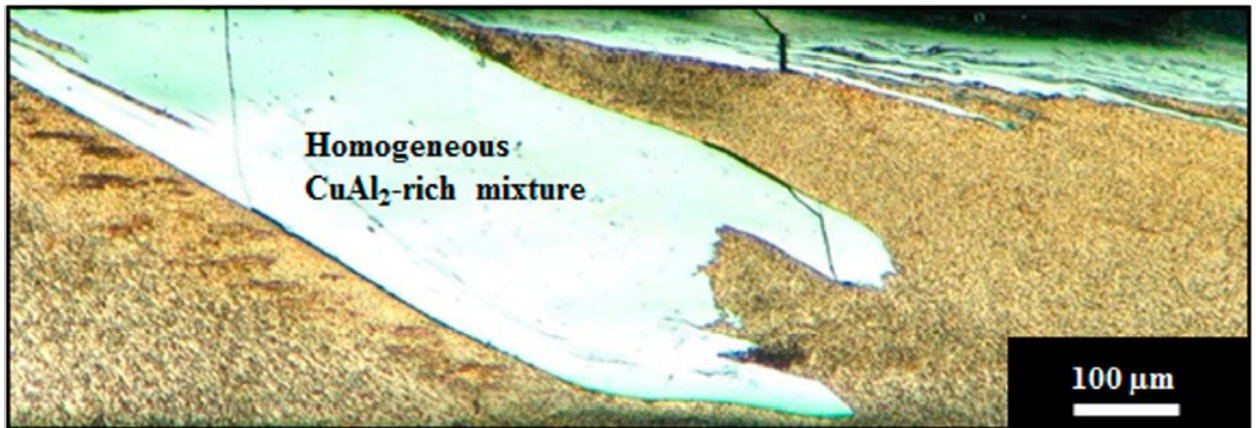
Figure 12 - Homogeneous mixture (adapted from Galvao *et al.* [35])

The composite-like structures are composed of Cu, Cu-rich or IMC particles dispersed in an Al or Al-rich matrix. This morphology can range from being small and localized to covering the whole nugget. The morphology has been reported by researches such as Xue *et al.* [40]-[42] and Al-Roubaiy *et al.* [43].
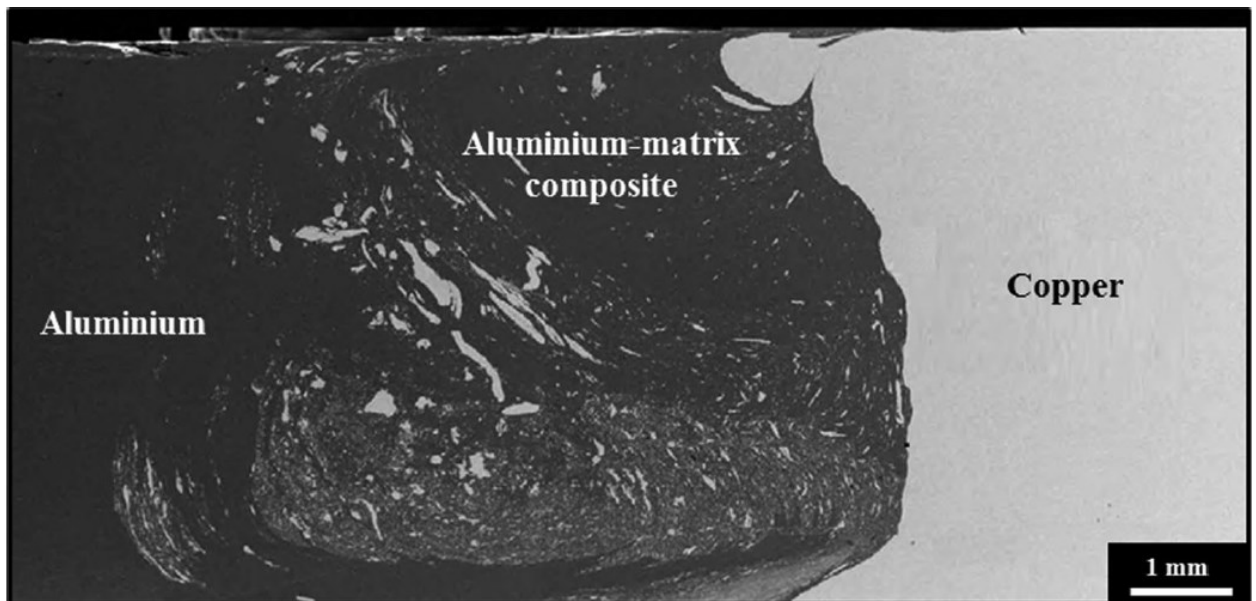

Figure 13 - Composite structure (adapted from Xue *et al.* [42])

2.3.4 Intermetallic Compounds

During FSW, different Al-Cu phases are formed because of the heat input and flow of the base materials while subject to intense pressure. These phases are called intermetallic compounds (IMCs). These IMCs also occur in Al-Cu welding using various other joining methods like explosive and friction welding [42], [44]. The most commonly formed IMCs are Cu_9Al_4 and $CuAl_2$ [35], [45]. These IMCs are brittle and to achieve sound FSW of Al-Cu joints it is important to avoid excess formation and keep them as a thin, uniform and continuous layer at

the base material interface [41], [42]. The Al-Cu phase diagram and a table detailing the chemical composition of the most relevant phases can be seen in Figure 14.
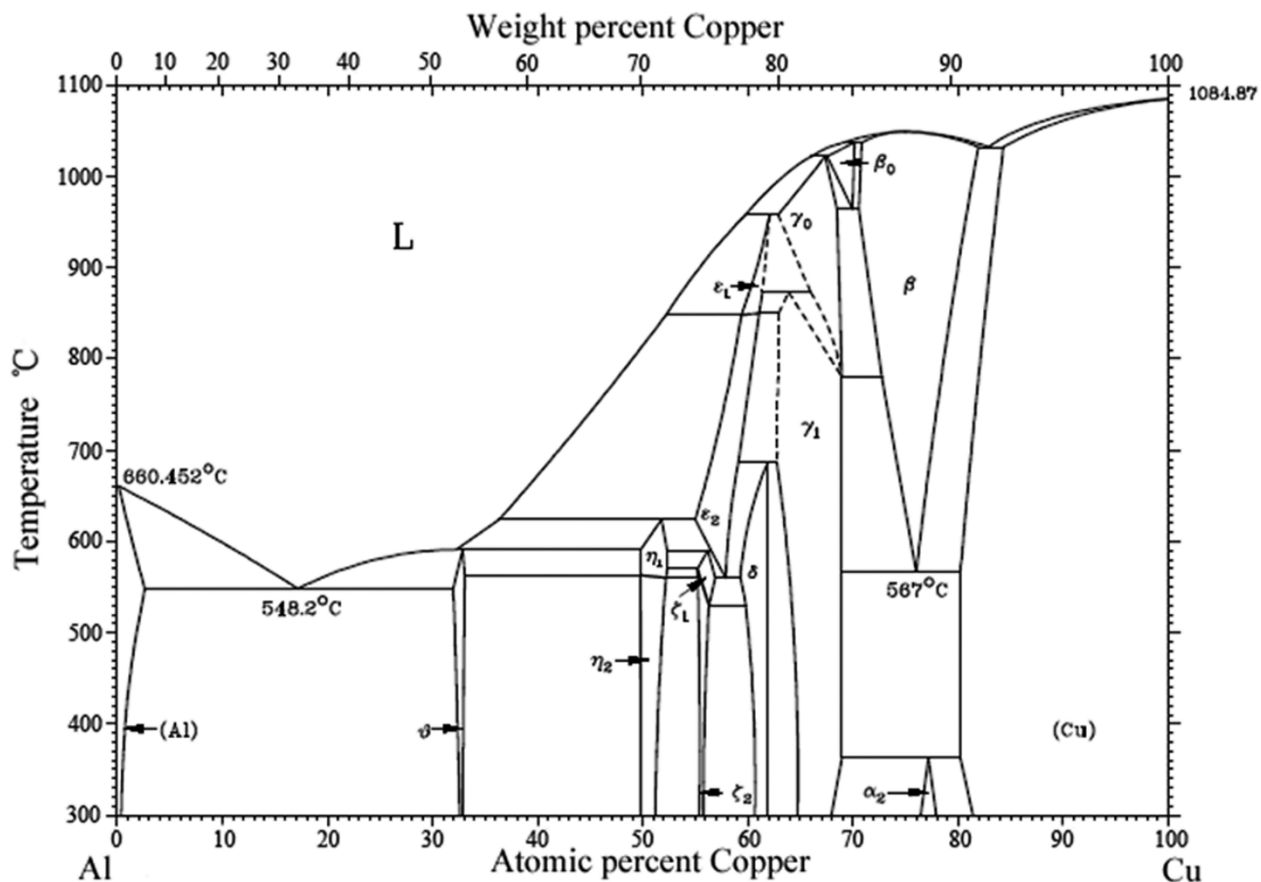
Figure 14 - Al-Cu phase diagram [46]

Table 3 - IMC chemical formulas

Phase	Chemical formula
γ1	Cu_9Al_4
δ	Cu_3Al_2
η1&η2	$CuAl$
ζ1&ζ2	Cu_4Al_3
θ	$CuAl_2$

Numerous works have detailed the formation of IMCs during FSW of Al-Cu and the effects they have on the weld. Few reasons for the formation mechanism have been reported although Galvao *et al.* [17] pointed out a thermomechanically activated solid-state diffusion phenomenon that controls the formation of the two most commonly seen IMCs in the FSW of Al-Cu, Cu_9Al_4

and $CuAl_2$. Because the chemical reactions that occur under the thermal cycles of the FSW process are not close to the equilibrium condition, the formation cannot be understood solely based on the phase diagram. In addition, the fusion temperature of Cu_9Al_4, which is 1030°C is much higher than the temperatures reached in the process. Thus, it is reasonable to say that only a thermomechanically induced solid-state diffusion process could form an IMC with such high fusion temperatures. Galvao *et al.* argue that Cu_9Al_4 is formed by the incorporation of Al atoms into the Cu structures, which can be assumed as a mechanical process resulting from the stirring during FSW. Intense plastic deformation is believed to accelerate the rate of diffusion in solid-state welding, which enables the sufficient atomic concentration for IMCs to form even at low temperatures.

H. Barekatain *et al.* [45] reported that the microstructure of the stir zone consists of Cu particles from the base Cu surrounded by IMCs layers.

Li Xia-wei *et al.* [47] on the other hand reported no IMCs in the weld nugget of a sound 1350 Al alloy to Cu FSW but observed a complex microstructure consisting of vortex-like pattern and lamella structure.

T.K. Bhattacharya *et al.* [32] reported a continuous IMC layer of 3.6 µm between the Al and Cu in a FS butt weld, which had a tensile strength joint efficiency of 86.5%.

Braunovic *et al.* [48] investigated the effect the IMC layer has on the electrical resistance of the Al-Cu joint. IMC layers with thicknesses up to 100 µm were tested. The findings were that the formation of the IMC layer has a very detrimental effect on the electrical properties of the joint. The electrical resistance of the joint interface rises linearly with the thickness of the IMC layer, around 0.5% for every 1 µm. As in FSW of Al-Cu the thickness of the IMC layer is usually just a couple of µm it should only result in a minor increase in electrical resistance.

Savolainen *et al.* [49] studied the electrical resistance of an FSW Al-Cu butt joint. The material welded was 10 mm thick. After having measured the resistance of the welded component and then subtracting the resistance of the base materials they found the resistance of the joint to be around 0.4 µΩ.

M.N. Avettand-Fenoël *et al.* [50] studied the IMCs in dissimilar Al-Cu FSW. They found the penetration of Cu-particles into the Al and Al-particles into the Cu to result in the local formation of IMCs. Their X-ray diffraction analyses established the Al_4Cu_9 IMC to be rich in oxygen. According to their sources [51], the first IMC phase to form is the one with the most negative effective heat of formation at the composition of the lowest temperature of the liquids. In the FSW of Al-Cu this is the Al_2Cu phase at the Al side. The IMC that first forms at the Cu side is not the one that should be expected to form first. The first one to form at the Cu side is the Al_4Cu_9 phase, which should be the second phase to form on the Cu side according to traditional knowledge.

2.3.5 Defects and Failures

It is quite difficult to achieve sound FSW of Al and Cu. The most reported weld defects in scientific literature are internal discontinuities, cracking and bad surface finishing. Internal discontinuities occur usually due to improper mixing of the base materials at the Al-Cu interface as has been reported by Tan *et al.* [38], Liu *et al.* [37], Muthu and Jayabalan [36], Al-Roubaiy *et al.* [43], Celik and Cakir [52], Bhattacharya *et al.* [32], Bisadi *et al.* [53], Xue *et al.* [41] and Saeid *et al.* [33].
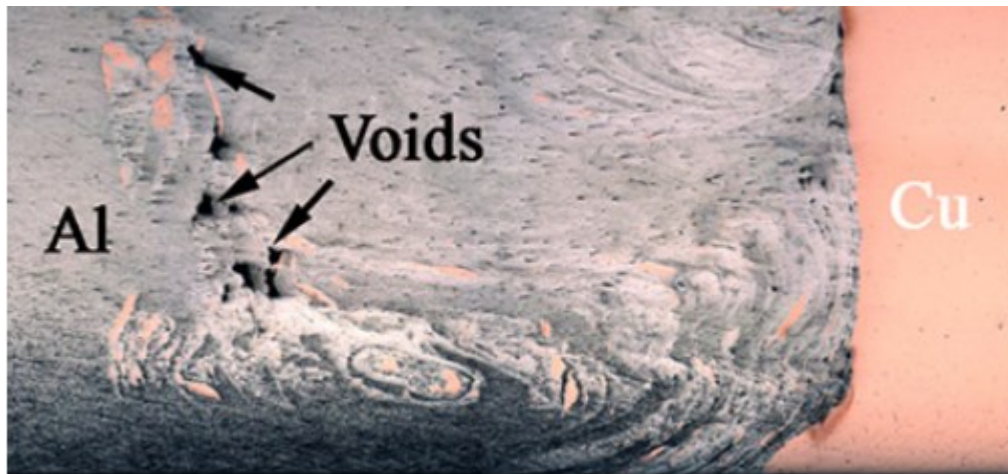

Figure 15 - Internal discontinuities (adapted from Xue *et al.* [41])

Cracking is caused by the high brittleness of the IMCs present in the welds. This has been reported in works by Liu *et al.* [37], Galvao *et al.* [17], [30], Muthu and Jayabalan [36], [54], Bisadi *et al.*[53], Saeid *et al.* [33] and Sahu *et al.* [55].
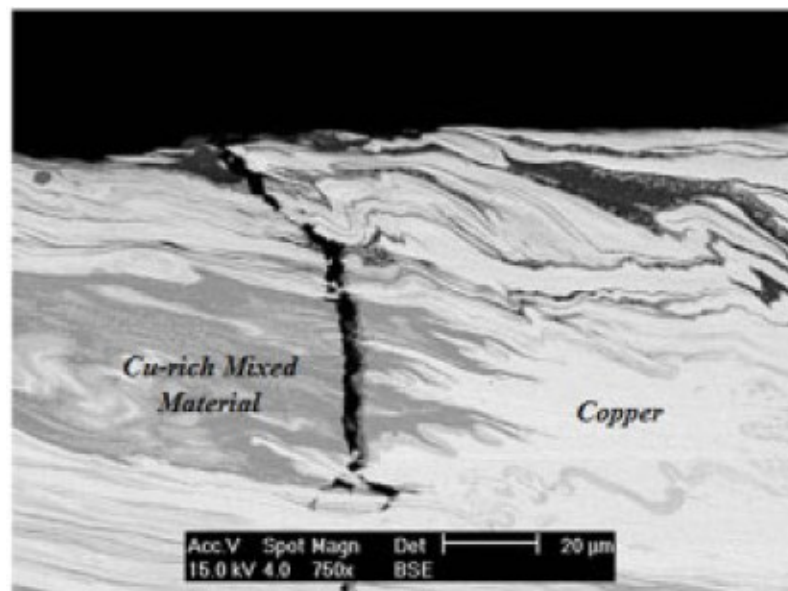

Figure 16 - Crack(adapted from Galvao *et al.* [17])

Bad surface finishing occurs mostly due to irregular distribution of IMC layers on the surface of the weld, which can result in flashes, grooves, pits and cracks as reported by Liu *et al.* [37], Muthu and Jayabalan [36], Al-Roubaiy *et al.* [43], Galvao *et al.* [1], [17], Xue *et al.* [41] and Barekatain *et al.* [45].
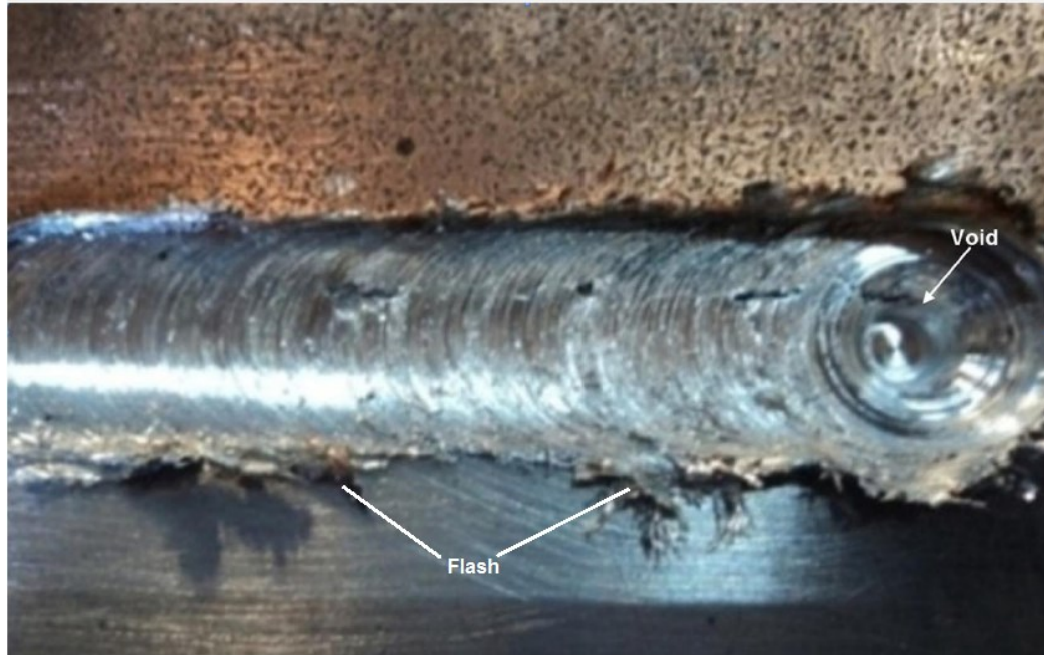

Figure 17 – Void and flash observed on the surface of an Al-Cu FS weld (adapted from Al-Roubaiy *et al.* [43])

According to Al-Roubaiy *et al.* [43] surface pits and grooves can form due to insufficient axial force and plunging depth, which results in inadequate refilling of the advancing side of the weld. By increasing the axial force, it is possible to minimize the formation of surface tunnels as well as collapsing internal voids and promote better mixing of the materials.

2.3.6 Influence of Heat Input, Rotational Speed and Travel Speed

Articles have detailed the effects of rotational and welding speeds on the resulting FSW Al-Cu weld. The rotational and welding speeds govern the heat input during the process, which also has been studied in detail. Correctly selecting the parameters value can be paramount to the outcome of the weld procedure.

With increasing heat input, that is; lower travel speeds and higher rotational speeds, the weld zone grows larger, which, along with more material mixing, can be beneficial for the weld properties. On the other hand, too much heat input increases the formation of IMCs, which increase the brittleness of the weld, and lower the tensile strength [52]. If the heat input is too low, as it is with high travel speeds, it cannot induce interfacial reaction between the Cu and Al [38].

T.K. Bhattacharya *et al.* [32] investigated the correlation between heat input, joint strength and welding forces. They noted that when they increased the heat input in the FS butt-welding of Al-Cu both the axial force and torque decreased. In their research, it was also observed that increasing the rotating speed from 800 RPM to 1000 RPM, and therefore the heat input, improved the joint strength significantly. This was for both of the travel speeds they used in their investigation, 20 and 40 mm/min.

H. Bisadi *et al.* [53] investigated the influences of rotational and travel speeds on FS lap-welds of Al-Cu. They found that both very low and very high welding temperatures lead to many joint defects. In their experiment, higher welding temperatures resulted in a joint surface quality reduction as well as increase in flash formation. Lower welding temperatures caused defects close to the sheet interface as well as some cavity defects. It reinforces the importance of balancing the heat input during FSW of Al-Cu in order to acquire sound welds.

Akinlabi *et al.* [30] found the electrical resistance of a FSW Al-Cu joint to increase with increasing heat input. This is likely due to the increased formation of IMCs.

A couple of articles have detailed the effects of the rotational speed on the weld. Their results have been compiled in Table 4.

P.K. Sahu *et al.* [55] when FSW AA1050 to Cu found that increasing the rotational speed up to 1200 RPM resulted in greater weld strength but once the rotational speed surpassed 1200 RPM the resulting strength started to decrease.

Liu *et al.* [37] found the tool rotational speed to have a significant effect on the distribution of Cu during their FS butt-welding of Al-Cu experiments. With a high rotational speed of 1000 RPM, they found the weld root to consist mainly of Cu, with a homogeneous distribution of structures. When the rotational speed was lowered to 600 RPM, they found large Cu fragment left on the Al alloy side as well as finding the distribution of Cu fragments in the weld to be very concentrated.

While it seems that with increasing rotational speed the surface quality of the weld decreases, it is important to balance it so that the tensile properties of the weld are sufficient as noted by P.Xue *et al.* [41]. In addition, they stated that with higher rotational speeds the IMC layer in the weld became less uniform in thickness.

Table 4 - Effect of rotational speed

Article	Materials	Thickness	Rotational speed	Issue highlights
Sahu *et al.* [55]	AA1050 Pure Cu	4 mm	600-2400 RPM	Medium rotational speeds produce better welds. Higher welding speeds lead to more flash formation and more material interaction.
Liu *et al.* [37]	AA5052 Pure Cu	3 mm	600-1200 RPM	Better Cu particle distribution with higher rotational speeds. Lower rotational speeds promotes less intermixing and cavity defects.
Bhattacharya *et al.* [32]	AA6063 Pure Cu	3 mm	800-1000 RPM	Better welds acquired with higher rotational speeds. Lower rotational speeds promoted less intermixing.
Celik and Cakir [52]	AA1050 Pure Cu	4 mm	630-2440 RPM	Medium rotational speeds promote a composite structure and high tensile strength in the weld. Higher speeds promote more IMC formation.
Xue *et al.* [41]	AA1060 Pure Cu	5 mm	400-1000 RPM	Thinner and more uniform IMC layer achieved at lower speeds. Surface quality deterred and IMC formation increased with higher speeds.

As seen from Table 4, the effect of rotational speed on the weld has been detailed by several articles. The works detailed in the table reach a consensus that increasing rotational speeds results in increased base materials interaction; more intermixing as noted by Liu *et al.* [37], Bhattacharya *et al.* [32] and Sahu *et al.* [55] and greater formation of IMC phases as noted by Celik *et al.* [52] and Xue *et al.* [41]. Effect on the surface quality was also noted in the works of Xue *et al.* [41] and Sahu *et al.* [55], where increasing rotational speeds contributed to worse surface quality of the welds.

The travel speed, how fast the FSW tool travels in the weld line during the procedure, controls the heat input of the welding procedure like the rotational speed. With slower travel speeds, the FSW tool dwells a longer amount inside the material and thus generates more heat.

H. Barekatain *et al.* [45] investigated the effects of different travel speeds and rotational speeds on the FSW of severely plastically deformed AA1050 Al and Cu sheets and found that for both rotational speed and travel speed there is an interval where the parameters chosen result in sound welds. The parameters cannot be too low since there needs to be a minimum heat input but setting them too high will be damaging. The acceptable parameters they found were travel speeds between 63-80 mm/min and rotational speed between 1200-1400 RPM.

Akinlabi *et al.* [56] researched the effect of travel speed on the properties of FS butt-welded Al-Cu sheets. The travel speeds investigated were between 50 and 300 mm/min. They found that at lower travel speeds the metallurgical bonding and mixing of the metals were improved because of high heat input and low axial force. This resulted in improved UTS.

Table 5 – Article compilation on the effects of travel speed

Article	Materials	Thickness	Joint design	Welding speed	Issue highlights
Tan *et al.*[38]	AA5A02 Pure Cu	3 mm 3 mm	Butt weld	20-40 mm/min	Higher welding speeds promote cavity defects and insufficient mixing. Lower speeds promote less flash formation, good appearance and proper mixing.
Bhattacharya *et al.*[32]	AA6063 Pure Cu	3 mm 3 mm	Butt weld	20-40 mm/min	Better welds acquired with lower travel speeds. Higher speeds produced less smooth material flow.
Saeid *et al.*[33]	AA1060 Pure Cu	4 mm 3 mm	Lap weld	30-375 mm/min	Higher welding speeds have lower vertical transport of material and promote cavity defects. Lower welding speeds increase the mixing of materials.
Akinlabi *et al.*[56]	AA5754 C11000	3.175 mm 3.175 mm	Butt weld	50-300 mm/min	Lower welding speeds improved mixing of both metals. Higher welding speeds did not achieve coalescence and proper mixing.
Al-Roubaiy *et al.*[43]	AA5083-H111 Cu-DHP R240	1 mm 1 mm	Butt weld	160-250 mm/min	Higher welding speeds reduce material mixing. Lower welding speeds enlarge the mixing area and increase IMC formation.

As displayed in Table 5, the effect of the travel speed on the weld has been detailed by several authors in both butt and lap welds. Tan *et al.* [38], Saeid *et al.* [33], Akinlabi *et al.* [56], and

Galvao *et al.* [17] are in agreement that lower welding speeds result in increased mixing of the base materials. Most authors did not report on the weld surface quality in their works although Tan *et al.* [38] noted less flash formation and better appearance with lower welding speeds.

2.3.7 Influence of Tool Offset, Material Positioning and Alloy type

Other factors of the process have an important influence on the outcome of the weld. Many works on the subject have detailed the influence of aspects such as tool offset and material positioning. A few have detailed the effects different alloys have on the process.

Tool offset has shown itself to be important to tool life and the overall quality of the weld. Tool offset is when, instead of the tool being centered at the joining line of the two materials, the tool is centered at a certain distance from the joining line. When the tool is placed more into the softer material, the Al, the tool life increases as less forces act on it from the harder material since it comes less into contact with the Cu.

Sare Celik and Recep Cakir [52] noticed that when FS butt-welding Cu to AA1050 alloy a full mixture of the materials could not be achieved without an offset between 1-2 mm (50-100% of probe radius). When the probe is located on either side of the joining line the weld zone shifts from the joining line towards the material the tool probe is offset to. Similar results were noted by P. Xue *et al.* [41] where good tensile properties were acquired when the tool offset was between 2 and 2.5 mm (67-83%), although too high offset is disadvantageous because of insufficiency in the reaction occurring between the Cu pieces and the Al matrix structure that forms during FSW. Tolephih *et al.* [57] also reported on the advantages of tool offset in an experiment where the highest weld strength was achieved using an offset of 33%.

P. Carlone *et al.* [31] also reported sound dissimilar FSW joints by offsetting the tool into the Al sheet. Al-Roubaiy *et al.* [43] reported successful welds with a high offset of 93%, although with an offset of 100% their specimens failed during preparatory machining because a near absence of stirring action on the Cu side. Li Xia-wei *et al.* [47] reported groove defects when using an offset of 100%.

Some researchers suggest that it might not be necessary to offset the tool in order to get a sound FS butt-weld between Al-Cu. T.K. Bhattacharya *et al.* [32] reported a joint efficiency of 86.5% without using an offset. M.N. Avettand-Feonël *et al.* [50] found offset in either direction, during FS butt-welding of Al-Cu, to increase the formation of IMCs within the weld, especially when the tool was offset into the Cu sheet.

Table 6 – Article compilation on the effects of tool offset

Article	Materials	Thickness	Offset [% radius]	Issue highlights
Sahu et al.[55]	AA1050 Pure Cu	4 mm	16.7-66.7	Increasing the offset up to 50% resulted in better welds. Going over 50% damaged the weld. Higher offset decreases the Cu in the nugget zone.
Tolephih et al.[57]	AA2024 Pure Cu	5 mm	50-83.3	Low offsets promote Al melting at the interface. High offsets weaken material bonding. Medium offsets produce sound welds.
Al-Roubaiy et al.[43]	AA5083-H116 Pure Cu	6.3 mm	86.7-100	100% offset resulted in improperly mixed welds. Low offsets promoted void defects.
Celik et al.[52]	AA1050 Pure Cu	4 mm	0-100	Full mixture could not be reached with 0% offset. 50% and over led to a homogeneous mixture and better properties.
Xue et al.[41]	AA1060 Pure Cu	5 mm	0-100	Sound welds could only be achieved with 66% offset or higher. Surface quality becomes worse and IMC formation increases with lower offsets.
Avettand-Fenoël et al.[50]	AA6082-T6 Cu-a1	5 mm	0-33, both materials	Offsetting the tool into either material increased IMC formation, especially for offset into Cu.

From table 6, it can be seen that most researchers agree on the benefits of tool offset. Although it differs from work to work, there is a certain interval in these works where the offset seems to promote successful welds. Too high offsets, especially close to 100%, promote improper material mixing according to Al-Toubaiy et al. [43], Tolephih et al. [57] and Sahu et al. [55]. However, these works do not reach a full consensus on the benefits of the tool offset. Avettand-Fenoël et al. [50] reported increased IMC formation in welds for offsets in both direction which results in less sounder welds. The lack of consensus might stem from differences in the alloys used or the thicknesses of the materials. It can be concluded that offsetting the tool into the softer material promotes better welds for some conditions but not all.

Positioning of the dissimilar materials to be joined via FSW, as stated before, is of great importance due to the flow mechanics that are in effect during the weld procedure. When the tool moves forward and is turning clockwise the material on the left side of the tool flows along the front end of the tool towards the other side, the left side in this example is therefore called the advancing side while the right side is called the retreating side. This creates a vacancy on the advancing side and material from the retreating side is transported at the rear end of the tool

to the advancing side to fill that vacancy [52]. The resulting microstructure is thus significantly governed by the relative positioning of the materials.

Researchers at Shenyang, China, observed that sound welds of FSW Al-Cu could only be obtained when the Cu was placed at the advancing side and not the other way around [41]. This knowledge has been reinforced by several other researches [30], [31], [49], [55] and has been attributed to the flow mechanism that occurs during the process. The material on the retreating side is transported via the shoulder towards the advancing side at the top of the plates while the advancing side pushes into the retreating side at a lower depth. Because of the softness of the Al it is pushed away from under the shoulder area, when it is positioned on the advancing side, by the hard Cu which is pushed down by the shoulder. This produces flash formation and hinders Al-Cu mixing which is much more successful when the Cu is placed at the advancing side.

Figure 18 – Effects of material positioning (adapted from Liu *et al.* [37])

On the other hand, C.W. Tan *et al.* [38] reported sounder welds with the Cu on the retreating side than the advancing side when slow travel speed (20 mm/min) was used.

Liu *et al.* [37] made multiple experiments with Al both placed on the retreating and advancing side. They found that all the joints welded with Al on the advancing side had poor appearance, contained grooves flashes as well as cracks and pits. Once they had changed the Al to the retreating side, the appearance became much better and the joints were without continuous defects.

Although not every research addressing the positioning of the base materials during FS butt-welding of Al and Cu is in agreement on which positioning is better it is clear that due to the flow mechanism of the weld procedure there is a large difference in result depending on which material is positioned where. The vast majority of works detailing the issue note the improved

weld that results from placing the Cu on the advancing side and it seems to be the standard procedure in the field [35].

Since FS lap-welds have not been as thoroughly researched as butt-welds fewer works detail the influence the material positioning has on the weld using that joint design. Akbari *et al.* [58] investigated the effect of materials position during FS lap welding of Al-Cu. In the research it was noted that for all the different rotational and welding speed tested the strength of the joint is always higher when the Al is placed on top of the Cu during the process. This was contributed to differences in the thermal conductivity of the materials. One of the main sources of heat is the friction between the shoulder and the upper sheet and placing the Al, which has lower heat conductivity, on top will therefore concentrate the weld zone to a smaller area and result in less coarse mechanical properties and a sounder weld. This seems to be in agreement with general practices in FS lap-welding of Al-Cu as the vast majority of works is made with the Al on top.

Although there exists a variety of different alloys with different properties for both Cu and Al only a limited amount of works have detailed the effect different alloys have on the weld properties and success. Most works focus on one combination of Cu and Aö, most often using pure or nearly pure Cu, as the purpose is often to maximize the joint properties of that particular material combination. Galvao *et al.* [59] investigated the effect that two different Al alloys had on a dissimilar Al-Cu lap weld. The alloys investigated were AA6082 and AA5083, the former being a heat-treatable alloy while the latter being non-heat-treatable. They found the difference in plastic properties of the alloys to have a considerable effect on both the metallurgical phenomena and material flow during lap welding. While the AA5083 welds had an excellent surface finish and poor Al-Cu interfaces, the AA6082 welds had poor surface finish but strong mixing of the base materials. This was contributed to the greater softening of the AA6082 alloy compared to the AA5083 alloy.

2.3.8 Effect of Tool Geometry

The geometry of the tool used during FSW has considerate effect on the flow of the materials and thus the final properties of the weld, especially in welding of dissimilar materials. A few previous works have detailed the effects of different tool designs on the properties of dissimilar Al-Cu FSW.

Muthu and Jaybalan [54] investigated the effects of three probe profiles on the weld properties of dissimilar Al-Cu FS welds. The profiles tested were whorl probe profile, plain taper probe profile and taper threaded probe profile. They concluded that among these three profiles the best results were obtained by using a plain taper probe profile that they attributed to a defect-free stir zone and dispersion strengthening.
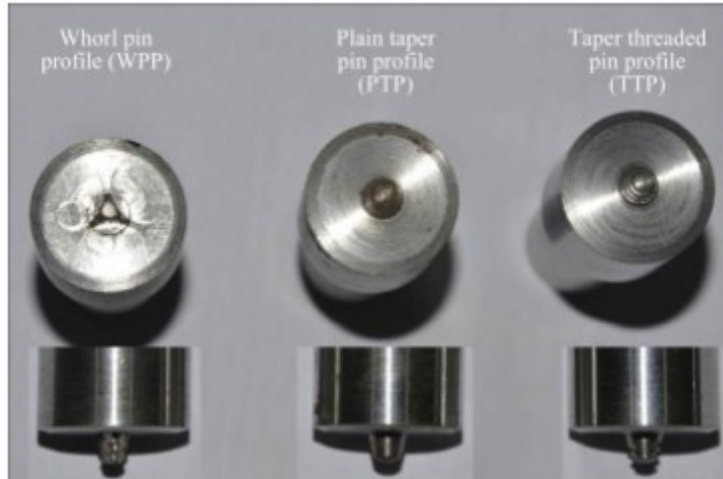
Figure 19 - Three different probe profiles (adapted from Muthu and Jaybalan [54])

Galvao *et al.* [1] investigated the influence of shoulder geometry on the properties of dissimilar Al-Cu FS welds. Two different shoulders were tested: a scrolled shoulder and a concave shoulder. The same welding parameters were used for both shoulders and the investigators observed that with different shoulders the weld nuggets had completely different intermetallic content. The researchers reported that the scrolled shoulder promoted formation of a mixed region almost exclusively made of $CuAl_2$ while the concave shoulder promoted the formation of a more diverse mixture of $CuAl_2$, Cu_9Al_4, Cu and Al as well as lower intermetallic content. The scrolled shoulder produced better surface finish.

Figure 20 - A concave and a scrolled shoulder

E.T. Akinlabi [9] looked into the effects of the shoulder diameter on the properties of FSW. 3 different shoulder diameters were tested, 15, 18 and 25 mm. The results were so that using the 18 mm shoulder resulted in the best mechanical properties. 15 mm diameter was also superior to the shoulder with 25 mm diameter. This was credited to the difference in heat generation when using the three different shoulders. The base materials were 3.175 mm thick.

2.3.9 Applications

The applications of dissimilarly welded materials are numerous and depend on the properties of both joined materials. Cu is mostly applied where its conductive characteristics are needed, such as in electrical or heat transference. Al is a conductive material as well although its properties are not as ideal as for Cu. On the other hand, Al is a much cheaper material and therefore can be used to replace the Cu in applications where some sections do not need the full effect of the Cu characteristics. It can be very cost-effective to be able to replace parts of Cu with Al where the Al properties suffice [60]. This can also be reversed in order to improve certain sections of electrical or heat transferal applications by replacing Al with Cu.

Figure 21 – Conventional monolithic Al bus bar

The last example is exactly one purpose of this work. By replacing the ends of Al bus bars with Cu, the overall characteristics of the bus bars should improve significantly. The ends of the bus bars are electrical hotspots. Their resistance is higher than the middle section of the bar, as they are both thinner and in bolted contact with other parts of the electrical system, which results in a locally higher resistance at the connection. This means that the temperatures of the bus bar rise while the system is in use. The ends are under high forces from the bolt and due to thermal cycles, the material slowly deforms over time. This lowers the bolted force, which increases the local electrical resistance that results in further elevated temperatures. Thus, the bus bar joints need to be re-tightened periodically in order to prevent failure. Cu has higher electrical and thermal conductivities, which results in lower local temperatures in the bus bar ends. The Cu also has 30% lower thermal expansion than Al, so the deformation due to thermal cycles should be much lower [61].

2.4 Evaluation of Weld Properties

The quality of the dissimilar FSW joint needs to be assessed and evaluated considering the desired application for the joints. The joints are to be used in the manufacturing of Al spiral bus bars with a Cu end. Three joint characteristics were selected to be evaluated based on the intended purpose of the joints:

- Tensile strength
- Bending ability
- Electrical resistance

Tensile strength and bending ability detail the mechanical strength and formability of the joint as it is required to withstand the forces affecting it while the bus bar is formed into a spiral. The electrical resistance of the joint needs to be minimal as to minimize the electrical power losses in the bus bar while in operation.

Tensile and bending tests both deliver many outputs and it can be difficult to compare different welds when using these values separately. To simplify the analysis of the outputs two coefficients are used; Global Efficiency to Tensile Strength, GETS (1) and Global Efficiency to Bending, GEB (2) [62].

$$GETS = CE\frac{E_i}{E_{BM}} + C\sigma_y\frac{\sigma_{y\_i}}{\sigma_{y\_BM}} + C\sigma_{UTS}\frac{\sigma_{UTS\_i}}{\sigma_{UTS\_BM}} + CA\frac{A_i}{A_{BM}} + CU_T\frac{U_{T\_i}}{U_{T\_BM}} \qquad (1)$$

Where E is the Young modulus, σ_y is the yield stress, σ_{UTS} is the ultimate stress, A is the elongation and U_T is the toughness.

$$GEB = CF\frac{F_i}{F_{BM}} + Cd\frac{d_i}{d_{BM}} + CU_B\frac{U_{B\_i}}{U_{B\_BM}} \qquad (2)$$

Where F is the maximum load, d is displacement at maximum load and U_B is the consumed energy until a certain minimum load is reached after the maximum load has been passed.

In both equation the different C values are weights, which consider the level of importance of the mechanical properties in the intended application of the joint [62].

To evaluate the electrical resistance of different Al-Cu welds the resistance of the joints is measured. An electric resistance coefficient, conductive efficiency (σ_{eff}), is used for this purpose.

$$\sigma_{eff} = \frac{R_{Al} + R_{Cu}}{R_{Al} + R_{Cu} + R_{Joint}} \qquad (3)$$

Where R_{Al} is the resistance of the Al side of the joint, R_{Cu} is the resistance of the Cu side of the joint and R_{Joint} is the resistance of the joint. The joint length is considered to be the same as the diameter of the shoulder used to produce the joint. The conductive efficiency compares the resistance the welded joint to an ideal welded joint without contact resistance.

2.4.1 Tensile Tests

Tensile test is a destructive test where a tensile force is applied to a test specimen, which is pulled apart at a constant rate until fracture. The specimen is machined with two wide "gripping ends" and a thinner "neck" in the middle, where the fracture is intended to take place.
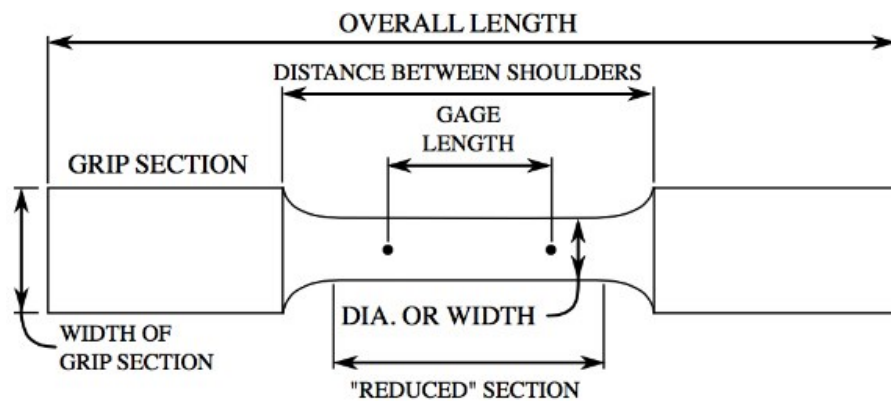
Figure 22 – Tensile test specimen [63]

The load on and elongation of the specimen is monitored and the first result of a tensile test is a load-versus-elongation curve. The data is then normalized for the original geometry of the specimen to obtain an engineering stress-versus-strain curve. Engineering stress, σ, and engineering strain, ε, are defined below [64].

$$\sigma = \frac{P}{A_0} \tag{4}$$

$$\epsilon = \frac{l - l_0}{l_0} = \frac{\Delta l}{l_0} \tag{5}$$

Where P is the load on the sample, A_0 the original cross-sectional area of the sample, l is the gauge length at a certain load and l_0 is the original length.
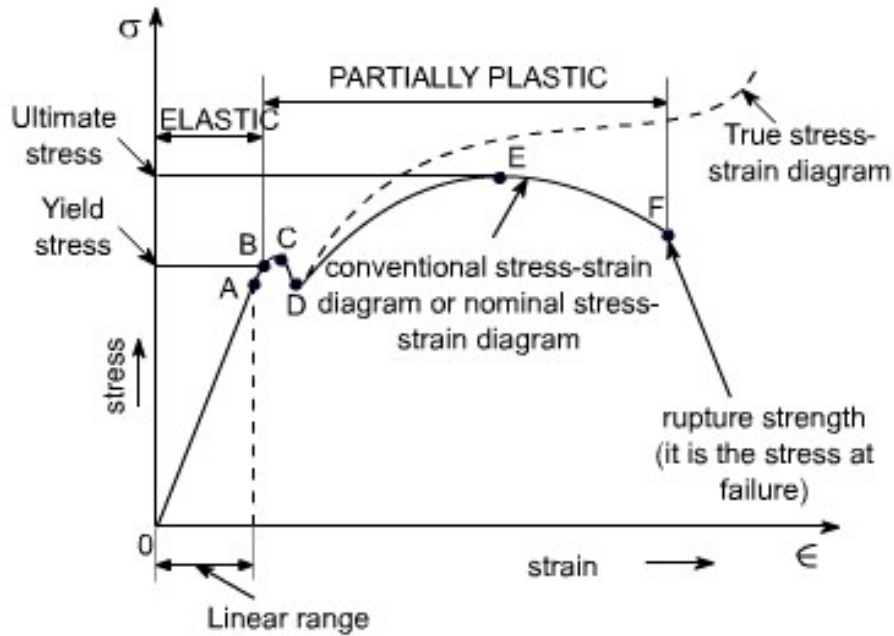
Figure 23 – An example tensile test stress-strain diagram [65]

In the first segment of the curve in Figure 23, where it is the steepest, the material experiences elastic deformation. Elastic deformation is a temporary deformation and a material will take its original shape once the load is removed. When the material has been strained past the elastic region it becomes plastically deformed and will not recover its original shape. Yield strength, σ_y, is the point where plastic deformation starts to take place. It can be hard to specify precisely it but conventionally it is defined as the intersection of the curve with a straight line parallel to the elastic part of the curve offset 0.2% on the x-axis. In other words, the yield strength is the stress needed to permanently deform the material by 0.2%. The slope of the elastic part of the curve is called modulus of elasticity, E.

The ultimate tensile strength (UTS), or tensile strength, is the maximum stress reached during the test. When the material starts to reach that point the cross-sectional area where fracture will occur experiences reduction. Therefore, the original area of the sample cannot be used to model the true stress, σ_T, defined below [64].

$$\sigma_T = \frac{P}{A_{actual}} \tag{6}$$

For most metals it is possible to approximate the true stress - true strain (ϵ_T) curve between the yield stress and ultimate tensile stress using the equation defined below [64].

$$\sigma_T = K \, \epsilon_T^n \tag{7}$$

Where K and n are constants, which vary for each material.

35

The final value acquired from tensile test is the toughness of the material. Toughness describes the combination of strength and ductility and is the material's ability to absorb mechanical energy up to the point of failure. It is equal to the total area under the stress-strain curve [64].

$$U_T = \int_0^{\epsilon_f} \sigma d\epsilon \qquad (8)$$

Where U_T is toughness and ϵ_f strain upon failure.

2.4.2 Bending Tests

Bending tests, or flexure tests, are used for the characterization of weld joints when the bending ability of the joint is an important property, such as it is in this work. The most common bending test method is the three point bending test. Three point bending tests are conducted so that the bar to be tested is mounted on top of two cylinders, one under each end. A third cylinder then presses on top of the middle of the bar with a constant speed so that the bar starts to bend in the middle. The test is ended when either the bar has been fully bent to 180° or the joint fractures.
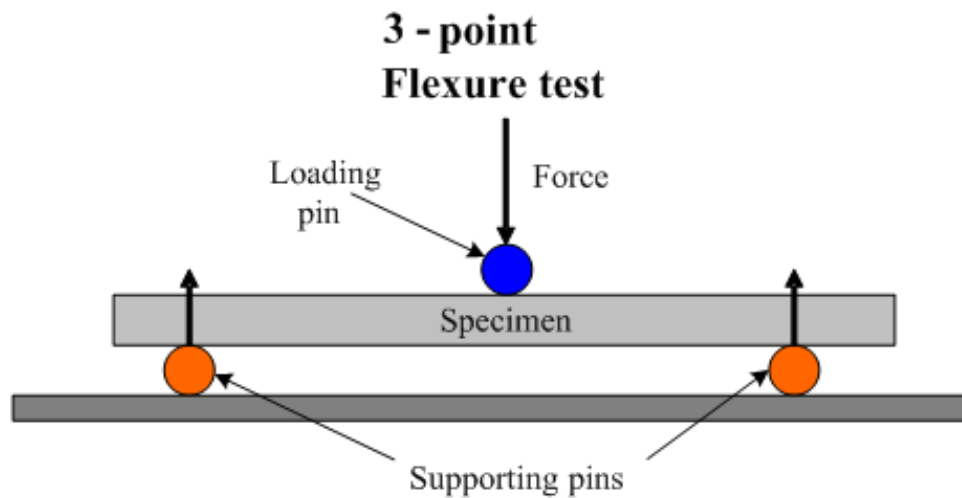

Figure 24 – 3-point flexure test [66]

The reason for conducting bending tests is to be able to determine the GEB of the welded joints. Thus, the important results from bending tests for this work is the maximum load on the loading pin, the displacement at maximum load and U_B, the energy consumed until the force lowers to a minimum specified load after the maximum load has been reached. The energy consumed is equal to the area under the bending stress-bending strain curve. Equations 8 and 9 below detail how the stress and strain in a 3-point flexure test is calculated.

$$\sigma_f = \frac{3FL}{2bd^2} \tag{9}$$

$$\epsilon_f = \frac{6Dd}{L^2} \tag{10}$$

Where σ_f is the flexural stress, F is the force, L is the length between the two supporting pins, b is the width of the specimen, d is the thickness of the specimen, ϵ_f is the flexural strain and D is the displacement of the specimen [67].

2.4.3 Electrical Resistance Tests

Accurately measuring low electric resistances can be difficult with traditional hand held instruments such as multimeters, which are rather used for high resistance values. When low resistances of joints are measured it is better to have a current flow through the joint and measure the voltage drop occurring over it. The resistance can then be calculated based on the voltage drop. This is known as four-terminal sensing.
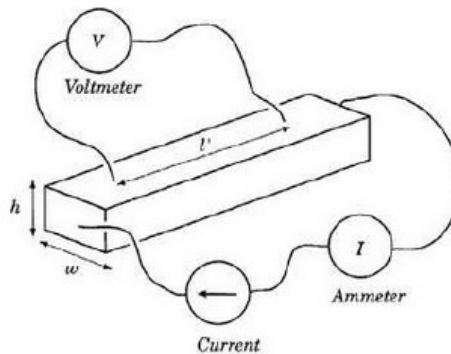

Figure 25 - Four-terminal sensing [68]

Four wires are attached to the bar, which is to be measured. Constant current is forced through the two outer wires while the voltmeter measures the voltage drop occurring between the two inner wires. The resistivity of the bar can then be calculated as follows [68].

$$\rho = \frac{Vwh}{Il^1} = \frac{Rwh}{l^1} \tag{11}$$

Where ρ is resistivity, V is the voltage difference measured, w is the width of the bar, h is the height of the bar, I is the current flowing through the bar, R is resistance and l^1 is the distance between the two wires measuring the voltage.

This is the operational principle of microhmmetres, which have been used to measure the resistance of Al-Cu joints in previous works [48]. To evaluate the resistance of the joint itself the total resistance from one side to the other is first measured. Then the base material contribution of resistance is subtracted to acquire the welds resistance.

$$R_{Joint} = R_{Measured} - \frac{1000(60 - l_a)\rho_{Cu}}{w_{Cu}h_{Cu}} - \frac{1000(l_b - 60)\rho_{Al}}{w_{Al}h_{Al}} \tag{12}$$

Where w and h are the widths and heights of each side of the weld and ρ is resistivity, l_a and l_b are explained in Figure 26. The equation is tuned to distances being measured in millimeters.
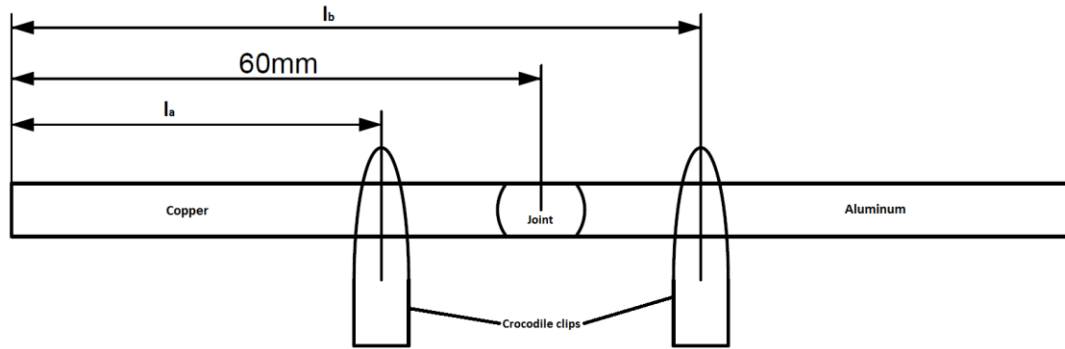

Figure 26 – Schematic of electrical resistance measurements

2.4.4 Hardness Tests

Hardness tests measure the resistance of a material to indentation. The hardness of a material is an indication of its strength. The test is conducted so that an indenter, made of a much harder material than the material to be tested, is pressed on the surface of the tested material with a certain force. Afterwards, the indentation is measured and the material's hardness has an inverse relation to the area of indentation [64].

There are a few different types of hardness tests, the most common ones being Brinell, Vickers and Rockewell hardness tests. During the course of this work Vickers hardness tests were used to characterize the hardness of both base materials and welds. Vickers hardness test uses a diamond pyramid indenter, which produces a pyramidal indentation.
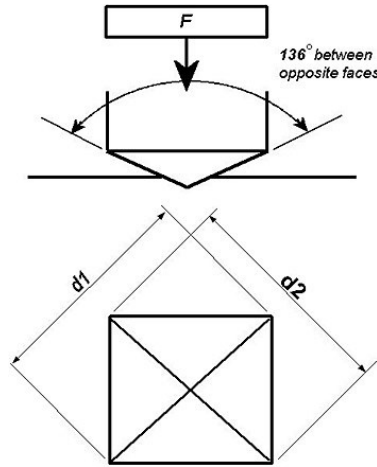
Figure 27 – Vickers hardness test [69]

The hardness is calculated after the indentation has been measured:

$$VHN = 1.72 \frac{F}{d_1 \cdot d_2} \qquad (13)$$

Where VHN is Vickers hardness number, F is the force of the indentation and d_1 and d_2 are the distances between opposite corners of the indentation [64].

2.5 Design of Experiments

In order to acquire valid results from a test program it is necessary to design it statistically. Statistical DoE gives unambiguous answers to important questions with minimal cost. It also allows for the measurement of experimental error, quantification of effects and gives insight into interactions of variables [70]. A common form of DoE is the factorial design, which can be used to investigate the effects of parameters in a process by testing all the possible combinations of the different levels of the parameters. When a process is governed by many different parameters, a factorial design becomes very time-consuming. Investigating such processes can be made more efficient by using other methods such as the Taguchi one.

2.5.1 Taguchi Method

The Taguchi method, developed by Dr. Genichi Taguchi, is a collection of methodologies that has become popular for designing experiments with the purpose of optimizing a set of control parameters of a process and is used in multiple industries [71]. The key variables of a process are studied and optimized in order to improve certain desired characteristics. The variables are investigated using an orthogonal set of experiments and the desired output is expressed as scalar functions to be optimized by the method [72]. The main benefit of the Taguchi method compared

to other DoEs is the usage of an orthogonal experimental set. This allows for much fewer number of experiments which makes the method both less expensive and more efficient than its alternatives.

There are three main concepts from Taguchi, which form the foundations of his methodologies [71]:

- Quality should be designed into the product and not inspected into it.

- Quality is best achieved by minimizing the deviation from a target. The product should be designed so that it is immune to uncontrollable environmental factors.

- The cost of quality should be measured as a function of deviation from the standard and the losses should be measured system-wide.

Traditionally, a product either meets certain design specifications or it doesn't. In production, this might result in products not being manufactured optimally, since as long as they meet the specification it satisfies the producer. Taguchi developed another way of depicting quality, which follows a parabolic function:

$$L = k(y - m)^2 \tag{14}$$

Where L is loss, k is a constant, y is the actual size of the product and m is the theoretical target value of mean value.

This way of thinking encourages companies to further improve their products, beyond just meeting the products' specifications.
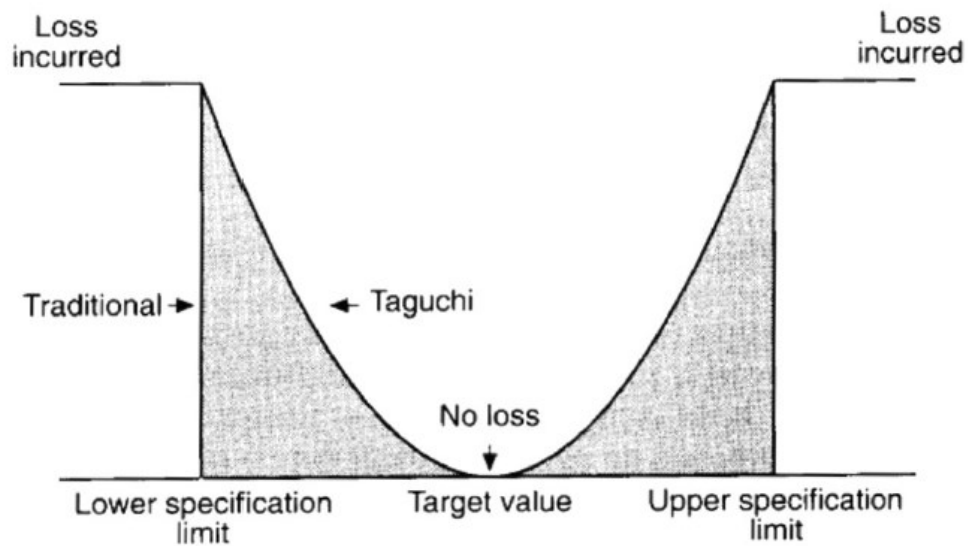

Figure 28 – Loss function, traditional and Taguchi's [73]

2.5.2 Taguchi Method Implementation

Implementation of the Taguchi method can be divided into eight steps [72]:

1. Identify the main function, side effects and failure mode
2. Identify the noise factors, testing conditions and quality characteristics
3. Identify the objective functions to be optimized
4. Identify the control factors and their levels
5. Select the orthogonal array matrix experiment
6. Conduct the matrix experiment
7. Analyze the data, predict the optimum levels and performance
8. Perform the verification experiment and plan the future action

Knowledge of the process that is to be optimized is needed before using the Taguchi method. What is the process, what are its side effects and how does it fail? Noise factors, which cannot be controlled such as room temperature and vibrations, should be identified as well as the testing conditions. The quality characteristics of the product must be selected and described as objective functions, which the Taguchi method seeks to optimize. There are three possible objective functions: Rated the best (e.g. dimension), higher the better (e.g. bending ability) and lower the better (e.g. cost). The control factors are also known as the process parameters. In FSW these are parameters such as rotational speed, travel speed and forging force to name a few. The minimum and maximum levels of these parameters should be selected so that the optimal levels are likely to fall within that interval and that the desired characteristics of the process results, when using those limits, can be measured.

Once the process itself has been detailed to fit the Taguchi method the set of experiments in the form of an orthogonal array matrix needs to be selected depending on the number of control factors and their levels. These experiments are then conducted and the desired characteristics measured from all the different results. The mean desired characteristics, mathematically expressed as performance parameters, resulting from each parameter level is extracted from the Taguchi experimental results. The process parameter levels giving the highest performance parameter results on average are identified and their average results are combined with the total means of each performance parameter in an algebraic model to calculate the optimum weld performance. ANOVA statistical analysis is then used to further interpret the results from the experiments using the Signal-to-Noise ratios (S/N) of the process output. ANOVA estimates the proportional contribution of the process parameters on the desired characteristics. Another algebraic model uses the proportional contribution of each process parameter and the highest performing process parameter levels on each process parameter to calculate the optimal process parameter levels [74].

The mathematical models mentioned here are further detailed in chapter 5, which covers how these methods are used in the optimization of process parameters for the FSW of Al-Cu butt joints.

3 Selection and Characterization of Base Materials

3.1 Introduction

Al bus bars are generally made of extruded 6000 series Al. Extruded Al alloys are subjected to multiple deformations during manufacturing that gives them tougher and stronger characteristics compared to chemically similar Al plates, which are rolled or laminated. Work-hardened alloys are more difficult to FSW and are generally not ideal for the mass manufacturing of long FSW bus bars because welding them one at a time would not only prove to be very slow but also a material wasting process.

During this work, a few different Al alloys were selected for characterization based on the wishes of Promeco Oy and ABB Drives Oy. These were extruded alloys and thus a similar rolled alloy was also chosen for characterization as it would prove to be a better choice for the mass manufacturing of bus bars while otherwise possessing similar characteristics important to the transmission of electricity such as low electric resistance. This chapter covers the characterization of the base materials chosen for the production of Al-Cu bus bars.

3.2 Material Selection

Three different Al alloys were selected for characterization: Extruded AA6060-T6, extruded EN-AW-6101-T4 and rolled AA1050-H14/H24. The first one was ordered and sent by Promeco Oy in the form of long bars, the second is the alloy of an Al bus bar, which was further investigated in chapter 7. The third one was chosen as it is a chemically similar alloy to the former two and is rolled as a plate. These three Al variants had their hardness tested. On the other hand, AA1050-H14/24 was the only Al tested for its bending and tensile strength as well as its electrical resistivity as it was the Al chosen for the optimization of weld parameters.

The Cu chosen is a high purity, oxygen free, non-phosphorus-deoxidized Cu alloy that does not contain any vacuum evaporating elements. Generally, it is simply known as oxygen free copper or Cu-OF. The particular variant used during this work was Cu-OF-04. The thickness of the two materials meant for bus bar production was chosen to be 6 mm.

3.3 Material Characterization

To be able to evaluate the properties of the weld joints the base materials need to be characterized and their properties documented to give a comparison. Knowing the initial composition and microstructure of the base materials helps in knowing their susceptibility to form IMCs, which should be minimized.

3.3.1 Hardness

The hardness of all the selected materials was tested using HV05 Vickers method. The Vickers hardness is measured by indenting the material using a pyramidal diamond indenter with a certain force. In the case of HV05, half a kilogram of force is used, which equals to 4.9 N. The hardness number is the determined by calculating the force-area ratio, using the area the

diamond indents into the base material. For every material, three surfaces were tested; the top surface, the longitudinal surface and the transversal surface. Conventional bus bar ends have a clamping area, which is flattened and thinner than the extruded part of the bus bar. Thus, both the extruded and the flattened parts had their hardness investigated. Nine tests were made for each sample and the indentations made so that they formed a square as can be seen below from Figure 29. Table 7 shows the measured hardness of each material's three surfaces.
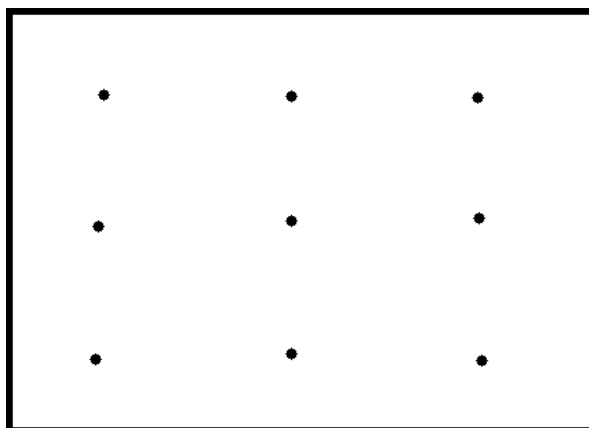
Figure 29 – Hardness indentations for base materials

Table 7 - Vicker's microhardness of the selected materials

Material	Top surface	Longitudinal surface	Transversal surface
Cu-OF-04	87.1 ± 3.4	90.2 ± 4.0	86.7 ± 1.7
AA6060-T6	70.8 ± 1.5	69.4 ± 1.3	69.7 ± 5.5
AA1050 H14/H24	39.5 ± 1.0	39.3 ± 3.0	39.7 ± 1.2
EN-AW-6101-T4	60.6 ± 2.5	58.2 ± 2.9	59.3 ± 1.0
EN-AW-6101-T4 (Flattened)	92.3 ± 4.2	90.1 ± 3.8	87.6 ± 5.5

As can be seen in the table above, AA6060-T6 is the hardest as-formed Al. EN-AW-6101-T4 is softer, but once its end has been flattened, the hardness increases and exceeds the hardness of AA6060-T6. Interestingly, the hardness of the flattened bus bar material is similar to that of Cu-OF-04.

3.3.2 Tensile Strength

To be able to evaluate the tensile strength of the final weld joint it is important to be able to compare it to the tensile strength of the base materials that compose the joint. Thus, the tensile strengths of AA1050-H14/24 and Cu-OF-04 were investigated.

Both the longitudinal (extrusion or rolling direction) and transversal tensile strengths were tested, three tests for each direction. The sample sizes for the Al and longitudinal direction of the Cu were the same, a standard sized tensile strength test specimen with a neck length of 65 mm. Because the width of the Cu bar is only 60 mm, a smaller specimen had to be made to test the transversal tensile strength of the Cu. Figure 30 shows the dimensions of the specimens.
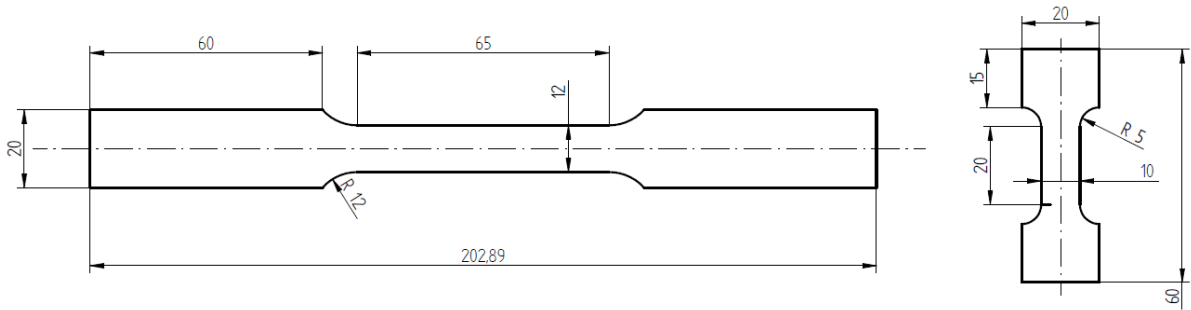
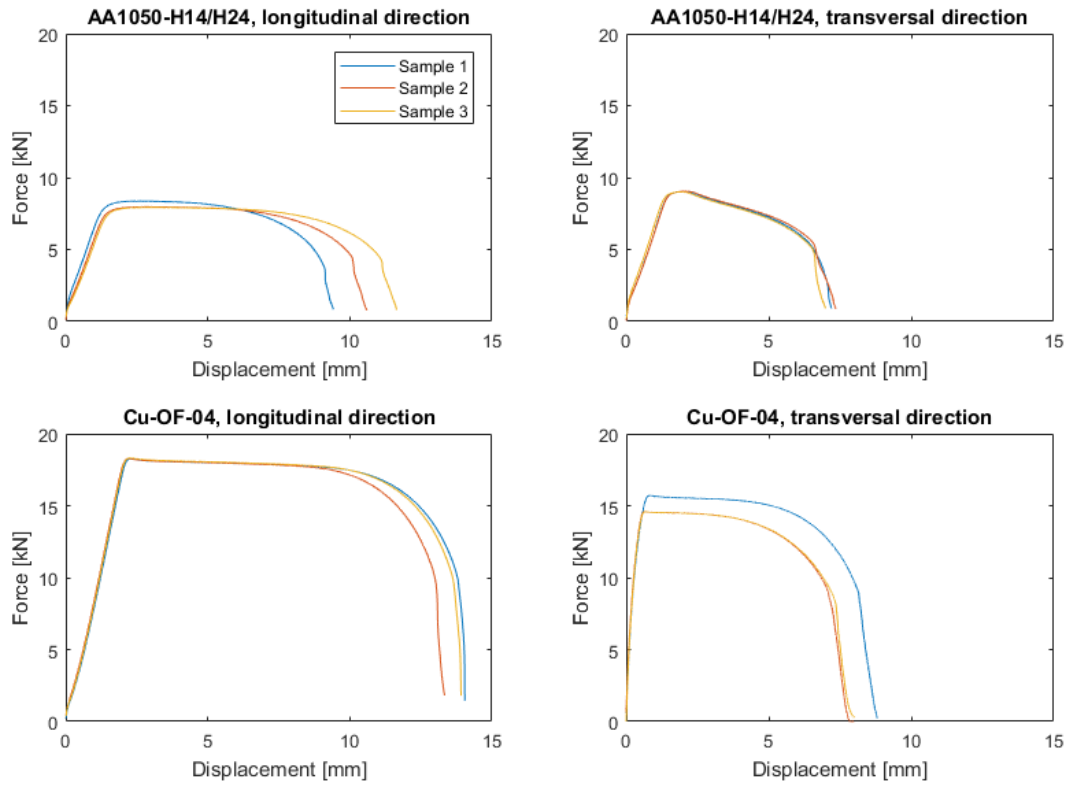Figure 30 – Tensile test specimen drawings for base materials

Figure 31 – Force-displacement graphs for all base material tensile tests

44

Due to the small length of the transversal Cu specimens, it was not possible to mount an extensometer on them. Therefore, the tensile test results are more limited for it. The transversal directional AA1050-H14/24 sample also had problems of necking occurring outside of the extensometer. Figure 31 shows the raw force-displacement data from the tensile tests. In Figure 32 are the main results of the base material tensile tests. Some values are empty for some materials due to the problems in testing mentioned here.
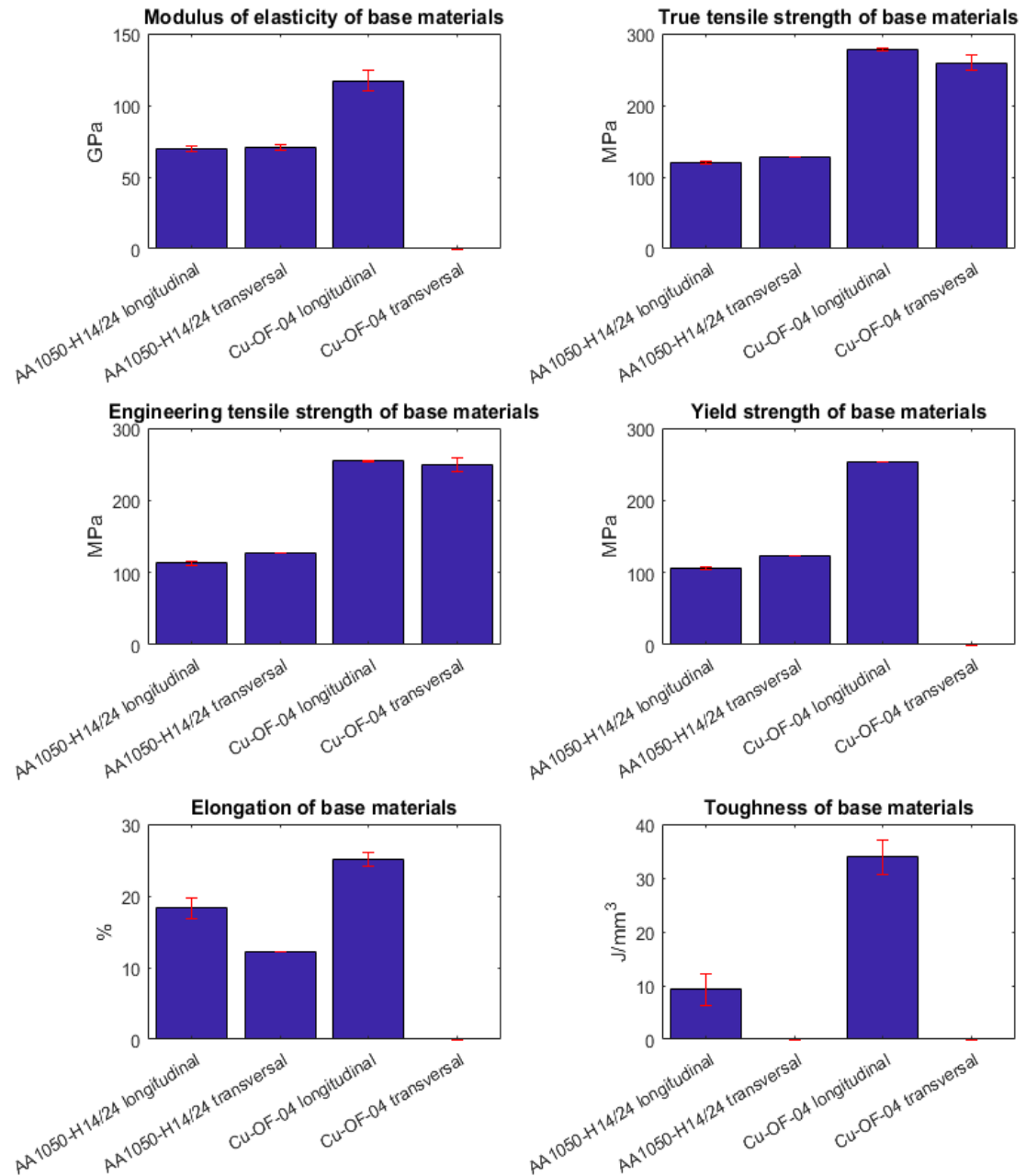
Figure 32 – Base materials tensile test results detailing the 6 different tensile properties

3.3.3 Bending Strength

Three longitudinal samples were machined and tested for each base material, AA1050-H14/24 and Cu-OF-04. Three-point bending tests were made using MTS 810 material test system. The width of each specimen was 20 mm and the distance between the supporting rollers was 78 mm. All specimens bent fully and no cracks were observed on their surfaces.
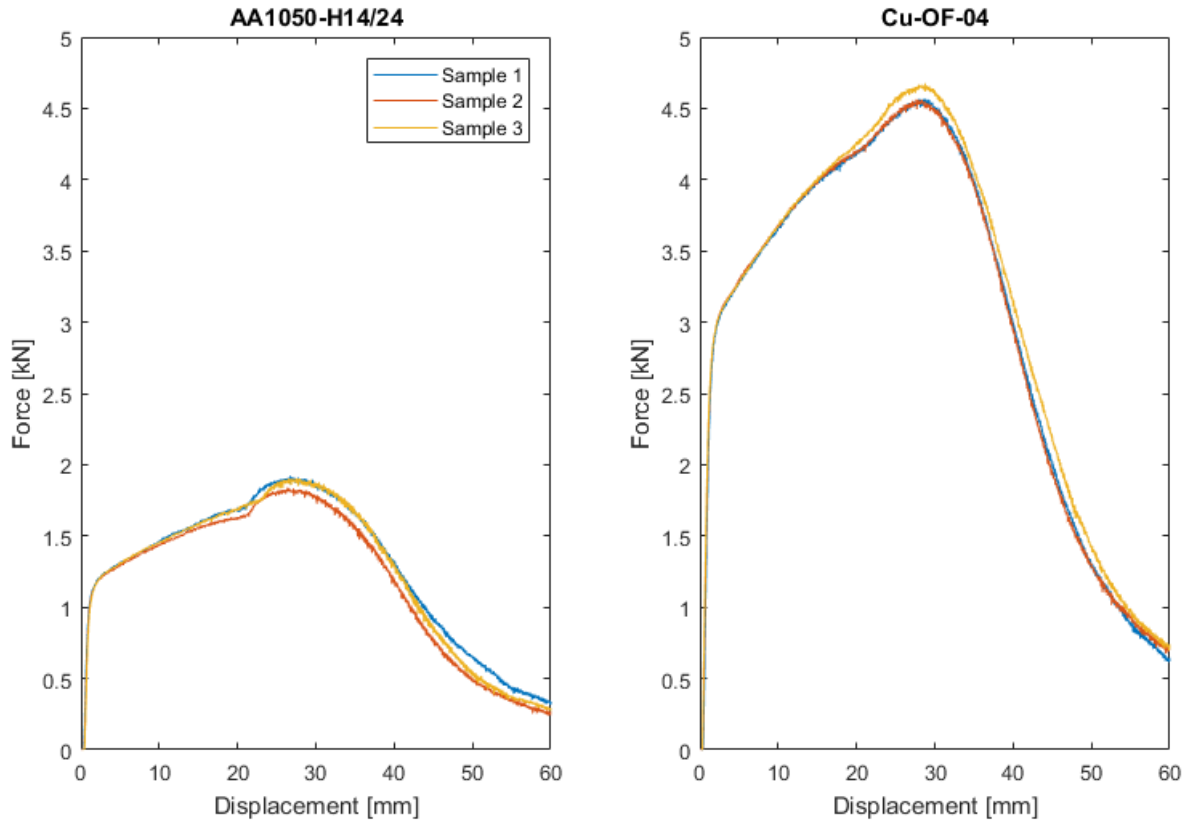

Figure 33 – Bending test force-displacement graphs for base materials

Based on the force-displacement graphs, three characterizing values were extracted or calculated. These values are maximum force, F, displacement at maximum force, d, and the energy consumed until a minimum specified load is reached after the maximum load is exceeded, U_B. The minimum specified load was chosen to be the equal to the maximum force. The results from the bending tests can be seen from Figure 34.
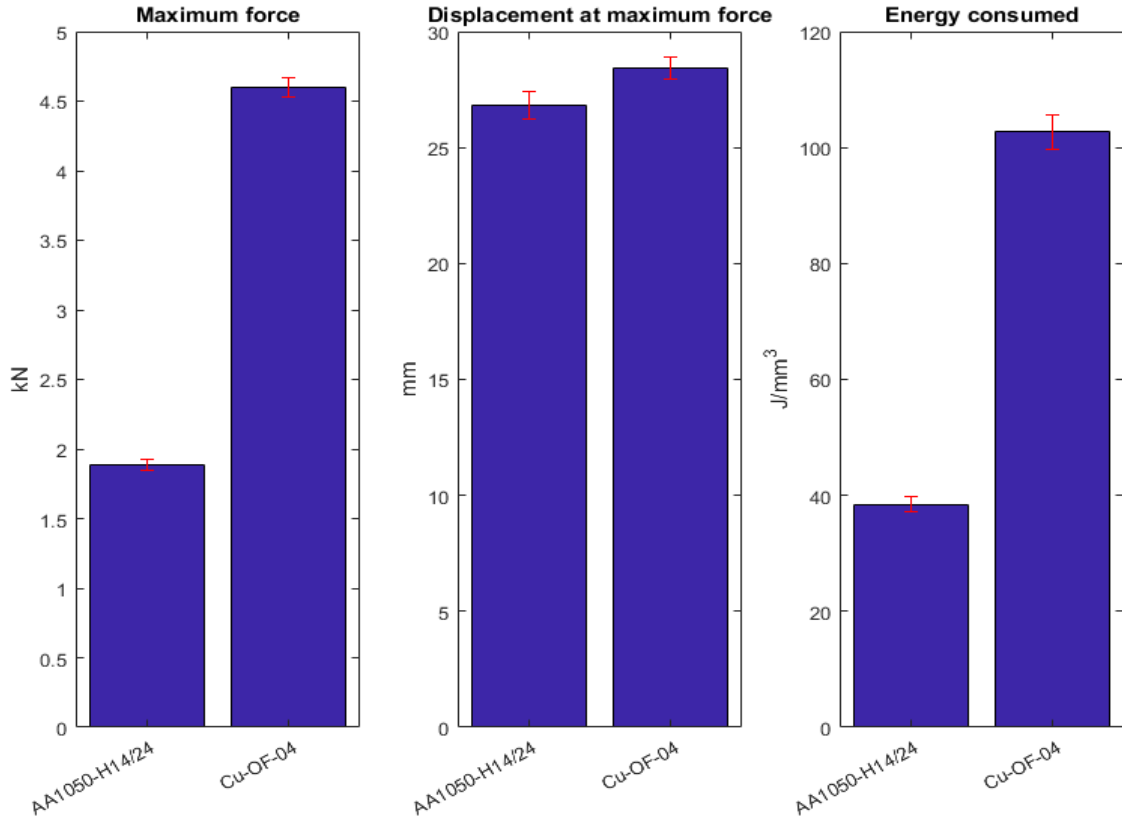
Figure 34 – Bending characteristics of base materials

3.3.4 Electrical Resistivity

The base materials, AA1050-H14/24 and Cu-OF-04, were cut into small bar samples for electric resistance measurements. Two samples were measured for each material using Cropico D07 microhmmeter. The device measures electrical resistance using 4-terminal sensing principle and returns the absolute resistance between two crocodile clips which are attached to the sample being measured.
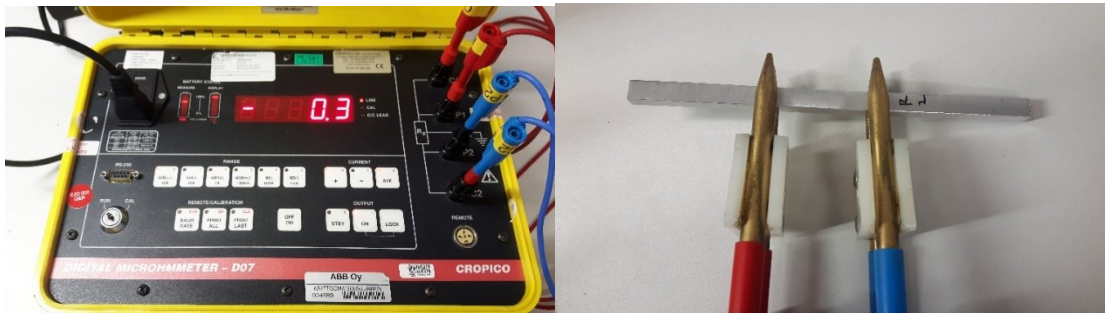

Figure 35 – Cropico D07 digital microhmmeter & an Al sample being measured

The width and height of the bars was measured as well as the distances, l_a and l_b, from one end of the bars to the center of each crocodile clip. Thus, the resistivity of the base materials could be calculated using equation (11). The error of the distance measurements was evaluated to be 0.1 mm.

Table 8 – Measured variables for evaluating the resistivity of the base materials

Sample	Width [mm]	Height [mm]	l_a [mm]	l_b [mm]	R [μΩ]
Cu-1	4.95	5.95	44.5	77.8	20.5
Cu-2	4.99	5.98	38.3	74.5	22.0
Al-1	5.06	5.95	44.6	73.6	29.3
Al-2	5.00	5.95	46.5	80.4	33.6

Table 9 – Resistivity of base materials

Material	Cu-OF-04	AA1050-H14/24
Resitivity [Ω·m]	0.0181 ± 0,0001	0.03 ± 0,0007

In addition to measuring the electrical resistivity of the base materials themselves, the contact resistance between them was also measured using varying contact forces. The base material samples were cut into smaller pieces and their ends milled. Then they were clamped together using a small vice and the resistance over the contact measured for low, medium and high forces. The lowest force was so that the samples would stay in place but could easily be moved by hand. Medium force was so that the samples could not be moved by hand and high force was when the vice was tightened as much as possible. Three samples of each material were measured for each varying force and the resulting contact resistance can be seen in Table 10. The contact resistance is the total resistance measured subtracted by the resistance contribution of the materials themselves.

Table 10 – Contact resistance between base materials

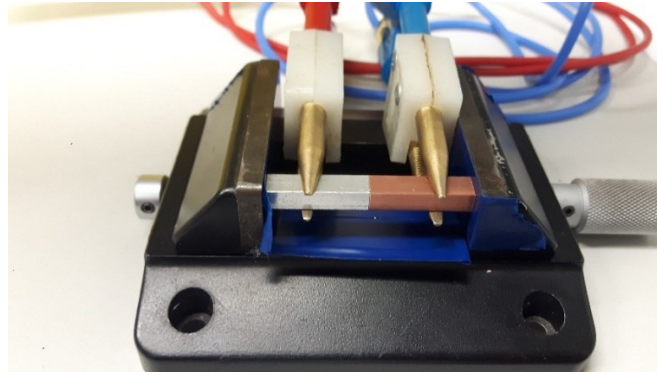| Force	Contact resistance [μΩ]
Low	8000 ± 2000
Medium	340 ± 30
High	110 ± 30

Figure 36 – Contact resistance between base materials being measured

The contact resistance is highly dependent on the contact force between the material, especially when low force is compared to a medium one. This is due to the increase in contact spots between the materials, which correlates with the increase in force [75]. These measurements were made in order to have a comparison for the resistance of the dissimilar FSW joints, which is a subject of chapter 6.

3.3.5 Metallurgical Features

The metallurgical features of the base materials, AA1050-H14/24 and Cu-OF-04, were investigated using an optical microscope. Both materials are close to being pure, with negligible amount of alloying particles. The structure of the Al plate stays homogeneous within the sample but as the Cu is extruded, there is a difference in the grain structure within the cross-section of the bar from which the sample was taken.
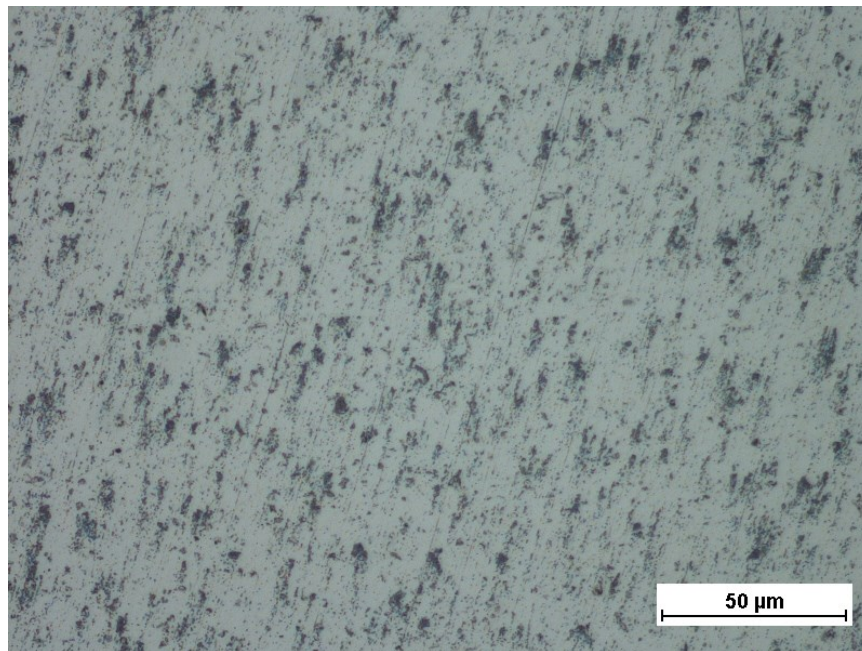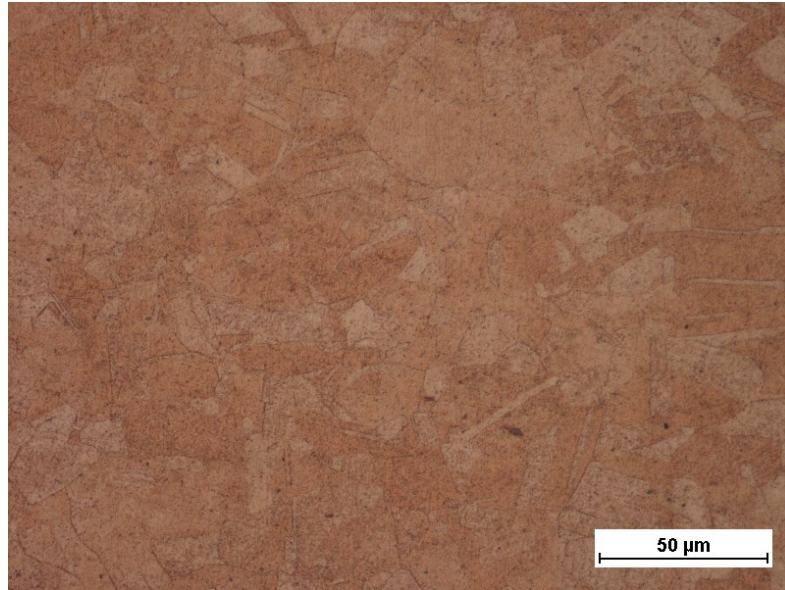

Figure 37 – AA1050-H14/24 microscopic image

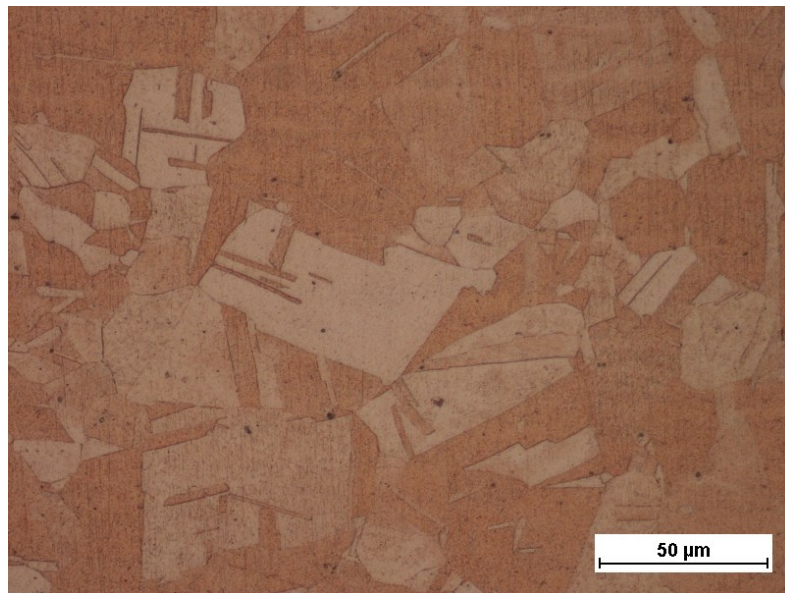Figure 38 – Cu-OF-04 grains at one end of the cross-sectional sample

Figure 39 - Cu-OF-04 grains in the middle of the cross-sectional sample

As can be seen from Figure 38 and Figure 39 the grain structure of the Cu varies within the extruded cross-section. At the middle of the cross-sectional sample, the grains are large and can be seen clearly. This is not the case at the end, where the grains are on average much smaller. This kind of change in the microstructure was not detected in the Al. This is due to the difference in the manufacturing process of the materials. The Al, being rolled, is not subject to the high forces and deformation the Cu experiences when the extruded bar is made straight after extrusion and therefore the grain structure remains more stable within the sample compared to the Cu.

50

4 Development of Tooling for FSW

4.1 Introduction

A considerate part of the work is the tool design. The tool material and geometry is vital to the success of the weld and the tools need to be customized and designed to fit the application. Finding the suitable manufacturer is also vital as heat treatment and material strengthening greatly influences the final properties of the tools. Few companies have the expertise of making durable and reliable FSW tools that can withstand the high forces of the process for an extended period without wearing out and failing.

In addition to designing and ordering the manufacturing of conventional FSW tools, a SSFSW tool module was designed and manufactured at Aalto University. The module was designed to be attached to the university's ESAB Legio FSW machine.

This chapter details the design and manufacturing of conventional FSW tools and an SSFSW tool module. The conventional tools were further used in subsequent chapters for the optimization of weld process parameters. The SSFSW tool module was designed and manufactured but not tested during the work of this thesis.

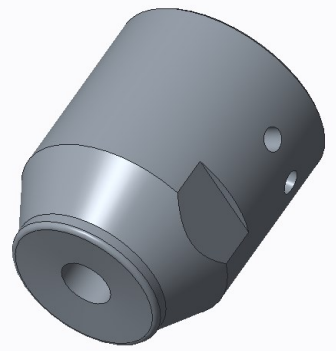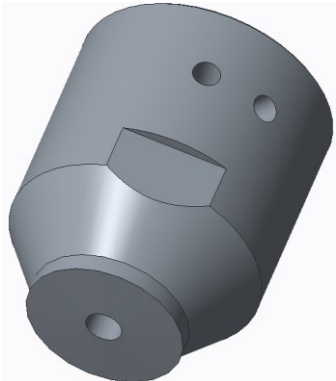## 4.2 Design and Manufacturing of Conventional FSW Tools

The tools were designed for a modular tool holder, which holds a shoulder and a probe. This probe holder was already designed by a colleague in the department and was available for use. The designed tool geometries were based on geometries found in dissimilar Al-Cu FSW research works.

Tools were designed to fit three different base material thicknesses: 6, 8 and 10 mm. After designing multiple potential geometries, four probe designs and five shoulder designs were chosen and sent to manufacturing. H13 tool steel was chosen as the tool material. Preliminary welds had been made using H13 tool steel tools and it proved to be strong enough to withstand the application. The tools were machined, quenched, tempered and surface hardened using ionic nitration by João Luís in Portugal, a machinist experienced in the manufacturing of FSW tools.

The inner diameter of a shoulder is the same as the major diameter of probes intended for usage with that particular shoulder and other shoulders having the same inner diameter. It was decided after consulting with Pedro Vilaça that the inner diameters of the shoulders would be equal to the thicknesses of the materials their usage was intended for. Thus, tools were designed with 3 different sizes, A, B and C mm inner diameter shoulders along with matching probes. It was decided that for 6 mm thickness, more variable geometries would be designed for testing as the project's focus had been set on the welding of 6 mm thick base materials. For the larger diameter tools only concave shoulders, threaded probes and threaded probes with scrolls were made. These designs were also made for A mm diameter tools but additionally convex, convex scrolled, and two flat scrolled shoulders were designed and ordered for that particular diameter as well as flat taper and threaded taper probes with flutes. As the outer

diameter of shoulders has considerable effect on the heat input of the weld process, two sizes of concave shoulders were designed and ordered for each intended probe diameter. Most tool geometries were based on geometries found in previous Al-Cu FSW works apart from the fluted probes and convex shoulders. The intended purpose of the fluted probe design is similar to the scrolled one, which is to be able to break up the base material oxide layers to create new chemically active surfaces that produce better bonding between the welded materials. Table 11 details the shape, diameters and geometric details of the ordered shoulders as well as showing an illustration of the designs' general shapes. Table 12 shows the shape, major and minor diameters, length of welding geometry, other geometric details and illustrations of the ordered probes.

Table 11 - Shoulder designs chosen for manufacturing

Shape	External diameter	Internal diameter	Geometric details	Illustration
Concave	D1 D2 D3 D4 D5 D6	A A B B C C	N/A	
Convex	D7	A	N/A	
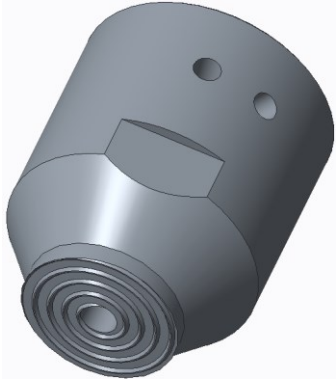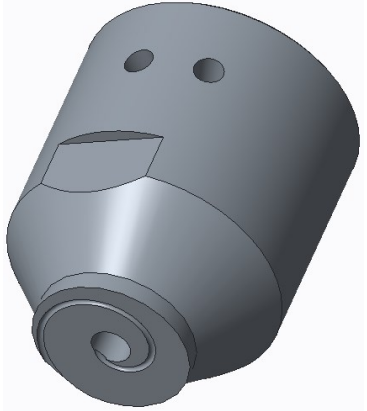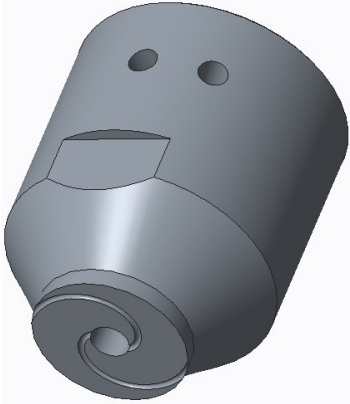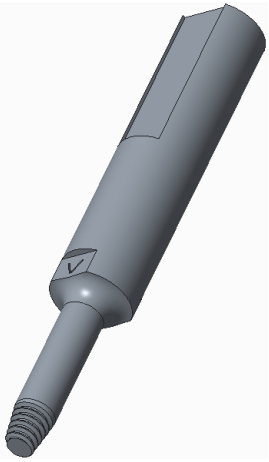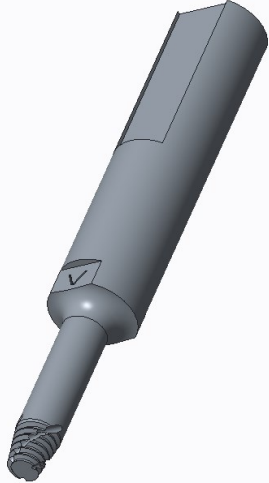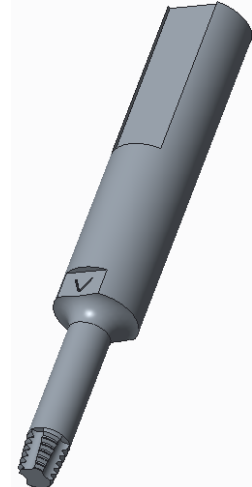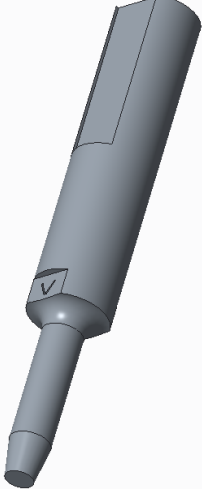
Convex with one positive scroll	D8	A	N/A	
Flat with one negative scroll	D9	A	N/A	
Flat with two negative scrolls	D10	A	N/A	

Table 12 - Probe designs chosen for manufacturing

Shape	Major diameter	Minor diameter	Probe length	Geometrical details	Illustration
Threaded taper	A B C	E F G	H I J	N/A	
Threaded taper with scrolls	A B C	E F G	H I J	N/A	
Threaded taper with flutes	A	E	H	N/A	

Flat taper	A	E	H		

After having received the tools from manufacturing they were tested for their surface hardness. The back surface of a single shoulder was polished. Then its hardness was tested using HV30 indentations. The material had average hardness of 683 HV. This equals to 57.9 Rockwell C hardness, which is above the range of tempered H13 tool steels (38-53 Rockwell C hardness) [76]. The surface hardening had therefore increased the material's hardness considerably.

Figure 40 – Manufactured conventional FSW shoulders and probes

Afterwards, several welds were made to test different tool geometries. The concave shoulders immediately performed very well, which was to be expected since it is the shoulder design mostly used in Al-Cu FSW research. Other shoulder designs did not show the same potential and were therefore not used more throughout the course of this work. Two probe designs, threaded taper and threaded taper with scrolls, gave the best results for the probe designs tested. The threaded taper one was selected for the optimization of the weld parameters as its geometry is simpler and more conventional than the other's is.

4.3   Design and Manufacturing of a Stationary Shoulder Tool Module

As previously stated, a Stationary Shoulder Friction Stir Welding (SSFSW) tool module was designed and manufactured during the process of this work. Stationary shoulders are a recent advancement in FSW technology and is highly desired in Aalto's material joining lab. Promeco Oy's FSW machine is similar in design as Aalto University's, although their machine has more limited attachment capacities. The design was made based on certain specifications and the concept was highly influenced by Beckman and Sundström's design. It was decided, to keep cost down, that the whole module would be manufactured inside Aalto University.

4.3.1 Design Specifications and Concept

First, design specifications were compiled together as detailed in Table 13.

Table 13 – Stationary shoulder design specification

Design specifications
Attachable to Aalto's ESAB Legio FSW machine
Able to withstand up to 1500 RPM operational rotational speeds
Capable of producing long welds
Able to easily force the shoulder down from the probe after operation
Deflection while in operation < 0.1 mm
Width of shoulder ≤ 60 mm

The ESAB Legio FSW machine has slots and threaded holes on the three free sides above the spindle, which are intended to be used with attachable equipment. The module needed to be designed to be mounted there. FSW rotational speeds sometimes go up to 2000 RPM, which can be very demanding for bearings. Such high rotational speeds are not common so it was deemed acceptable for the design to be operational under 1500 RPM as otherwise it would require larger and more expensive bearings. A cooling channel close to the bearing was deemed necessary to be able to produce long welds. During FSW, material, especially Al, tends to stick to the tool and enter cavities between the probe and shoulder. This can cause the shoulder and probe to be difficult to separate, as the sticky material bonds them together and therefore it was specified that the design would allow the shoulder to be easily forced away from the probe. Deflection of the module needed to be kept at minimum to protect the bearing and probe and thus deflections under 0.1 mm were deemed acceptable. The width of the shoulder needed to be equal or less than 60 mm to be able to operate with the clamping system used for the course of this thesis.

A few different concepts were explored and in the end the most promising one chosen. The concept is made up of five main parts; 2 arms for mounting the module to the machine, a

shoulder that attaches to the arms, a probe holder, which holds the probe and is mounted to the spindle, and a probe. The following 3 figures display the final design of the module. Bill of Material (BOM) tables are also presented to explain the figures.
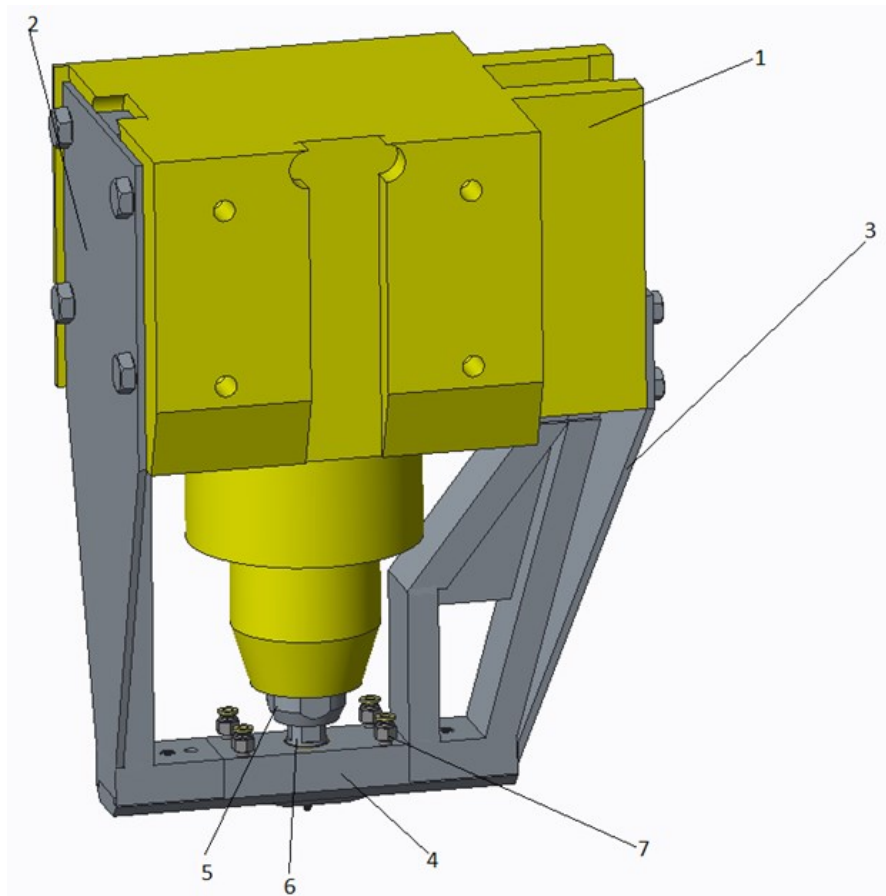
Figure 41 – SSFSW tool module Design overview

Table 14 – Overview BOM

Part no.	Part name
1	ESAB Legio FSW Machine
2	Left arm
3	Right arm
4	Shoulder
5	Probe holder
6	Probe
7	Cooling channel's quick connector
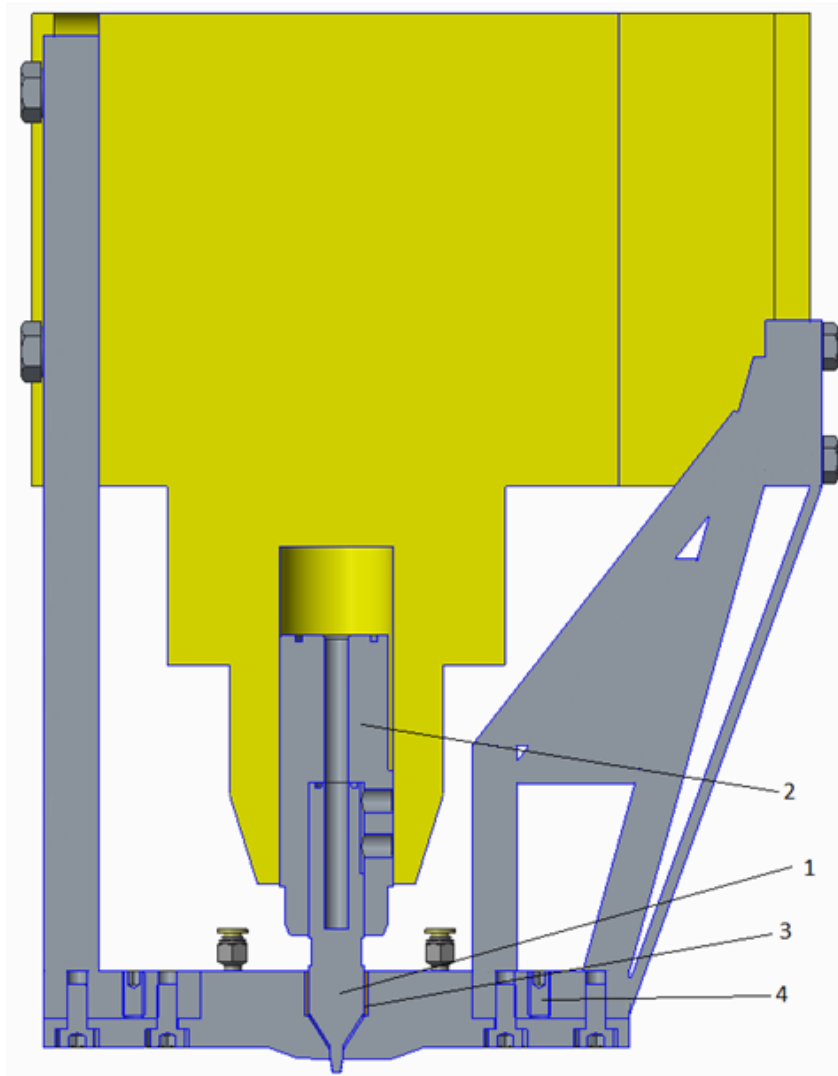
Figure 42 – A cross-section of the SSFSW tool module design

Table 15 – Cross-sectional BOM

Part no.	Part name
1	Probe
2	Probe holder
3	Sliding bearing
4	Extraction bolt

Figure 43 – A cross-section of a single cooling channel in the SSFSW tool module design

Table 16 – Cooling channel cross-sectional BOM

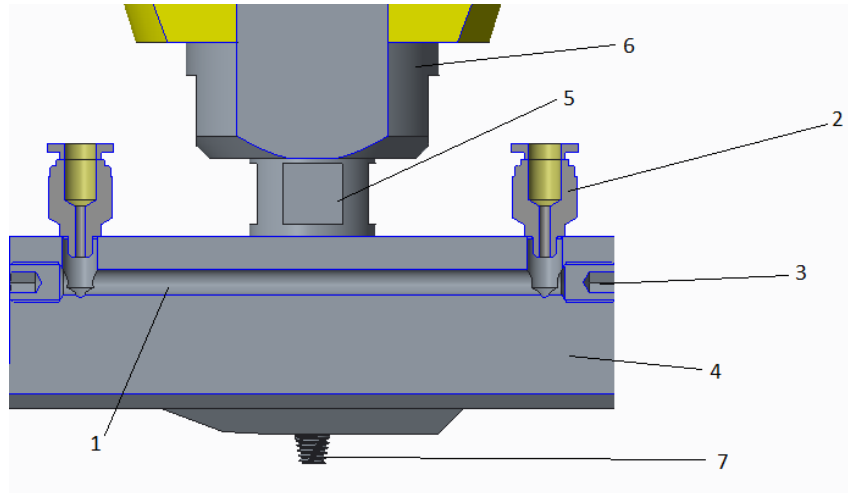| Part no.	Part name
1	Cooling channel
2	Quick-connector
3	Channel tap bolt
4	Shoulder
5	Probe
6	Probe holder
7	Probe end

All parts were designed to be fully machined except the arms, which were designed to be first welded and then machined, as they are too large to be fully machined cheaply. The tool module design was made to meet its specifications and the general design met all of them except for the deflection of the shoulder and the ability to operate using high rotational speeds, which both needed to be calculated. The deflection was evaluated using Finite Element Method (FEM) analysis and the arms were redesigned and optimized so that they would meet the design's specifications. The bearing's ability to withstand high rotational speed and forces during operation was evaluated using Lagermetall's online bearing calculator, but their EX3M slide bearing is the toughest one available on the market and was chosen as the sliding bearing for the tool module.

Lagermetall's online calculator calculates the PV-value, which is the product of the average contact pressure and sliding velocity, the bearing experiences based on the dimensions of the bearing, rotational speed and force. The force acting on the bearing was estimated to be 2kN at maximum. Using that force value, 1500 RPM rotational speed and the inner diameter and length of the bearing, the PV-value was calculated to be 7.85 N/mm² · m/s. This is lower than the

maximum recommended PV-value of the bearing, which is 9.6 N/mm$^2 \cdot$ m/s. The ordered bearing has diamond shape pockets on the sliding surface that hold grease, as the SSFSW module was not designed to include a grease pocket. The diamond pockets allow for the module to be re-lubricated after a certain amount of time. The frequency of lubrication needs to be determined by testing the module.

4.3.2 FEM Analysis

An FEM analysis was used to calculate the expected deflection of the module when in operation. The analysis was made so that both mounting surfaces of the arms were constricted and the load was defined to act on the bottom surface of the shoulder. After consulting with Pedro Vilaça the maximum forces acting on the shoulder during operation were estimated to be less than 20 kN in the z-direction and 10 kN in the x-direction, given that the materials to be welded are in the xy-plane. These values were used during the FEM analysis. Initial design, seen in Figure 45, was deemed insufficiently rigid and was therefore changed by adding a second load carrying bar and 2 stiffening plates, seen in Figure 46. After improvement the FEM analysis showed a maximum deflection under 0.1 mm which met the design specifications. It is to be noted that the coordination system in the FEM figures is wrong, y is z.
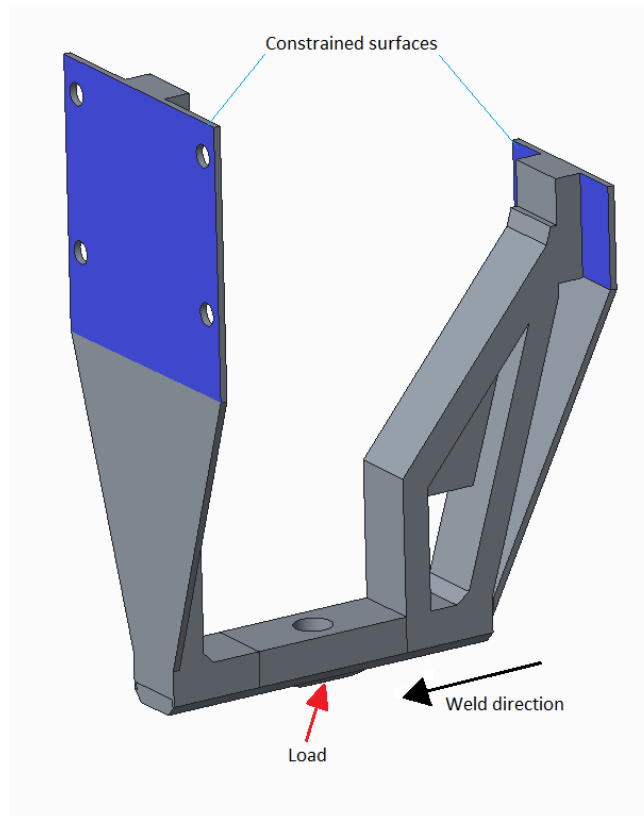
Figure 44 – Load direction and constrained surfaces used for FEM analysis
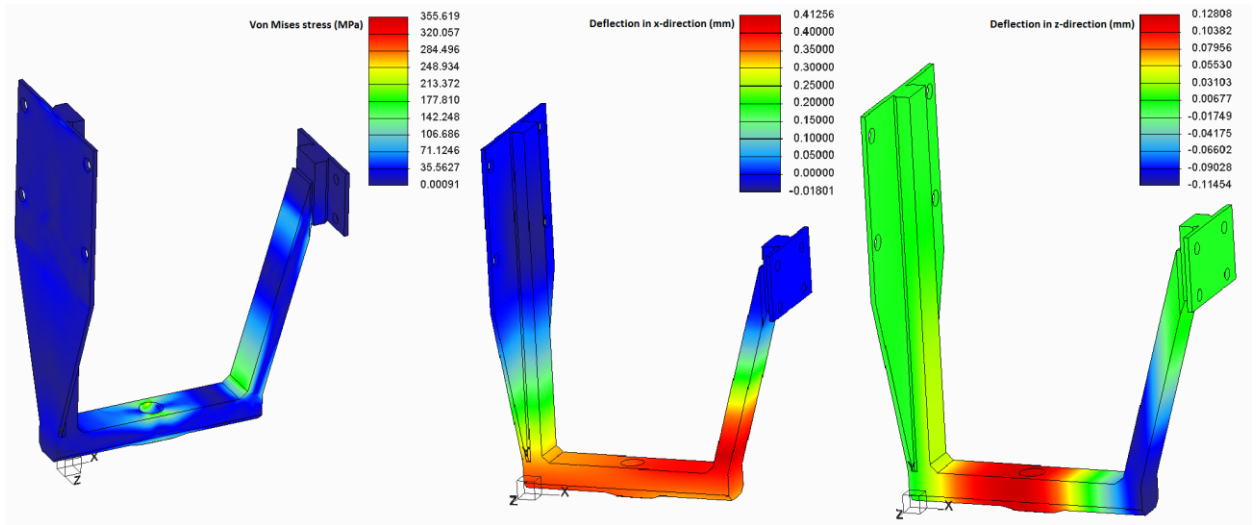
Figure 45 – FEM analysis before improvements of structural rigidity
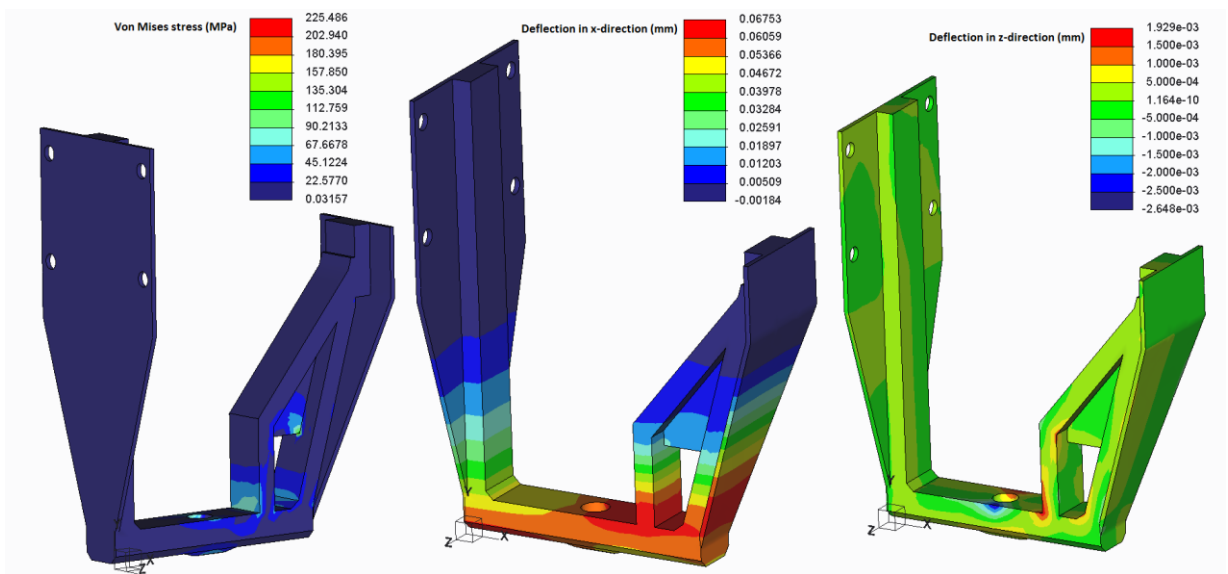
Figure 46 – FEM analysis after improvements of structural rigidity

Clear difference in structural rigidity of the two different arm designs is seen in Figure 45 and Figure 46. After changing the design of the right arm from a single bar to a more complex structure with two stiffening plates for both planar directions, the maximum x-deflection is reduced from 0.413 mm to 0.068 mm. Similarly, the z-deflection is reduced from 0.128 mm to 0.0019 mm. This allows for the module to meet its specifications of a maximum deflection of 0.1 mm.

4.3.3 Manufacturing

First, plates and bars were cut, machined and welded together into the general shape of the arms. The material chosen for the arms was structural steel. Afterwards, the arms were machined; the mounting holes, slots and threaded holes for the shoulder made. Meanwhile, the probe holder and probe were turned. The materials for the probe holder was H13 tool steel while the probe itself was turned from a QRO 90 Supreme steel rod from Uddeholm. The shoulder was then machined, everything except the hole for the probe. The hole was made after the arms and shoulder had been mounted on the FSW machine so that the actual center of the probe could be determined. Due to potential distortion, resulting from the welding of the arms, it was decided to position the hole for the probe in that way. The shoulder was machined from structural steel. After every part had been fully machined, the arms and parts of the shoulder were painted black. The assembled tool module can be seen below.

Figure 47 – The SSFSW tool module assembled on Aalto University's ESAB Legio FSW machine

5 Optimization of FSW Process Parameters

5.1 Introduction

To acquire process parameters sufficient for the production of Al-Cu bus bars they were optimized based on the Taguchi DoE method, which was conducted as described in chapter 2.5.2. Nine welds were made with statistically varying parameters using B major diameter threaded taper probe and a corresponding D3 diameter concave shoulder. The ØB probe was chosen even though the base material thickness was 6 mm because the smaller ØA probes proved to be unfit for manufacturing conditions as they tended to break after few welds. GETS, GEB and the conductivity efficiency of the joints were chosen as main functions while travel speed, tool plunge (weld position) and offset into the Al were chosen as the variable parameters to be optimized. This chapter details the optimization of FSW process parameters for 6 mm thick AA1050-H14/24 – Cu-OF-04 butt joints.

5.2 Performance Parameters

To assess the performance of the dissimilar Al-Cu FSW joints, three performance parameters were used: GETS, GEB and the conductivity efficiency (σ_{eff}). An emphasis was put on the ductility of the joints over their strength and so the performance parameters are as follows:

$$GETS = 0.05 \frac{E_i}{E_{BM}} + 0.2 \frac{\sigma_{y\_i}}{\sigma_{y\_BM}} + 0.2 \frac{\sigma_{UTS\_i}}{\sigma_{UTS\_BM}} + 0.25 \frac{A_i}{A_{BM}} + 0.3 \frac{U_{T\_i}}{U_{T\_BM}} \qquad (15)$$

$$GEB = 0.4 \frac{F_i}{F_{BM}} + 0.3 \frac{d_i}{d_{BM}} + 0.3 \frac{U_{B\_i}}{U_{B\_BM}} \qquad (16)$$

$$\sigma_{eff} = \frac{R_{Al} + R_{Cu}}{R_{Al} + R_{Cu} + R_{Joint}} \qquad (17)$$

The equations for GETS, GEB, R_{Joint}, R_{Al} and R_{Cu} were explained in chapter 2.4. For the equations above, the performance parameters scale from 0 to 1 and the quality of the joint is better when the value of the parameters is closer to 1.

5.3 Establishment of Test Matrix and Process Parameter Levels

The parameters to be optimized and their levels were chosen after multiple preliminary welds. The major parameters chosen for optimization were travel speed, weld position and offset into the Al as previously stated. The parameters used for the DoE optimization and their levels can be seen in Table 17.

Table 17 – Constant and variable parameters and their levels chosen for DoE optimization

Parameters	Symbol	Level 1	Level 2	Level 3
Variable parameters				
Travel speed [mm/min]	A	80	120	160
Weld position [mm]	B	N/A	N/A	N/A
Offset into Al [mm]	C	0	1	2
Constant parameters				
Rotational speed [RPM]	800			
Tool geometry	ØB threaded taper probe + ØD3 concave shoulder			
Clamping condition	Manually clamped – 25 mm from weld line for both materials			
Machine tilt [degrees]	2			
Probe length [mm]	N/A			
Dwell time [s]	5			
Acceleration length [mm]	20			

There are many orthogonal arrays available when using the Taguchi method and each array is to be used with specific number of variable parameters and levels. For 3 variable parameters with 3 levels each the corresponding orthogonal array is the so called L9 one. It is meant for understanding 4 different variable parameters with 3 levels each but can also be used with 3 different parameters, one column simply has to be eliminated. As there are 3 parameters with 3 levels each the total degrees of freedom is 26 and there are 27 possible parameter combinations. This is the number of tests that need to be made if a full factorial DoE method is being used but because the Taguchi test array is orthogonal it is possible to extract the effect of each variable parameter using only 9 tests [77].

Table 18 – L9 orthogonal array

Test no.	Parameters			
	A	B	C	D
1	1	1	1	1
2	1	2	2	2
3	1	3	3	3
4	2	1	2	3
5	2	2	3	1
6	2	3	1	2
7	3	1	3	2
8	3	2	1	3
9	3	3	2	1

With only three parameters one of the columns, D, can be eliminated and afterwards the table can be completed by filling in the parameters and their levels.

Table 19 – DoE test matrix

Test no.	Parameters		
	Travel speed	Weld position	Tool offset
1	80 mm/min	N/A	0 mm
2	80 mm/min	N/A	1 mm
3	80 mm/min	N/A	2 mm
4	120 mm/min	N/A	1 mm
5	120 mm/min	N/A	2 mm
6	120 mm/min	N/A	0 mm
7	160 mm/min	N/A	2 mm
8	160 mm/min	N/A	0 mm
9	160 mm/min	N/A	1 mm

5.4   FSW Procedure

To have accurate results from the DoE welds it is important to have all welds made under the exact same circumstances so that no extra noise skews the results. A certain procedure was followed for each weld after the FSW tool was assembled. This procedure is detailed in Table 20.

Table 20 – DoE weld procedure

| Step no.	Action
1	Mark a point on top of the Al plate where the FSW tool will plunge into, considering the offset of the weld.
2	Clamp the base materials using the Cu clamps and steel plate anvil. Place the ends of the Cu clamps 25 mm away from the joint line. Both base materials shall have the dimensions of 250x60mm.
3	Drill a hole where the tool will plunge using a ØB drill.
4	Insert the tool into the FSW spindle, tighten the O-ring seal by pressing the tool into a plastic block and then turn liquid cooling on.
5	Zero the FSW tool's z-position onto the Cu, 10 mm from the joint line, using 5kN force.
6	Set the offset by first centering the middle of the probe over the joint line and then increase the distance into the Al by the required offset.
7	Move the tool towards the end spot of the weld to make sure that there is not a noticeable change in offset throughout the weld.
8	FSW the base materials together, weld length should be 200 mm.
9	Save the log-file of the weld to a USB drive for future analysis.
10	Clean the tool using a lathe.
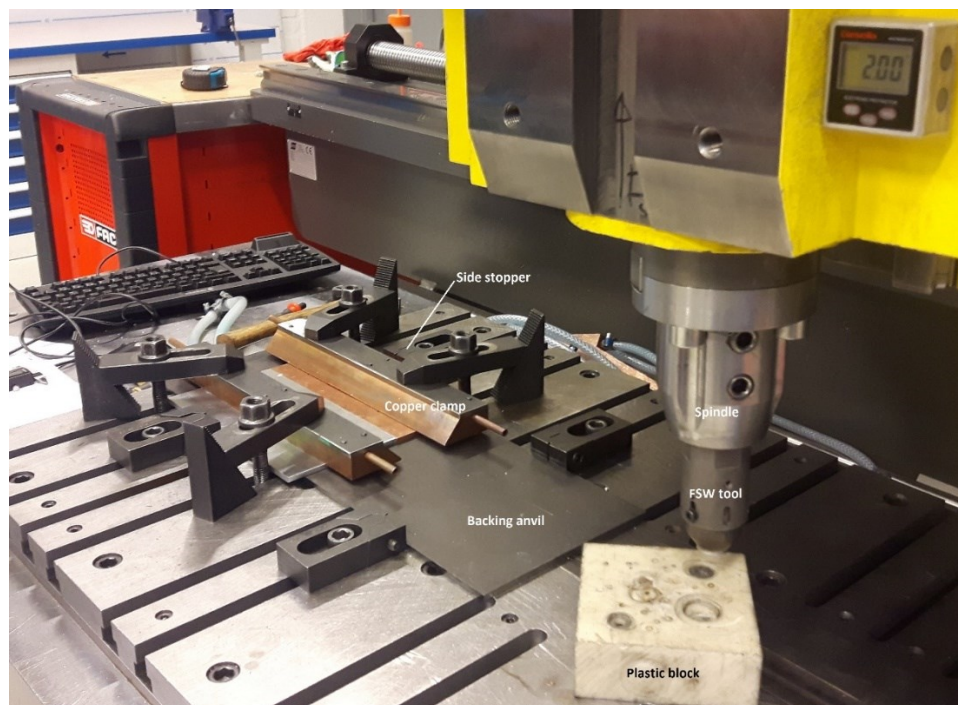
Figure 48 – DoE weld setup

The materials were clamped using Cu clamps which have the option of being liquid cooled, although cooling was not used for these welds, and side stoppers that prevent the base materials from separating when the tool plunges into the joint line. A 6 mm thick high strength steel plate was used as a backing anvil. All welds were made during the same day. The weld setup for the DoE welds can be seen in Figure 48.

As it is quite difficult and time-consuming to fully clean the FSW tool between welds, which makes it economically inefficient in production, all the welds were made with a "dirty" probe but a clean shoulder, which is much easier to clean. A preliminary weld was made before the first DoE weld in order to make the probe dirty so that all welds would be made under the same conditions. Figure 49 further explains the difference between a clean and a dirty tool.

Figure 49 – An unused probe and clean shoulder vs. shoulder and probe filled with sticky Al

5.4.1 Clamping system

A very important factor for FSW is the clamping system used for the process. It is vital to the success of the weld that the base materials are thoroughly clamped so that they stay completely still during the process. Insufficient clamping can cause multiple problems. The materials can rise around the area the welding force acts on, preventing the root side of the weld from staying flat. This occurs when the clamping force is either not close enough to the joint line or is simply too low. This problem occurs much more seldom if a hole is drilled where the probe will plunge. When welding butt joints it can be important to use side stoppers to prevent the materials from sliding away from each other when the tool is plunging into them. This is certainly the case in Al-Cu FSW.

For all welds done during the work of this thesis a certain clamping system was used, seen in Figure 50. The system is composed of 2 Cu clamping bars, a steel backing anvil, 4 clamps and 2 side stoppers. Clamping was made so that the edges of the Cu clamping bars were 25 mm from the joint line. The start position of each weld (the red circle) and the advancing and retreating sides are also marked on the figure.
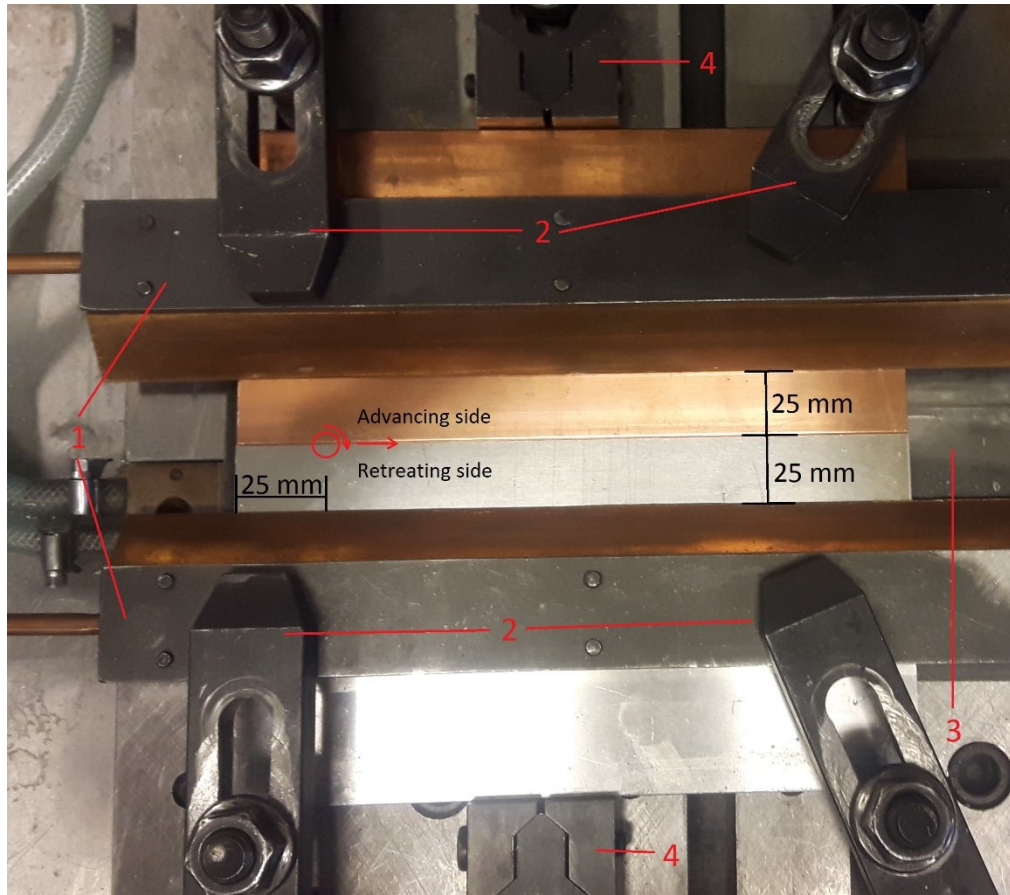
Figure 50 – Clamping system setup and weld direction for all welds made during this work

Table 21 – Clamping parts seen in Figure 50

Part no.	Part name
1	Cu clamping bars
2	Steel clamps
3	Backing anvil
4	Side stoppers

5.4.2 Surface Characterization and Specimen Extraction Plan

After all 9 welds had been made their surface characteristics were analyzed and then they were cut into tensile, bending and electric resistance specimens as detailed in Figure 52. The surface characterization was fully observational. The top surfaces of the welds were inspected to characterize their flash, concavity, width regularity and striade regularity. The roots of the welds were also inspected to characterize the flatness, uniformity and evidence of joining of the welds.
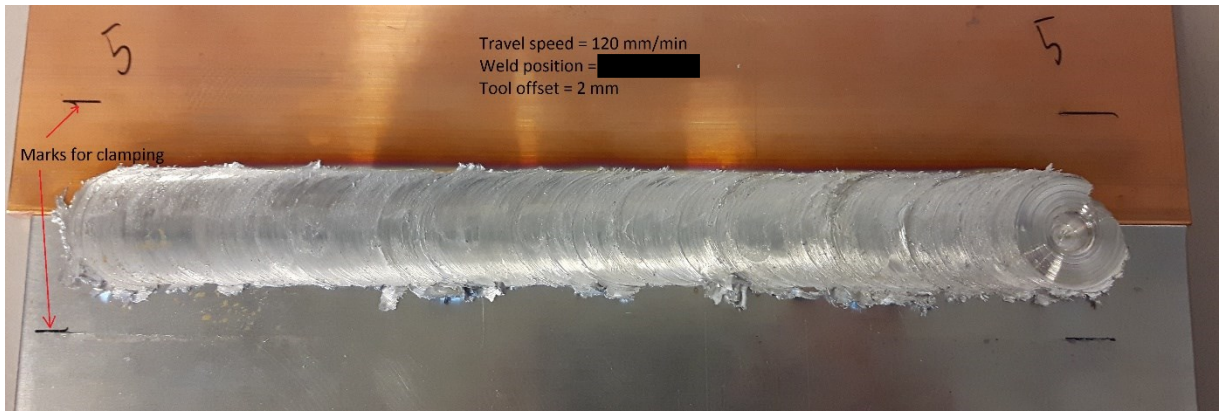
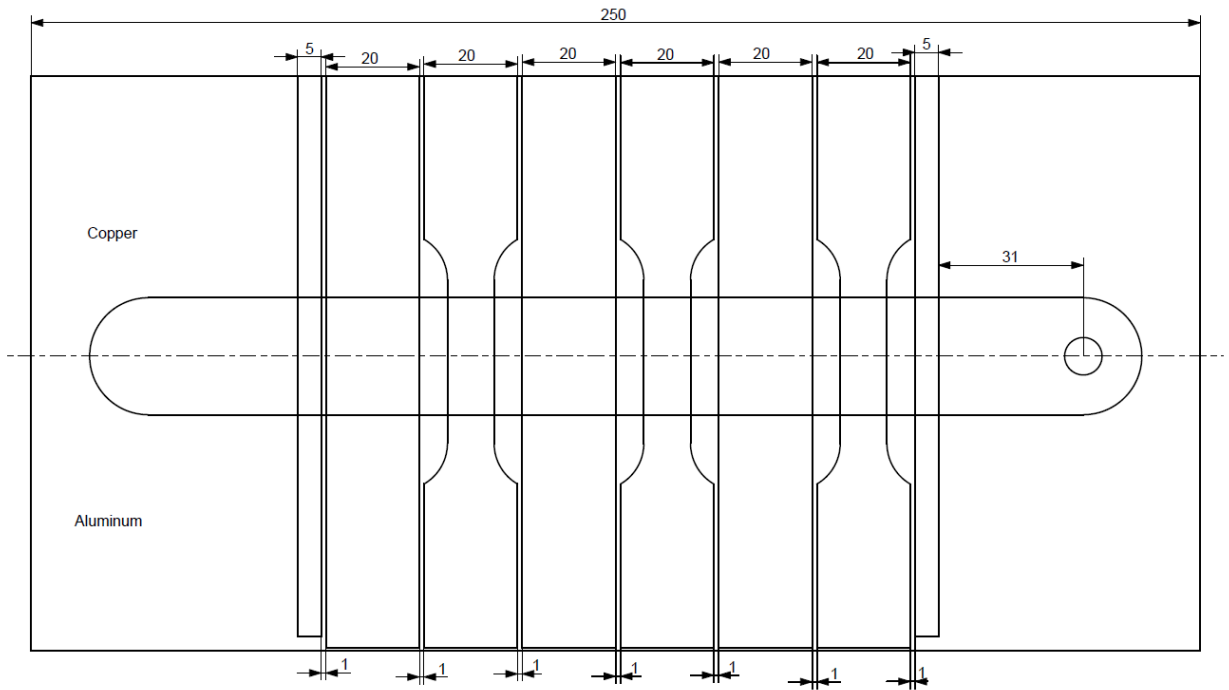Figure 51 – Visual surface analysis of the most aesthetically pleasing DoE weld, weld no. 5

Figure 52 – Extraction plan for mechanical and electrical specimens used for weld characterization

Table 22 – Surface characterization of DoE welds

Weld no.	Face of the weld													Root of the weld						Observations
	Flash			Type of flash		Removal of flash		Width regularity		Striade regularity		Concavity		Flatness		Evidence of joining		Uniformity		
	None	Little	Significant	Continuous	Granular	Easy	Difficult	Regular	Variable	Semi-Regular	Variable	Minimal	Significant	Flat	Irregular	Apparent	Dubious	Regular	Variable	
1		X			X	X		X			X	X		X		X			X	Surface crack
2		X			X		X		X		X	X		X		X			X	Surface cracks
3		X			X		X	X			X	X		X		X			X	Surface and root cracks
4		X			X	X		X		X		X		X		X		X		
5		X			X	X		X		X		X		X		X		X		
6			X	X		X			X		X		X	X		X			X	Surface and root defects
7		X			X	X		X		X		X		X		X		X		
8		X			X	X		X			X	X		X		X			X	Surface and root defects
9		X		X			X	X			X	X		X		X			X	Root defects

70

5.5 Performance of the DoE Welds

After the welds had been analyzed and their performance parameters calculated the effect of each process parameter on the performance parameters could be evaluated. Table 23 presents the variable parameters and the experimental results for the GETS, GEB and σ_{eff} of each weld.

Table 23 – Experimental results for DoE welds

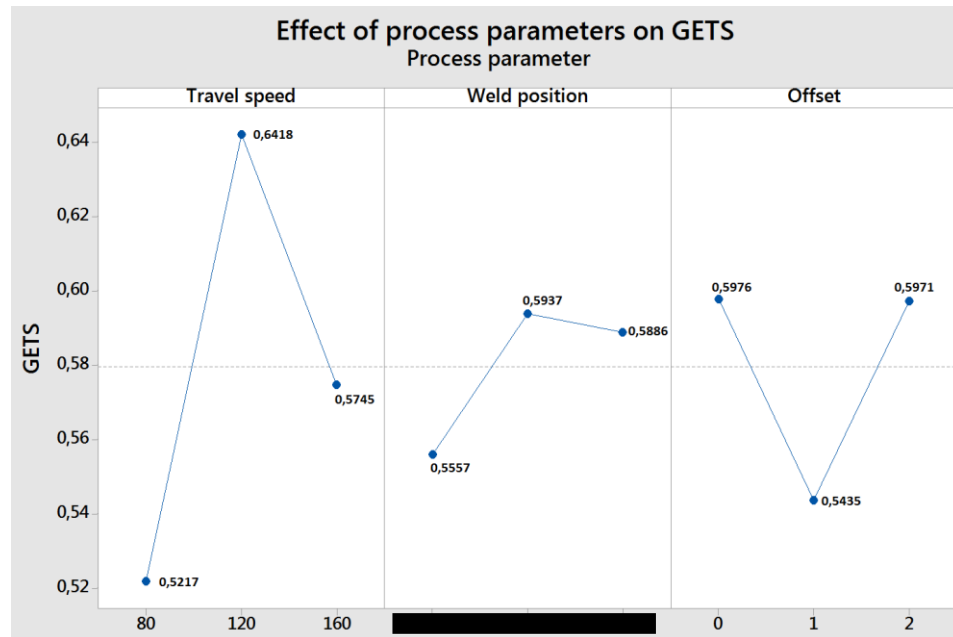| Test no. | Parameters | | | GETS | GEB | σ_{eff} |
	Travel speed [mm/min]	Weld position [mm]	Offset into Al [mm]			
1	80	N/A	0	0.629	0.559	0.887
2	80	N/A	1	0.473	0.252	0.947
3	80	N/A	2	0.463	0.255	0.863
4	120	N/A	1	0.562	0.375	0.929
5	120	N/A	2	0.753	0.468	0.967
6	120	N/A	0	0.610	0.167	0.863
7	160	N/A	2	0.575	0.259	0.912
8	160	N/A	0	0.554	0.222	0.935
9	160	N/A	1	0.595	0.248	0.945

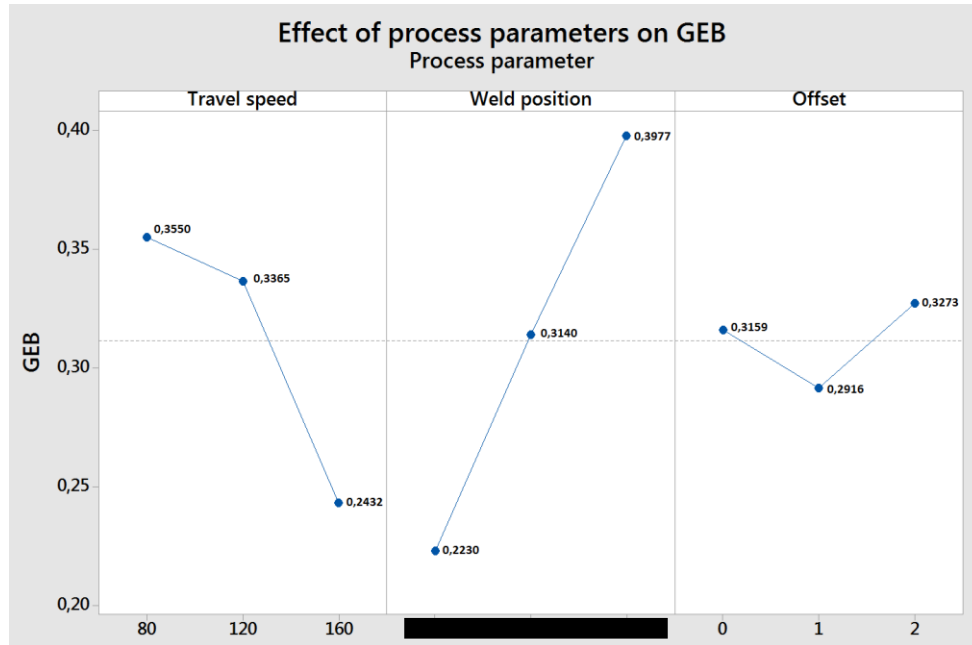

Figure 53 – Effect of process parameters on GETS

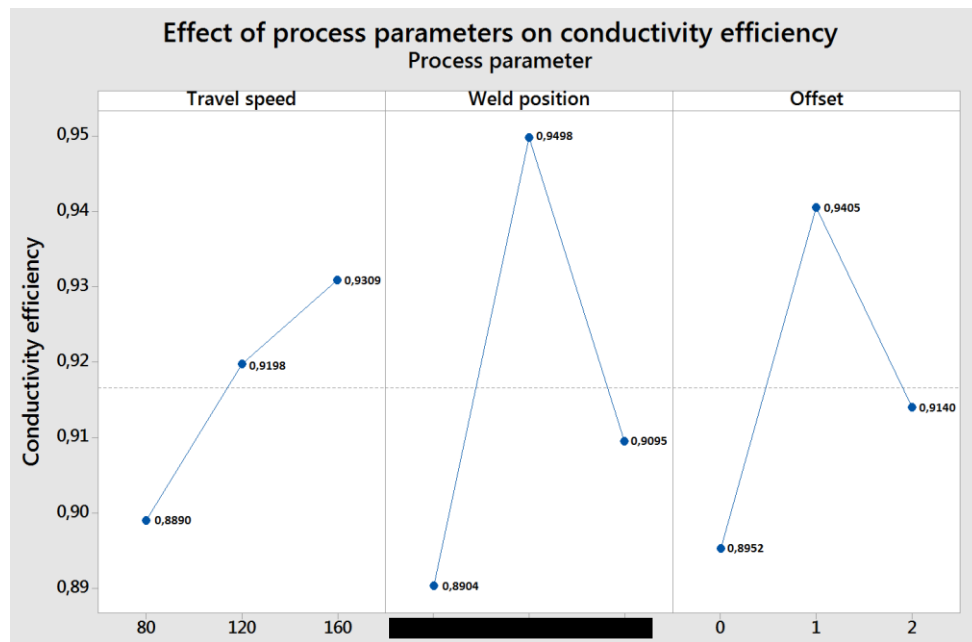Figure 54 – Effect of process parameters on GEB

Figure 55 – Effect of process parameters on conductivity efficiency

It can be seen from the three previous figures that the variable parameters have different effects on different performance parameters. A medium level travel speed results in high GETS performance of the weld while low speed increases the GEB and high speeds increase the electrical conductivity efficiency. High speeds form thinner IMC layers which could explain

better conductive characteristics for higher travel speeds while lower speeds soften the base materials, which promotes better bendability of the joint area. Similarly, the different mixing characteristics caused by the offset might explain why the conductive efficiency is highest for a medium offset while the mechanical performance parameters prefer either a high or a low level offset.

5.6   Analysis of Variance

Analysis of Variance (ANOVA) is used to find out how significantly each process parameter affects each quality characteristic. The proportional contribution each process parameter has on the quality characteristics can be calculated using ANOVA. This is accomplished by separating the total variability of the Signal-to-Noise (S/N) ratios, which is measured by the sum of the squared deviations from the total mean S/N ratio, into contributions by each of the design parameters and the error. The total sum of the squared deviations, SS_T, can be calculated using equation (18) [78]:

$$SS_T = \sum_{i=1}^{n} (Y_i - Y_m)^2 \tag{18}$$

Where n is the number of experiments, 9 in this case, Y_i is the experimental results for test i. Y_m is presented in equation (19) below.

$$Y_m = \frac{1}{n} \sum_{i=1}^{n} Y_i \tag{19}$$

SS_T can be divided into two parts: the sum of SS_P, the squared deviations of each process parameter, and the sum of the squared error SS_e. Equation (20) presents how SS_P is calculated.

$$SS_P = \sum_{j=1}^{r} \frac{(SY_j)^2}{r} - \frac{1}{n} \left[\sum_{i=1}^{n} Y_i \right]^2 \tag{20}$$

Where one of the parameters is represented by P and j is the level of that parameter, r is the number of repetition which is 1 here and SY_j is the experimental result sum of the experiments that include parameter P and level j. SS_e can then be calculated using equation (21).

$$SS_e = SS_T - SS_A - SS_B - SS_C \tag{21}$$

Where SS_{A-C} are the square deviation sums for parameters A, B and C.

Then the total number of Degrees of Freedom (DoF) is determined for both the total number of tests and for each tested parameter. The DoF for the total number of tests is calculated by simply subtracting 1 from the total number of tests, so in this case the total DoF is 8. Similarly, for each tested parameter the DoF is calculated by subtracting 1 from the total number of factors, so in this case the DoF for each parameter is 2. The F-value, F_P, for each parameter and the proportional contribution of each parameter, ρ_P, are then calculated using equations (22) and (23):

$$\rho_P = \frac{SS_p}{SS_T} \tag{22}$$

$$F_P = \frac{V_P}{V_e} \tag{23}$$

Where V_P is the mean of squares deviations and V_e is the mean of the squared errors.

Using equations (18)-(23) the ANOVA for all three performance parameters was calculated.

Table 24 – ANOVA results for GETS

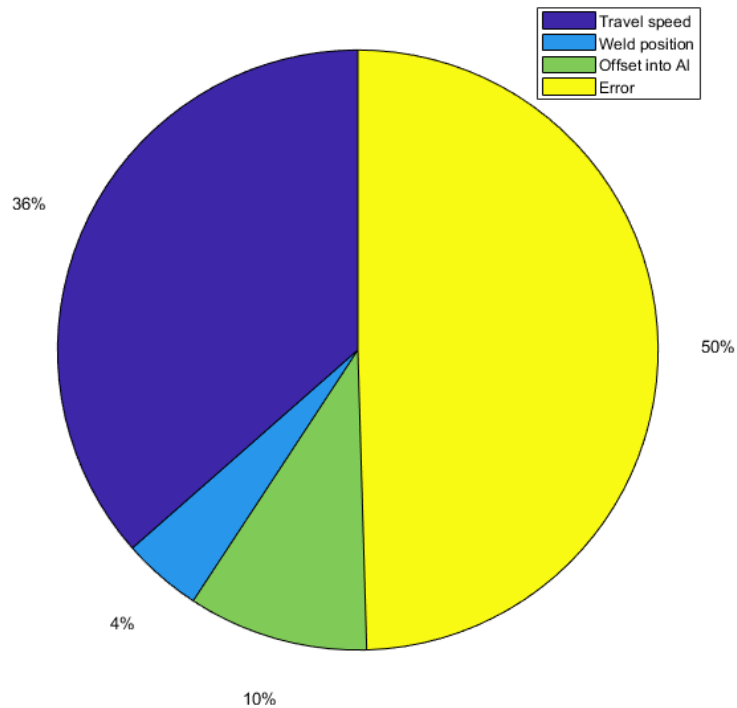| Factors	DoF	Sum of squares	Mean square	F-ratio	Contribution [%]
A	2	0.02175	0.01087	0.736616	36.48
B	2	0.00255	0.00128	0.086406	4.28
C	2	0.00579	0.00290	0.196148	9.71
Error	2	0.02953	0.01476		49.53
Total	8	0.05962	0.02981		100.00

Figure 56 – Proportional contribution of each parameter on GETS

Table 25 – ANOVA results for GEB

Factors	DoF	Sum of squares	Mean square	F-ratio	Contribution [%]
A	2	0.02155	0.01077	0.343844	16.33
B	2	0.04579	0.02289	0.730592	34.69
C	2	0.00199	0.00099	0.031729	1.51
Error	2	0.06267	0.03134		47.48
Total	8	0.13200	0.06600		100.00

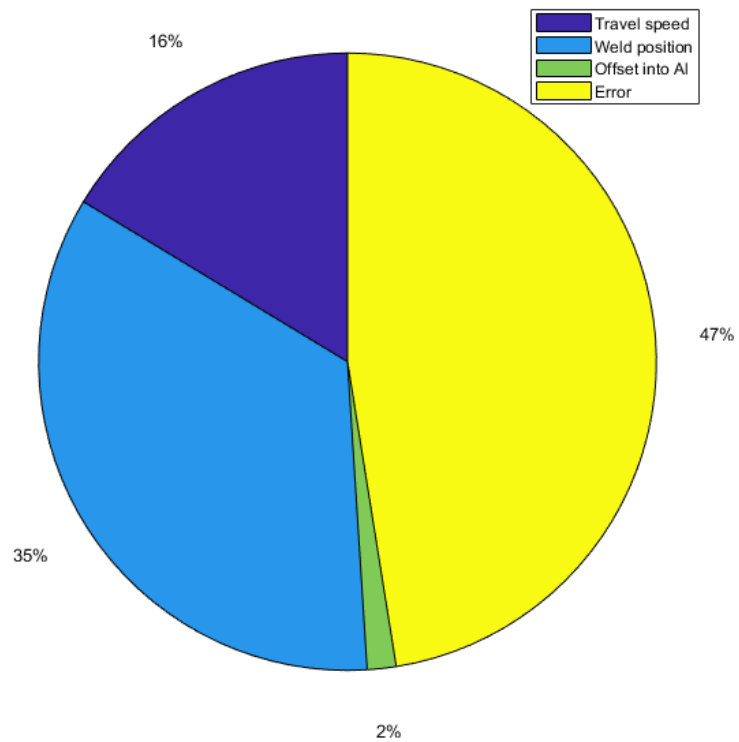

Figure 57 – Proportional contribution of each parameter on GEB

Table 26 – ANOVA results for conductivity efficiency

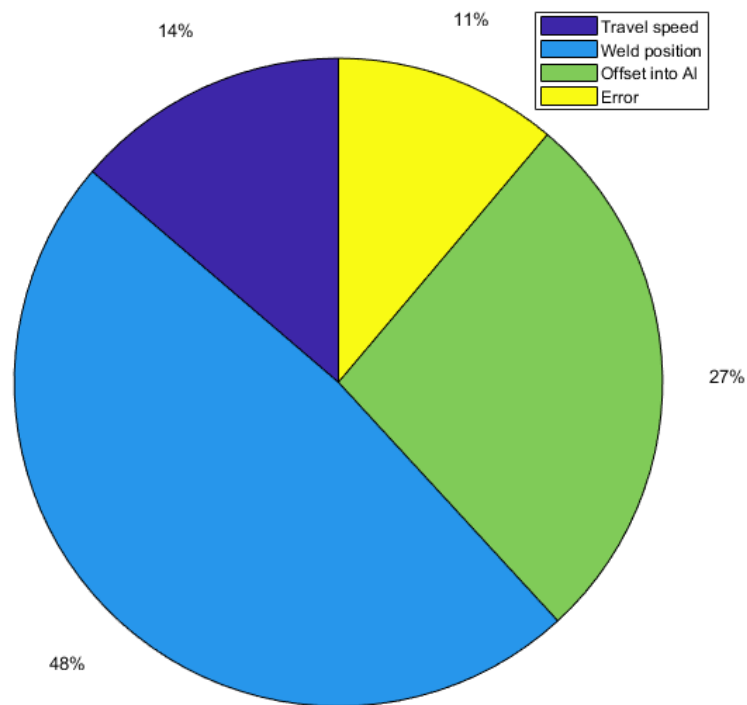| Factors	DoF	Sum of squares	Mean square	F-ratio	Contribution [%]
A	2	0.00157	0.00079	1.232140	13.73
B	2	0.00551	0.00276	4.314842	48.10
C	2	0.00310	0.00155	2.424512	27.02
Error	2	0.00128	0.00064		11.15
Total	8	0.01146	0.00573		100.00

Figure 58 – Proportional contribution of each parameter on conductivity efficiency

Proportional contribution of each variable process parameter on each performance parameter is presented in Figure 56-Figure 58. From the figures, it can be seen that error has a significant contribution on the mechanical performance assessment parameters. Looking past the error, while travel speed has the most effect on the GETS, the GEB and the conductivity efficiency are mostly governed by the weld position. The offset has almost no effect on the GEB as detailed by Figure 58.

5.7 Calculation of Optimum Performance Parameters

The results from ANOVA and the effect each parameter has on the performance parameters can now be used to predict the optimum performance of the process and the parameters that will results in that performance. By knowing the best performing performance parameter levels, seen from Figure 53-Figure 55, the optimum results can be estimated using equation (24) below:

$$Y_{Opt} = \bar{x} + (A_1 - \bar{x}) + (B_2 - \bar{x}) + (C_3 - \bar{x}) \qquad (24)$$

Where $\bar{x}$ is the mean of the results and A_1, B_2 and C_3 are the best responses. In the example of the optimization of GETS, the best responses would be A2, B2 and C1 as can be seen from Figure 53.

The optimum performance was calculated using equation (24) and is presented in the table below.

Table 27 – Calculated optimum performance

GETS	GEB	ρ_{eff}
0.674	0.457	0.988

The optimum parameters are acquired by multiplying together two matrixes, P and Q. Here, the columns of P are the best parameter levels for the performance parameters:

$$P = \begin{bmatrix} A2 & A1 & A3 \\ B2 & B3 & A2 \\ C1 & C3 & C2 \end{bmatrix} = \begin{bmatrix} 120 & 80 & 160 \\ N/A & N/A & N/A \\ 0 & 2 & 1 \end{bmatrix}$$

The columns of Q are the proportional contribution each process parameter has on each performance parameter. Table 28 below is used to assist in the construction of Q.

Table 28 – Proportional contributions of weld parameters

	Travel speed		Weld position		Offset into Al	
GETS	$\rho_{A.GETS}$	36.48	$\rho_{B.GETS}$	16.33	$\rho_{C.GETS}$	13.73
GEB	$\rho_{A.GEB}$	4.28	$\rho_{B.GEB}$	34.69	$\rho_{C.GEB}$	48.10
ρ_{eff}	$\rho_{A.Cond}$	9.71	$\rho_{B.Cond}$	1.51	$\rho_{C.Cond}$	27.02
Total	$\rho_{A.T}$	50.47	$\rho_{B.T}$	52.52	$\rho_{C.T}$	88.85

$$P = \begin{bmatrix} \dfrac{\rho_{A.GETS}}{\rho_{A.T}} & \dfrac{\rho_{B.GETS}}{\rho_{B.T}} & \dfrac{\rho_{C.GETS}}{\rho_{C.T}} \\[2mm] \dfrac{\rho_{A.GEB}}{\rho_{A.T}} & \dfrac{\rho_{B.GEB}}{\rho_{B.T}} & \dfrac{\rho_{C.GEB}}{\rho_{C.T}} \\[2mm] \dfrac{\rho_{A.Cond}}{\rho_{A.T}} & \dfrac{\rho_{B.Cond}}{\rho_{B.T}} & \dfrac{\rho_{C.Cond}}{\rho_{C.T}} \end{bmatrix} = \begin{bmatrix} 0.723 & 0.311 & 0.155 \\ 0.085 & 0.660 & 0.541 \\ 0.192 & 0.029 & 0.304 \end{bmatrix}$$

The optimum parameters can then be calculated as seen below:

$$\begin{bmatrix} Travel\ speed & x & x \\ x & Weld\ position & x \\ x & x & Offset \end{bmatrix}$$
$$= \begin{bmatrix} A2 & A1 & A3 \\ B2 & B3 & A2 \\ C1 & C3 & C2 \end{bmatrix} \begin{bmatrix} \dfrac{\rho_{A.GETS}}{\rho_{A.T}} & \dfrac{\rho_{B.GETS}}{\rho_{B.T}} & \dfrac{\rho_{C.GETS}}{\rho_{C.T}} \\[2mm] \dfrac{\rho_{A.GEB}}{\rho_{A.T}} & \dfrac{\rho_{B.GEB}}{\rho_{B.T}} & \dfrac{\rho_{C.GEB}}{\rho_{C.T}} \\[2mm] \dfrac{\rho_{A.Cond}}{\rho_{A.T}} & \dfrac{\rho_{B.Cond}}{\rho_{B.T}} & \dfrac{\rho_{C.Cond}}{\rho_{C.T}} \end{bmatrix}$$

The calculated optimal parameters for the dissimilar FSW of 6 mm thick AA1050-H14/24 and Cu-OF-04 is presented in Table 29 below.

Table 29 – Optimal parameters for the process

Optimal parameters	
Travel speed [mm/min]	N/A
Weld position [mm]	N/A
Offset into Al [mm]	N/A

6 Characterization of Optimized Weld

6.1 Introduction

Once the optimized FSW process parameters were calculated, it was time to test and characterize the optimal joints as well as the process itself. The welding process had its temperatures investigated and analyzed using strategically placed thermocouples. A weld was produced using the optimized parameters in the same fashion as the DoE welds were. Then the tensile, bending, electrical and surface properties of joint were characterized. The metallurgical properties were investigated using optical microscopy and Scanning Electron Microscopy (SEM) and the micro-hardness field of the joint established. This chapter details this characterization.

6.2 Temperature Analysis

The temperatures of the base materials were monitored using strategically placed thermocouples and analyzed. Ø1 mm holes were drilled into the base materials at positions seen from Figure 59. The strategical position was so that the thermocouples on each side were at same distance from the center of the stirred zone (weld line). The thermocouples were placed inside these holes along with thermal paste for improved thermal conductivity. The thermocouple wires were then attached to the base plates using epoxy adhesive to keep them stable during the weld. 16 thermocouples were placed in total. During the weld process, some of the thermocouples, especially on the Al side, were pushed away by the flash formed during the weld and the data they sampled was not used for further evaluation.
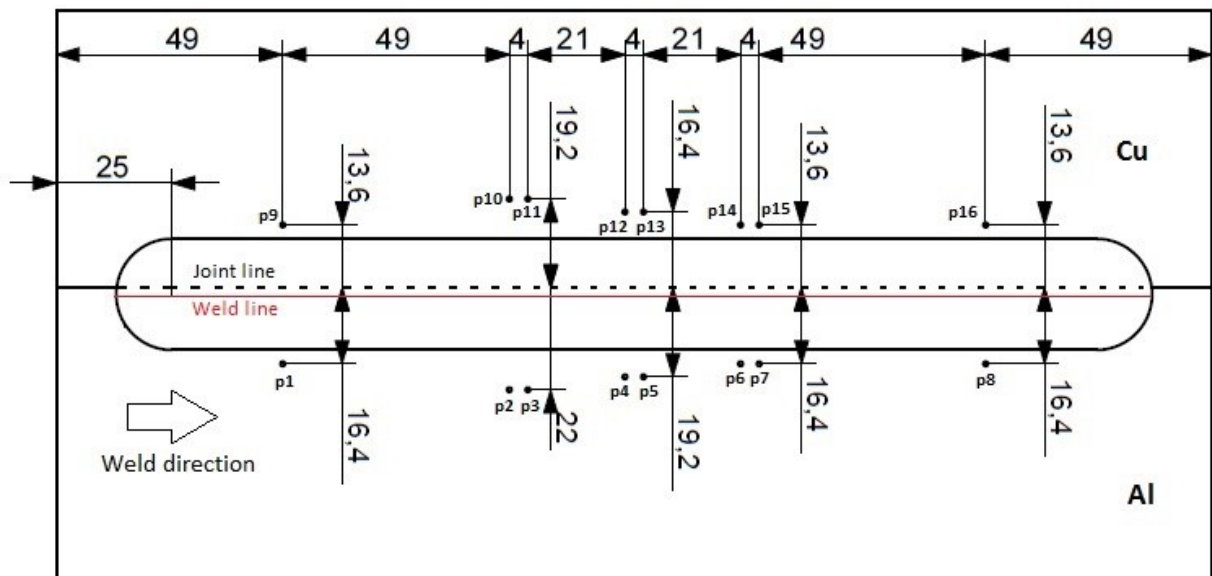

Figure 59 – Placement of thermocouples p1-16, showing both the original joint line and the offset weld line, dimensions in mm
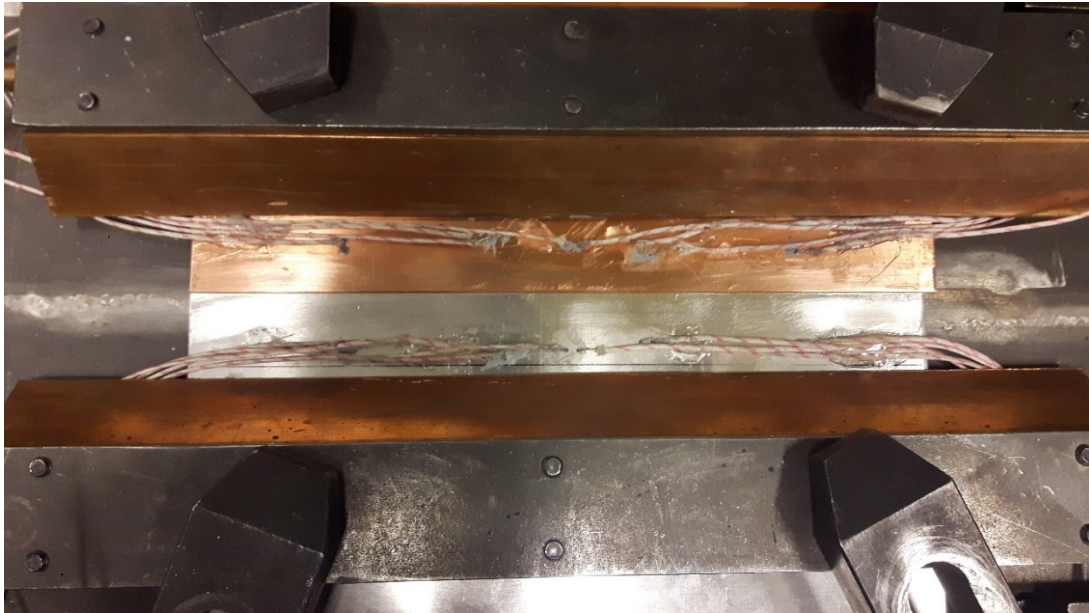
Figure 60 – Thermocouples inside clamped base materials before welding

After welding, the temperature data was analyzed and is presented here in two ways. Figure 61 details the top temperatures reached at certain distances from the center of the stirred zone for the Cu and the Al, excluding the thermocouples at the start and end of the weld. The actual position of the holes was measured once the weld had been cut into cross-sections to be able to measure the actual distances from the thermocouples to the center of the stirred zone. Figure 62 shows the temperature behavior at different points in both materials.
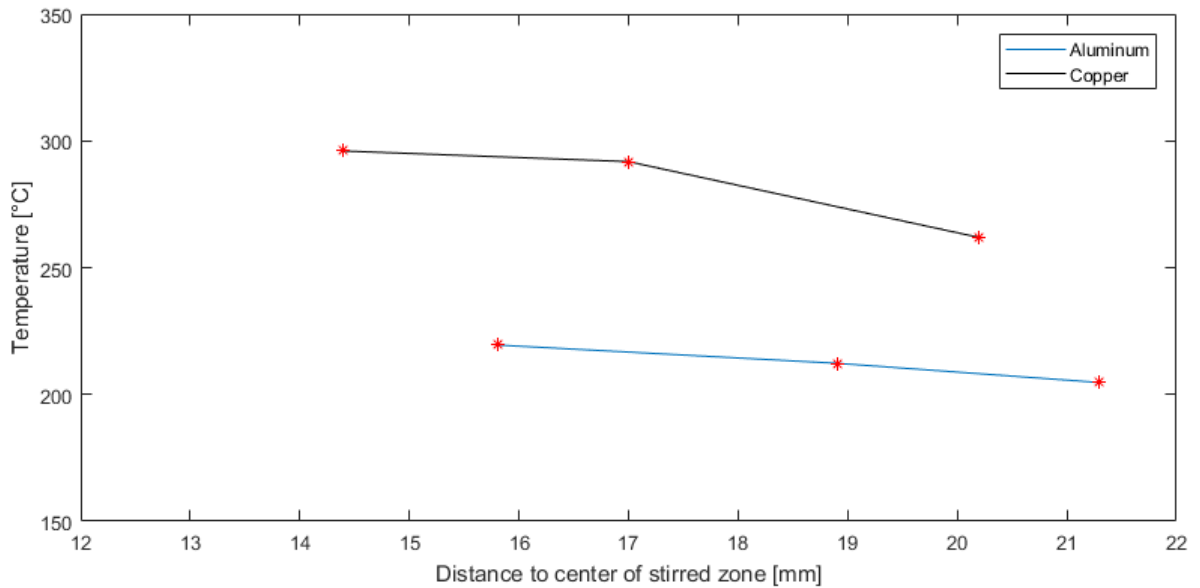

Figure 61 – Maximum temperatures reached at varying distances from the stirred zone in the base materials
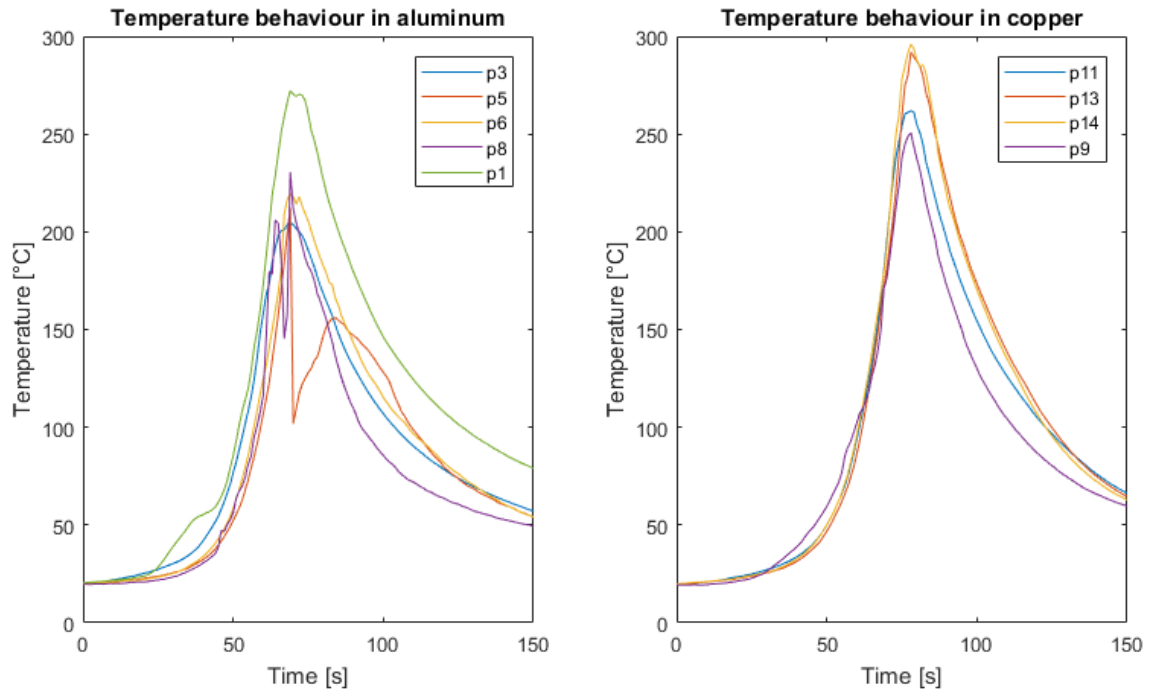
Figure 62 – Temperature behavior of different points in base materials

The temperature behavior highly differs depending on which base material is investigated. The highest temperatures reached in Cu are much higher than in Al, especially for thermocouples closer to the center of the stirred zone. By using interpolation, it was found that the maximum temperature in Cu at a 15.8 mm distance from the center of the stirred zone is 293.7 °C while the maximum temperature in Al at the same distance from the stirred zone is 219.5 °C. This can be contributed both to the higher heat conductivity Cu and the different heat input generated by the plasticization of Al compared to Cu. Cu generates more heat when deformed and thus the Cu side heats up more than the Al side. This also supports the notion that the majority of heat input generated by FSW is not a result of friction between the tool and the base materials but by their deformation and plasticization. The highest temperature reached in the Al is at p1, which is at the start of the weld. This is due to the high heat generated during the plunging of the probe into the materials. Because of the offset used in the process, the probe is in more contact with the Al side and heats it up more than the Cu side at the start of the weld. There is also less material around the start point for the heat to dissipate to and the dissipation into the Cu is slower than later in the weld as the materials have only been welded in a localized area at that point in the process.

6.3   Tensile Properties

The tensile properties of the optimized weld were characterized. Three tensile specimens were made and tested. Figure 63 shows the stress-strain curves for all specimens. Table 30 details the tensile values evaluated from the stress-strain curve.
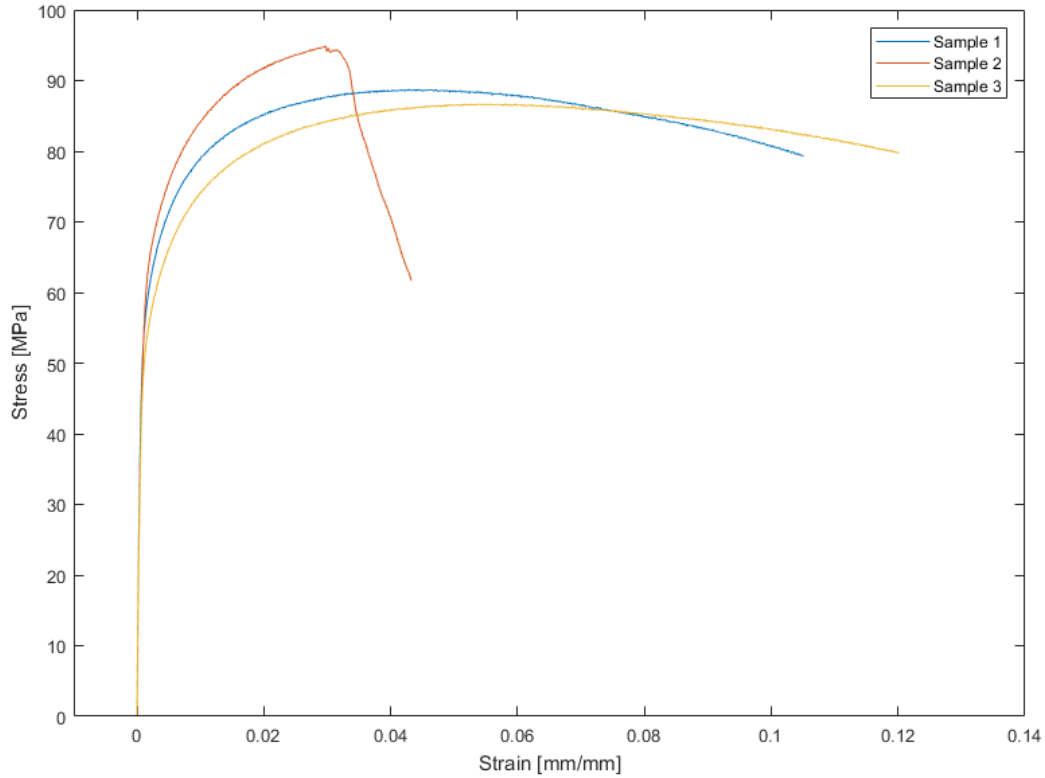
81

Figure 63 – Engineering stress-strain curves of the optimized weld

Table 30 – Tensile properties of the optimized weld joint

E [GPa]	σ_y [MPa]	σ_{UTS} [MPa]	A [%]	U_T [J/mm²]	GETS
90.54 ± 2	64.09 ± 2.9	90.14 ± 4.3	26.80 ± 4.8	4.32 ± 1.6	0.848 ± 0.1

There is some difference in the behavior of the three samples. While sample 2 is stronger, has higher modulus of elasticity and a greater ultimate tensile strength than the other specimens it lacks the toughness and elongation the other two samples have as can be seen in Figure 63. On average, the tensile properties are better than the best DoE welds, with both good strength and toughness, exceeding the calculated performance.

6.4 Bending Properties

Bending tests were conducted on the optimized weld. Both sides were tested, root and face side. Figure 64 shows the stress-strain curves of the bending tests and Table 30 details the maximum force, displacement at maximum force and energy consumed for both the face and root side of the weld.
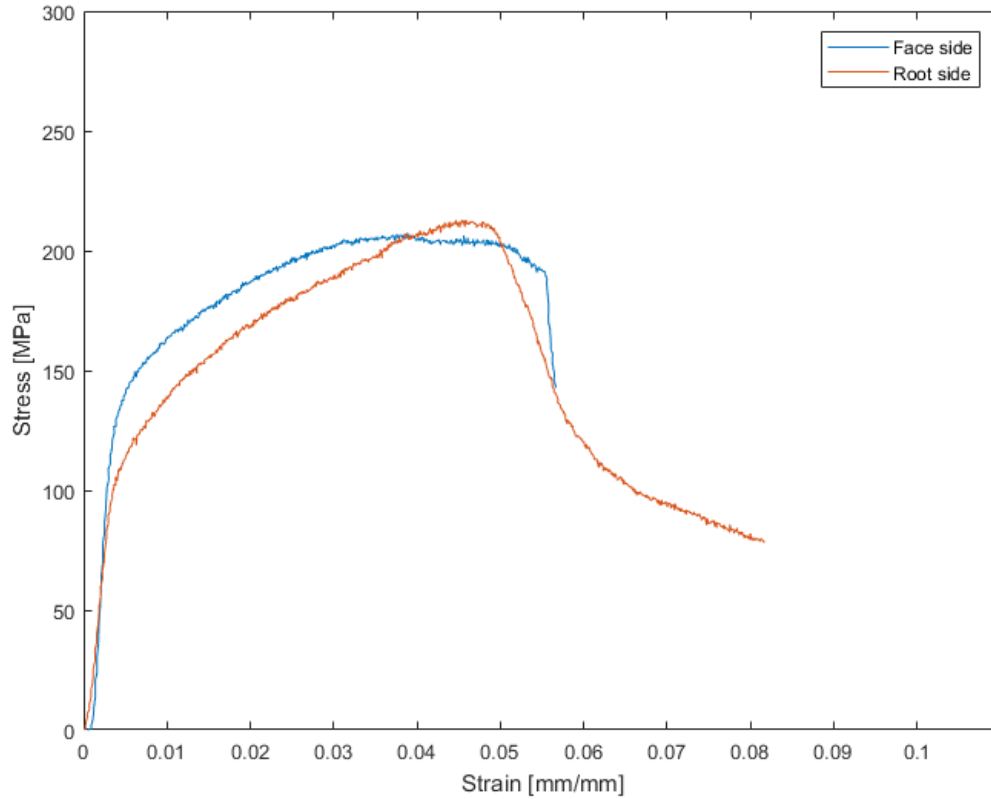
Figure 64 – Bending stress-strain curves of the optimized weld

Table 31 – Bending properties of optimized joint

Side	F_{max} [kN]	$d_{@Fmax}$ [mm]	U_B [J/mm³]	GEB	$GEB_{average}$
Face	1.28	6.56	6.64	0.396	0.408 ± 0.02
Root	1.31	7.55	7.26	0.419	

The GEB for the optimized joint is 0.05 lower than calculated. There is a small difference in the bending properties of the two different sides of the joint. The root side has better overall bending characteristics.

6.5   Electrical Properties

The electrical properties of the optimized joint were measured and characterized in the same manner as the DoE welds. The resistance, proportional increase of resistance compared to an ideal 24 mm joint without any contact resistance and conductivity efficiency are presented in Table 32.

Table 32 – Electrical properties of optimized joint

Joint resistance [μΩ]	Proportional increase [%]	σ_{eff}
0,55 ± 1	2.9 ± 5	0.972 ± 0.05

The joint resistance is extremely small compared to the contact resistance between machined base materials when pressed with high force, which is around 200 times higher. This amount of resistance cannot be measured using normal electrical multimeters and is almost negligible as the resistance is only around 3% higher than for a perfect resistless joint. The joint is highly capable of transferring electricity with minimal to negligible power losses.

6.6 Metallurgical Properties

The metallurgical properties of the optimized weld were investigated using optical microscopy and Scanning Electron Microscopy (SEM). Two samples were made from the middle section of the weld, one for each method used. The weld structure was investigated with different kinds of weld morphologies in mind. An IMC layer between the base materials was identified and its chemical composition mapped out with a line analysis. Intercalated lamae morphology was also identified and its chemical composition mapped out. Additionally the grain structure of the base materials after welding was investigated. Figure 65 shows the optical macrograph of the weld and marks the areas of interest that the following image shows further.

Figure 65 – Optical macrograph of the optimized weld, areas of interest detailed by Figure 66 are marked from 1 to 6
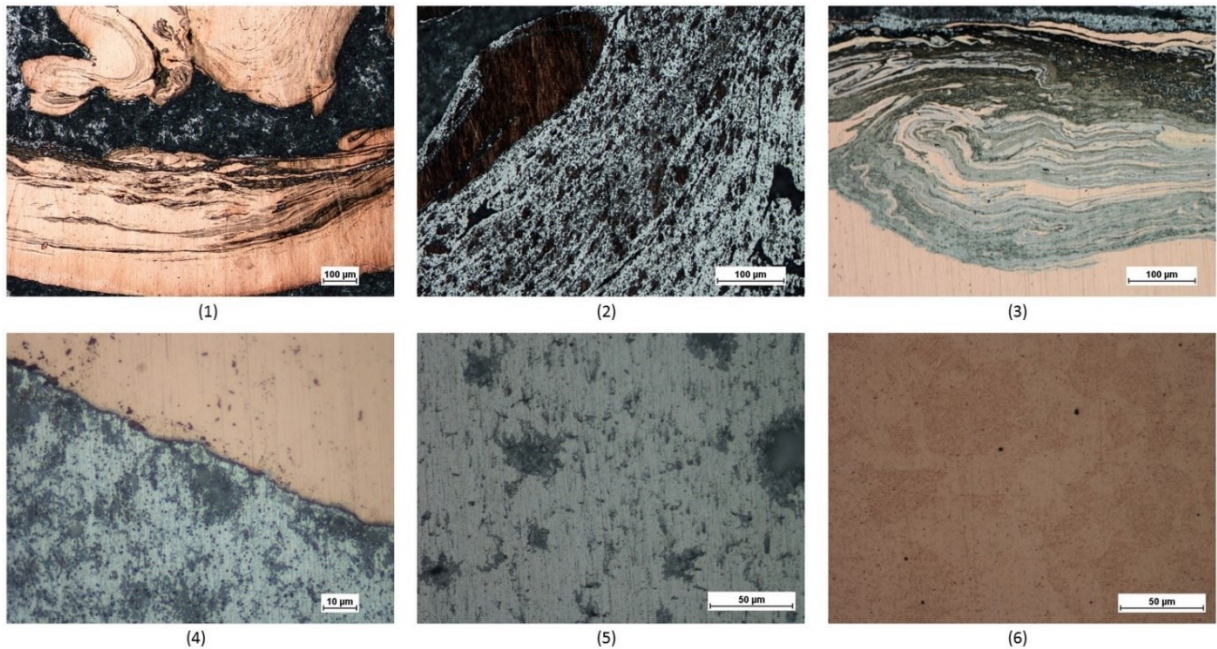
Figure 66 – Micrographs of the joint shown in Figure 65 from position 1 to 6, (1) Cu-rich mixed material inside the lower Cu tongue, (2) intercalated lamae, (3) layered structure inside the upper Cu tongue, (4) intermetallic layer, (5) Al grains, (6) Cu grains.

The two figures above detail the complexity of the Al-Cu weld structure. Within the weld, multiple Al-Cu morphologies can be identified. Cu-rich material mixtures are found within both tongues that have pushed into the Al during welding. The mixture in the bottom tongue (1) is similar to the one shown in Figure 16 while the mixture in the upper tongue (3) is a more homogeneous layered structure. An IMC layer forms in the less mixed zones where Cu meets Al (4). The layer at the tip of the upper tongue has thickness of around 1 μm.
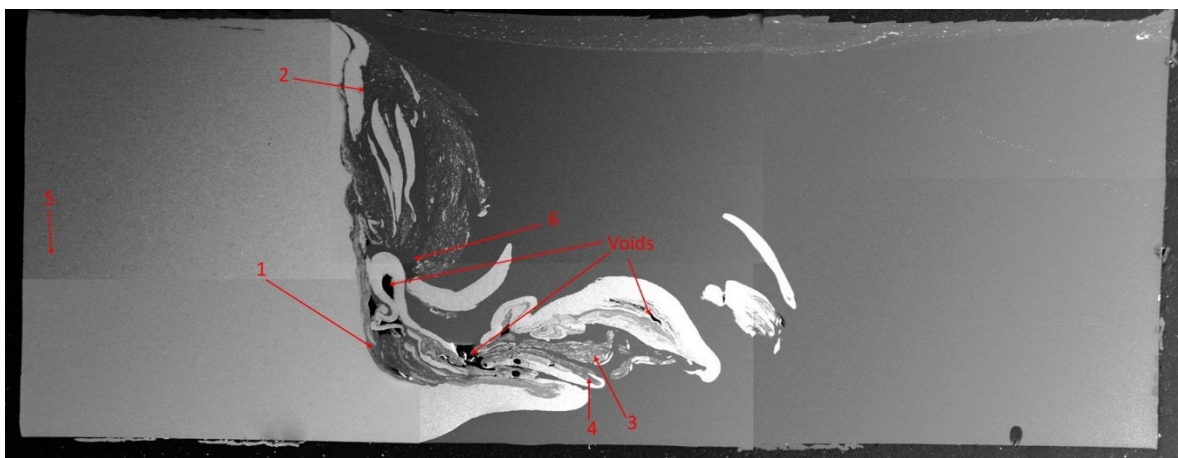

Figure 67 – SEM macrograph of the optimized weld, areas of interest detailed by Figure 68 are marked from 1-6
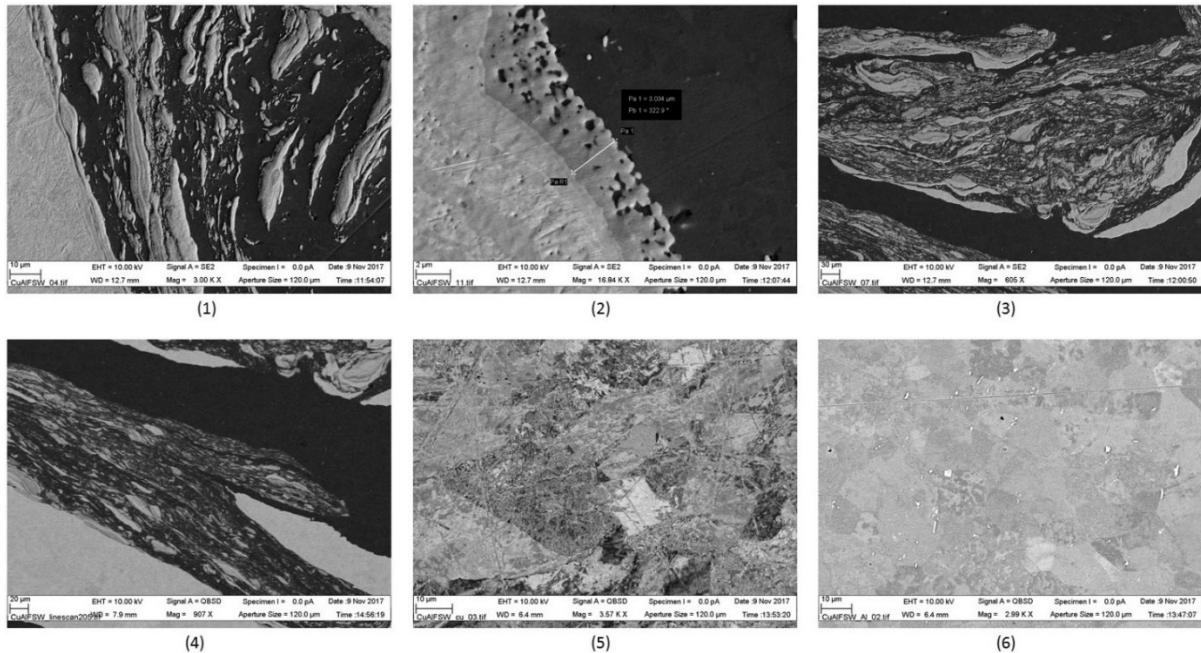
Figure 68 – SEM Micrographs of the joint shown in Figure 67 from position 1 to 6, (1) Al based composite matrix, (2) IMC layer at the Al-Cu interface, (3) intercalated lamae, (4) multilayered structure, (5) Cu grains away from the mixed zone, (6) Al grains with Cu particles in the stirred zone.

From the SEM imaging, multiple different Al-Cu mixed morphologies were identified, mostly resembling an Al based composite matrix or more Cu heavy mixtures such as the intercalated lamae (3) and multilayered structures (4). Similar mixtures were found in the optical macrograph in Figure 65 apart from the Al based composite matrix (1), which is easier to identify using SEM imaging. The IMC layer (3) identified here is thicker than the one previously identified with a thickness of around 3 μm. IMCs are also present within the Cu next the the layer. Using the SEM equipment the chemical composition of the IMC layer was determined using an X-ray diffraction line analysis.

A few voids can be seen within the processed zone in Figure 67. The voids are present in the processed zone on the boundaries between Cu and Al and within Cu dominated mixtures.
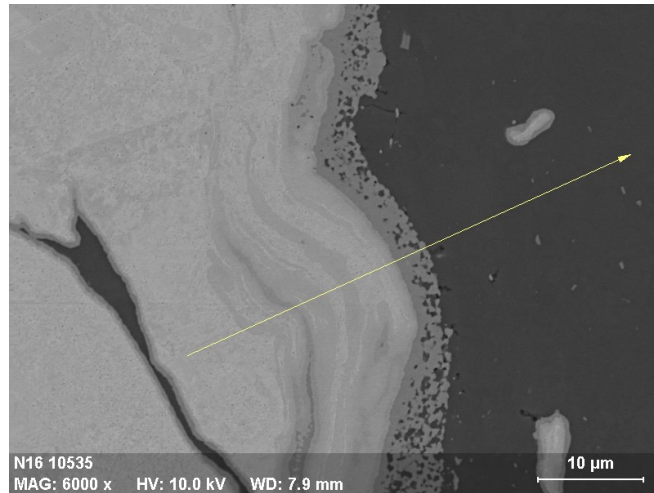
Figure 69 – The line used for the chemical analysis of the IMC layer in Figure 68 (2)
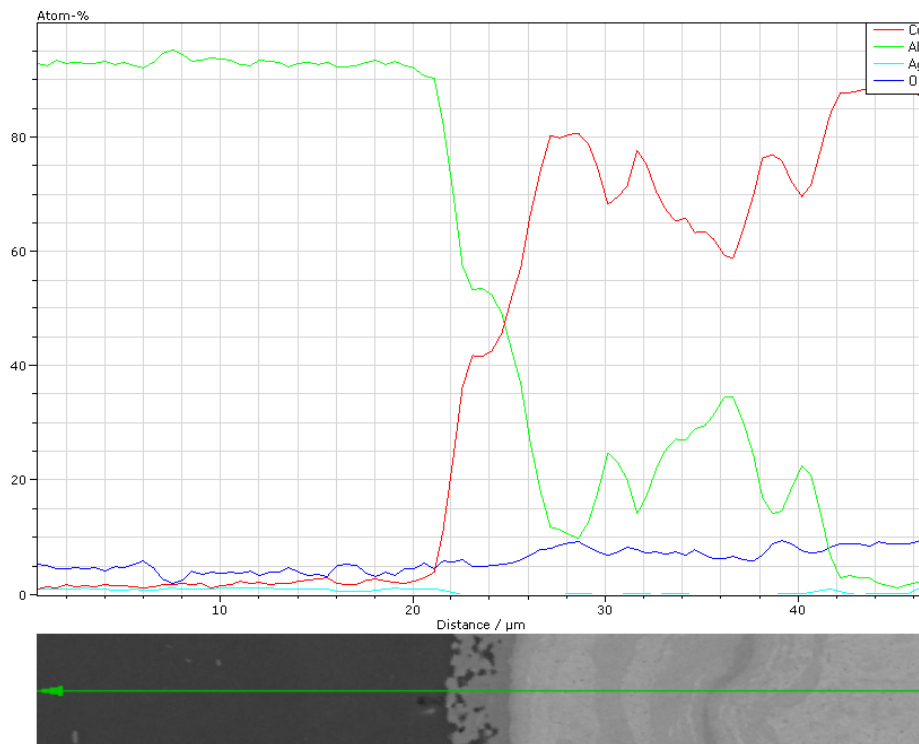

Figure 70 – Line analysis of the IMC layer

The line analysis uncovers the IMCs found in the Al-Cu interface. The dark gray layer next to the Al was identified as CuAl. Further into the Cu other more Cu-heavy IMCs are present such as Cu_9Al_4.
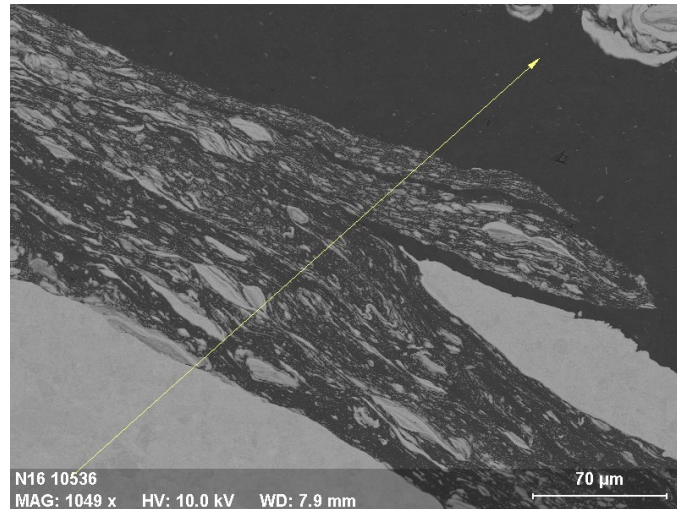
Figure 71 – The line used for the chemical analysis of the multilayered structure in Figure 68 (4)
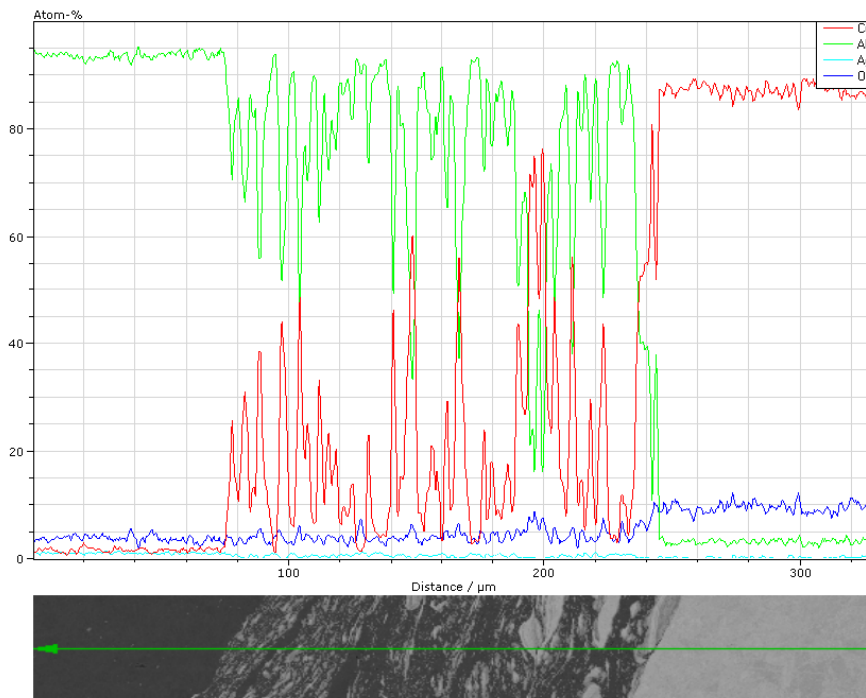

Figure 72 – Line analysis of the multilayered structure

The chemical composition of the multilayered structure is severally chaotic. Based on the line analysis the structure is mostly composed of layers of pure Al, IMCs and some pure Cu. This can be contributed to the intense mechanical mixing of Cu particles into the Al and diffusion occurring at the interface of the two materials.

6.7 Hardness Properties

The cross-sectional hardness of the optimized joint was investigated using a CSM micro-combi tester. 451 indentations using a force of 0.5 N were made, covering a 20x5 mm rectangular area and centered in the middle of the stirred zone. The Vickers hardness was measured using the Oliver and Pharr method (O&P) [79]. This method determines the Vickers hardness using the load and displacement information sensed while the indentation takes place. It can therefore not be directly translated into traditional Vickers hardness numbers that are determined based on the area of indentation, although they are similar.
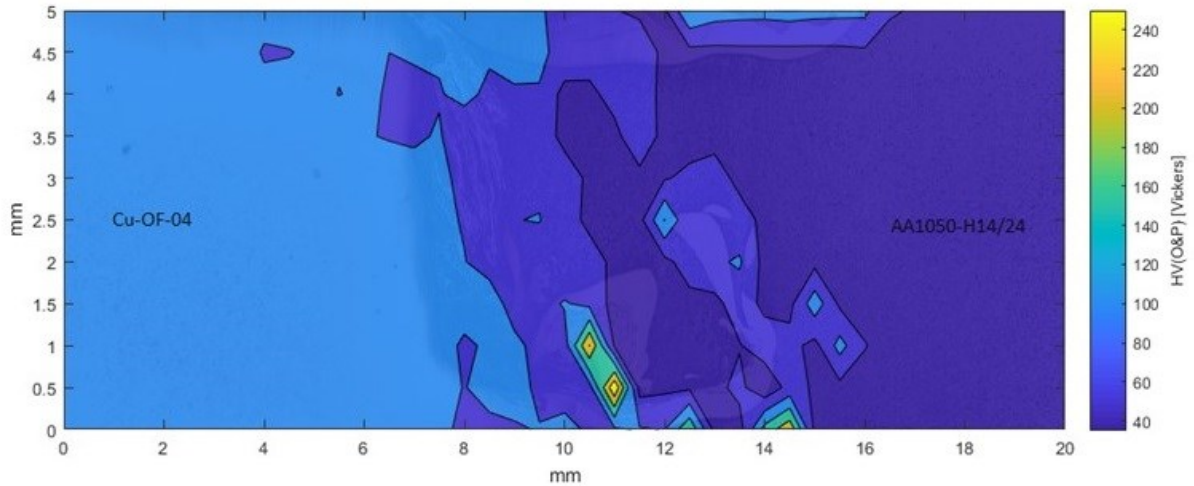

Figure 73 – Microhardness field of the optimized joint, with the optical macrograph from Figure 65 transparent in the background

Figure 73 shows the clear difference in the hardness of the base materials, on each side of stirred zone. The Cu has hardness of 120 Vickers while the Al is around 40 Vickers. The stirred zone itself has a more complicated distribution of hardness. Cu tongues and particles, with higher hardness, enter the Al and result in the locally higher hardness fields engulfed by the softer Al. IMCs form at the bottom of the stirred zone and cause the spikes in hardness seen there while the other mixed regions closer to the Cu have hardness values in between that of the base materials.

6.8 Surface Properties

The surface of the optimized weld was characterized in the same way as the DoE welds were. The results are presented in Table 33. It is to be noted that even though the flash was difficult to remove compared to some DoE welds there was less of it in general which is a sign of minimal loss of material and indicates a good weld. Comparing the surface finish of the optimized weld to the surface finish of DoE weld number 5 seen in Figure 51 shows that the optimized weld has poorer surface aesthetics, with weld 5 being quite smoother.

Table 33 – Surface characterization of optimized weld

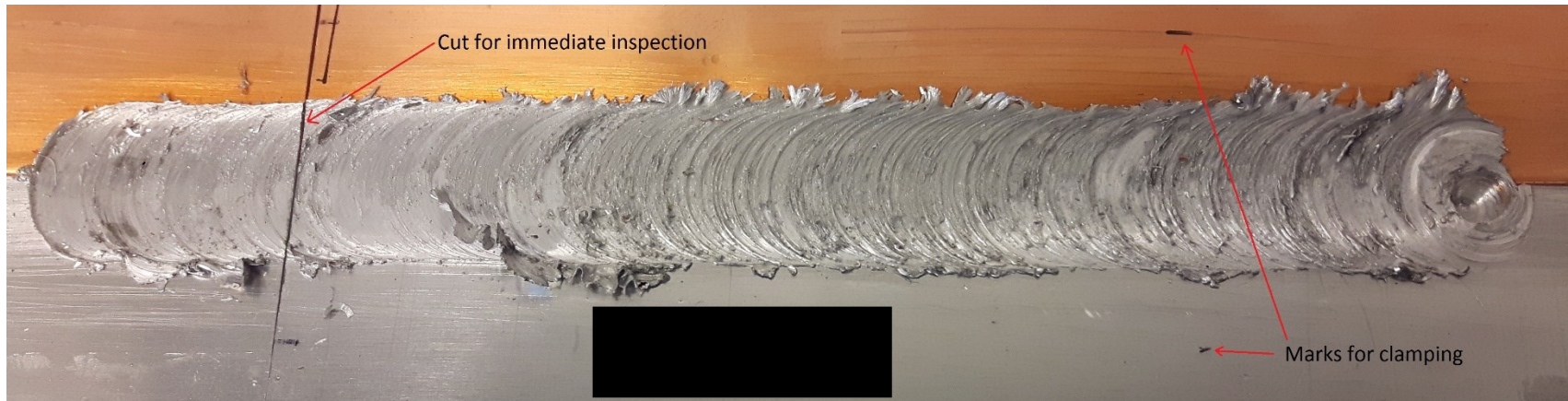| Face of the weld														Root of the weld						Observations
Flash			Type of flash		Removal of flash		Width regularity		Striade regularity		Concavity		Flatness		Evidence of joining		Uniformity			
None	Little	Significant	Continuous	Granular	Easy	Difficult	Regular	Variable	Semi-Regular	Variable	Minimal	Significant	Flat	Irregular	Apparent	Dubious	Regular	Variable		
	X		X			X	X			X	X		X		X		X			

Figure 74 – Visual surface analysis of the optimized weld

6.9   Global Analysis of the Results and Translation into Force Control

After having characterized the various properties of the optimized weld the results can be analyzed globally. The force logged during the process is also analyzed to give a translation between the control method used during this work, position control, and force control, which is the control method generally used in manufacturing.
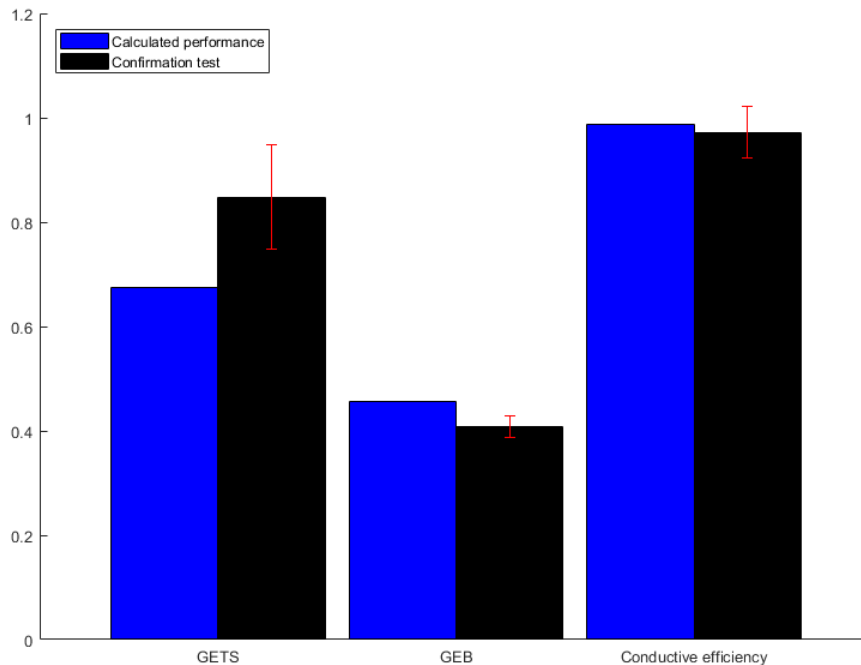

Figure 75 – Comparison between calculated and confirmed performance parameters

The performance parameters of the optimized weld are better than expected as can be seen in Figure 75. The tensile characteristics are especially good when compared to the calculated performance. The bending and electrical characteristics are quite close to the calculated performance. When compared to the various DoE welds, the optimized weld has superior tensile and electrical properties. The bending properties, on the other hand, are not as good as two DoE welds, weld 1 and weld 5.

When it comes to surface characteristics, the optimized weld is not as aesthetically pleasing as some of the DoE welds, mainly weld 5. The optimized weld has a rougher and less uniform surface. This is not a surprise, as surface and mechanical properties do not always correlate with each other and the weld was not optimized based on the surface characteristics but on the mechanical and electrical properties. Higher offsets result in less intense mixing of the base materials, which leads to a smoother Al layer at the top of the weld but can also lead to weaker bonding between the materials.

The process control method used for all the welds covered in this thesis is position control. This method is generally not used for long welds or in production where force control is favored. The usage of position control, that is that the z-position of the FSW tool stays fixed throughout the

weld after plunging, can result in a varying force throughout the weld process. Small differences in thicknesses of the base materials or backing anvil can cause the force to vary throughout the weld, resulting in non-uniform characteristics. Additionally, when the materials heat up and soften, the forging force they are subjected tends to decrease throughout the weld if the heat input is not in equilibrium with the weld position and the resulting forging force. For the optimized parameters, the welding force of the process was detailed so that it can be translated from position control into force control more easily.

Figure 76 shows the force logged by the FSW machine for the confirmation test. The force data is a bit chaotic due to problems with the load cell of the machine, which currently has up to 20% measurement error for loads around X kN. The force has been averaged out using the moving average, which should be closer to the actual force acting on the base materials during the weld. This load cell error was the main reason it was decided to use position control in the first place.
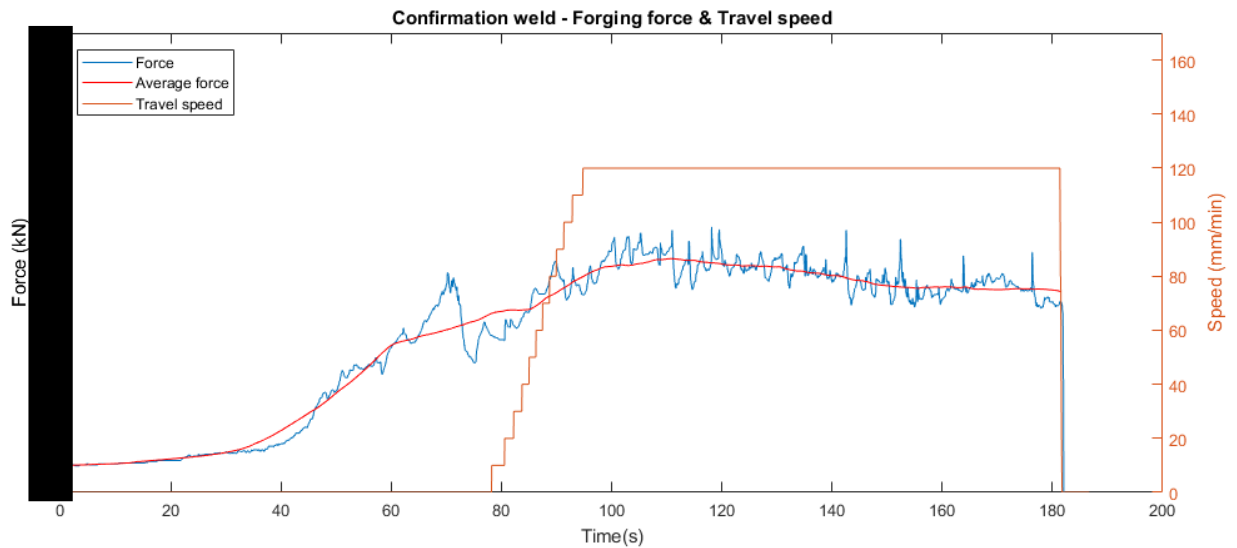

Figure 76 – Force-time graph for the confirmation weld, including the travel speed

From the figure above it can be seen how the force varies throughout the weld and how unstable it seems to be when the raw force curve is looked at. This noisy variation in the force data stems from the measurement error in the load cell of the machine and does not represent the actual force the weld process experiences. The average force of the weld varies a bit during the process. At the start of the weld it rises to X1 kN before slowly decreasing to around X2 kN at the end of the weld. It can be estimated that this weld's position control using weld position of N/A mm can be translated to a force control method with a weld force of around X3 kN.

7 Relaxation of Clamping Force Experiment

7.1 Introduction

One of the advantages of having a Cu end in dissimilar Al bus bars is that the Cu should deform and creep much slower than the Al while in operation, thus reducing the cost of maintenance as with Al ends the bolted connection of the bus bar needs to be periodically retightened. In order to establish that and to investigate the magnitude of improvement an experiment was designed and conducted.

While in operation, the bus bar ends experience both high clamping forces and large thermal cycles. This causes the material to expand and contract while under heavy load, which over time deforms it and reduces the clamping force of the bolt. When the clamping force lowers, so does the electrical and thermal conductivity of the bolted joint. To avoid a premature system failure the bolts need to be retightened with a certain frequency.

Standard creep tests are conducted by applying a constant stress to a tensile specimen under controlled elevated temperature. The extension of the specimen is measured by an extensometer and the test results are plotted as a strain-time graph [80].

Although creep might be a factor in the relaxation of the bolts' clamping force a standard creep test would not fully explain the operational difference between a Cu bus bar end and an Al bus bar end. Knowing the relaxation rate of the clamping force while the bus bar ends experience environment similar to what they experience while in operation is a better indicator of the integrity of the system.

When standard scientific tests do not fully explain the difference of two similar, but different systems, alternative tests are often composed, presented and conducted [81]. Sometimes they are also recognized as an improvement to similar tests and standardized [82].

The test protocol described in this chapter tests the bus bar ends in an environment similar to which it experiences while in operation. It should therefore give a better understanding of the rate of which the clamping force lowers than a standard creep test would. Further into the chapter, the conductance of the test and the results are presented.

7.2 Test Setup

The experimental set up, presented in Figure 77, is made of several parts. A donut load cell and the bus bar end are clamped together between a bolt and a nut, separated by ceramic washers. A ceramic sleeve is placed around the bolt to further insulate it. Behind the flattened mounting end of the bus bar, two cartridge heaters are placed and a cooling channel is made. To monitor the thermal cycles, three k-type thermocouple wires are strategically placed in small holes on the flattened surface. Two are placed side by side at the beginning of the flattened end for redundancy and increased accuracy. The third thermocouple is placed at the end of the flattened bus bar end, which allows for mapping of the temperature in the clamped zone.
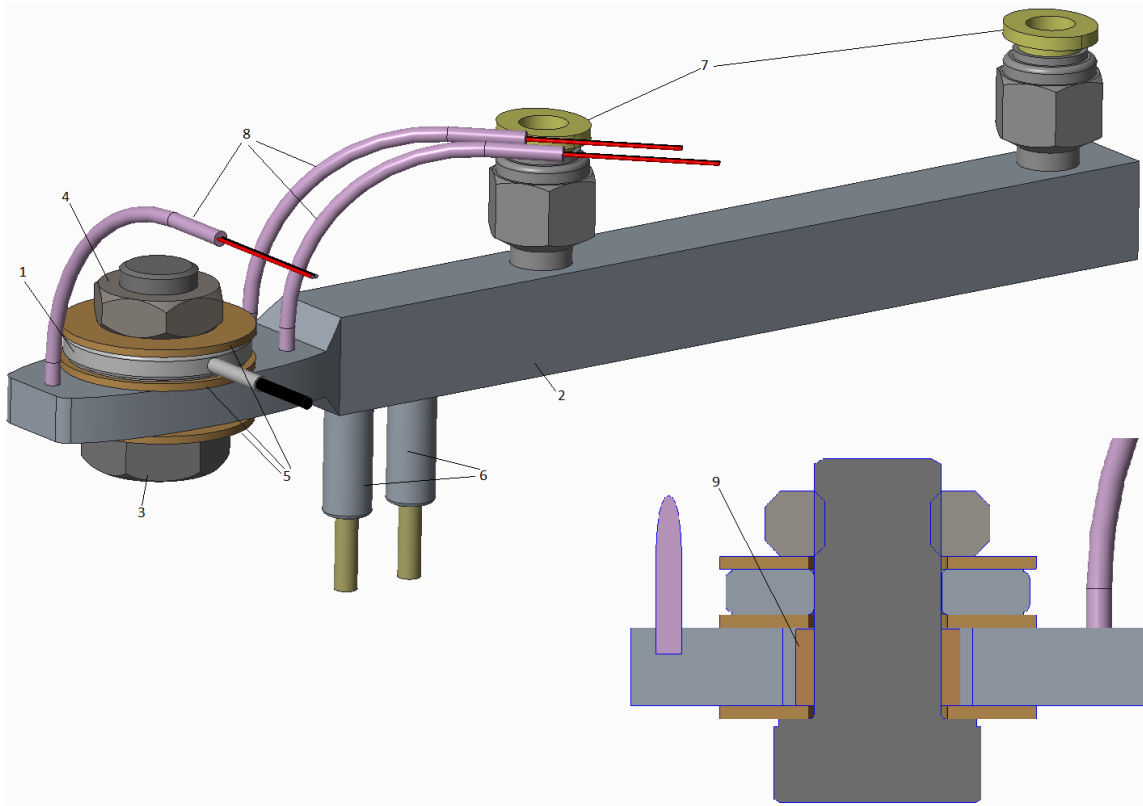
Figure 77 – Designed relaxation of clamping force experiment test setup

Part number	Part name
1	Donut load cell
2	Bus bar end
3	Bolt
4	Nut
5	Ceramic washers
6	Cartridge heaters
7	Cooling channel
8	Thermocouple wires
9	Ceramic sleeve

Table 34 - Test setup components

An electric circuit was designed and built in order to control the experiment via microcontroller. The heaters were to be turned on and off using relays. The load cell and three thermocouples were each connected to amplifiers which made the microcontroller able to accurately read the force and temperature values. The designed electrical circuit can be seen in Figure 78.
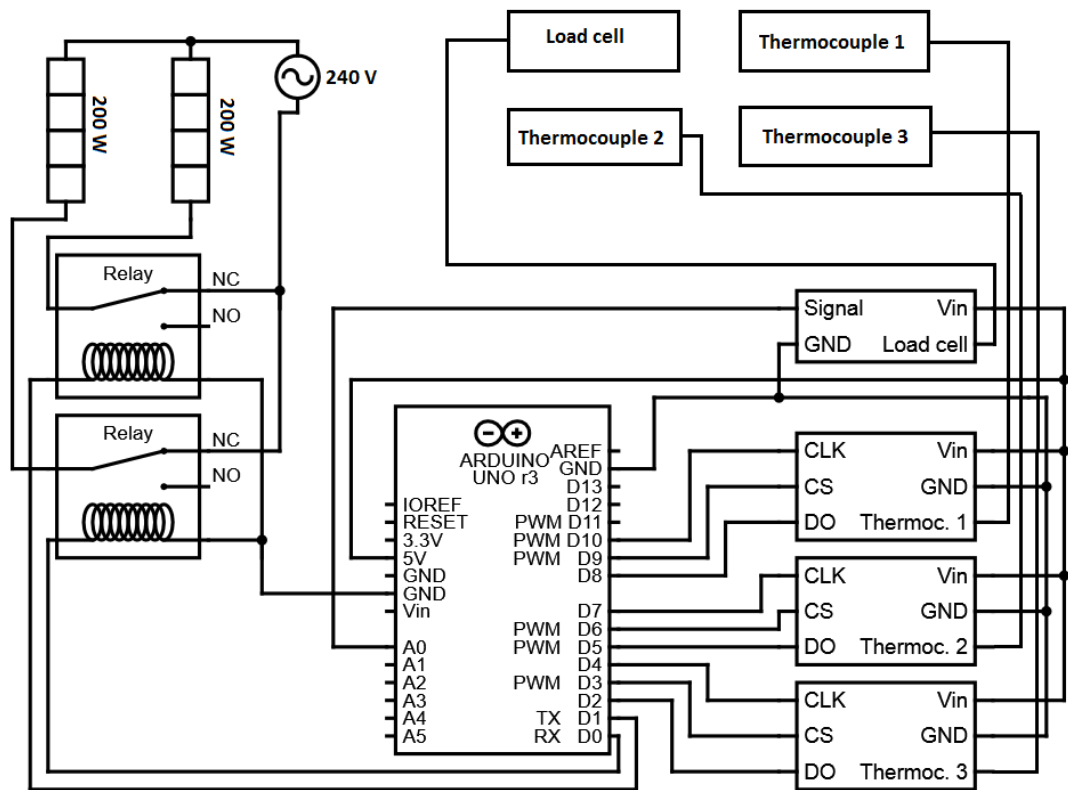
Figure 78 – Relaxation of clamping force experiment's electrical circuit

7.3   Procedure Specification

The test evaluates the rate of reduction in clamping force of the bolt due to creep of the clamped material occurring when the material is subjected to thermal cycles similar to which it experiences while in operation.

Table 35 – Test nomenclature

Symbol	Description	Units
F_0	Preload force	[N]
$F(t)$	Force at time t	[N]
F_{min}	Minimum force needed for cycle iteration	[N]
$T(t)$	Temperature at time t	[K]
T_{Hot}	High temperature in thermal cycle	[K]
T_{Cold}	Low temperature in thermal cycle	[K]
f_F	Sampling frequency of force	[s^{-1}]
f_T	Sampling frequency of temperature	[s^{-1}]
Δt_{Hot}	Length of time the temperature is held above T_{Hot}	[s]
Δt_{Cold}	Length of time the temperature is held below T_{Cold}	[s]
N_{max}	Maximum number of cycle iterations	[1]

The test is controlled by a microcontroller and is conducted as follows: The force and temperature monitoring is activated and the data is sampled and logged with certain sampling frequencies, f_F and f_T. The bolt is preloaded with a certain force, F_0, and the cooling flow is turned on. Then an iterative cycle begins. The heaters are turned on. After the temperature reaches a certain high point, T_{Hot}, it is held above it for a certain amount of time, Δt_{Hot}. Then the heaters are turned off and the temperature lowers until it reaches a certain low point, T_{Cold}, which it is held under for a certain amount of time, Δt_{Cold}. If either the number of cycles have reached a certain maximum, N_{max}, or the force is under a certain minimum, F_{min}, the cooling flow is turned off, the test is stopped and the data is analyzed. Otherwise, the process goes through another iterative cycle.

Figure 79 further explains the procedure specification. Figure 80 explains the thermal cycle the test specimen experiences.
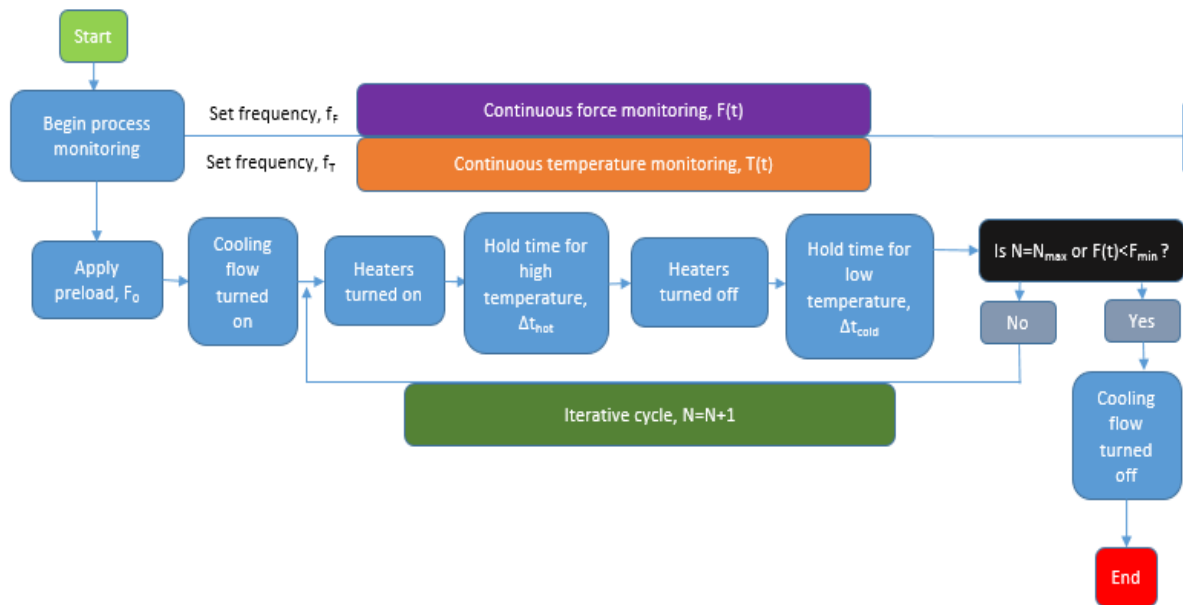

Figure 79 – Designed test protocol for the relaxation of clamping force experiment
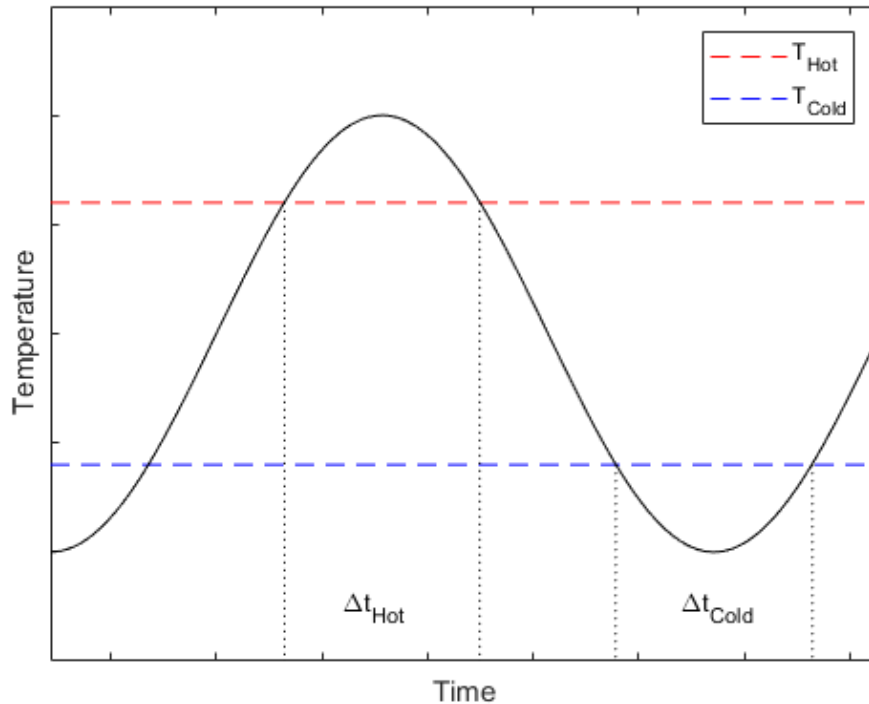
Figure 80 – Relaxation of clamping force experiment thermal cycle

7.4 Test Conductance

The actual setup of the experiment deviated slightly from the original design. The originally planned load cell was not useful for this type of test as it is piezo-electric and should not be used for taking measurements over a long time. Therefore, a strain gauge based load cell was purchased. It is much bigger than the originally planned one and therefore a load pyramid had to be designed and manufactured to transfer the load from the bus bar end to the load cell. The load pyramid was made out of Cu and with cooling channels to protect the load cell from excessive temperatures. Stainless steel washers were used in place of the ceramic components and the thermocouples were attached to the side of the bus bar end using an electrical discharge machine. A Cu bus bar end was manufactured for testing in similar dimensions as the smaller EN-AW-6101-T4 bus bar end used. Its material was Cu-OF-04.

Two experiments were made for each material using different temperature interval. The first experiment for each material had a peak temperature of around 150 °C while the second one had a peak temperature of around 195 °C. Both of these peak temperatures are the peaks measured by the thermocouple closest to the source of the heat, the cartridge heaters. The actual experimental setup for both materials can be seen in Figure 81 and Figure 82. The lower peak temperature tests were much shorter in timespan than the higher peak temperature ones as can be seen in next sub-chapter. The sampling frequencies f_F and f_T were both 1 second. For the lower temperature test, the heating cycle was so that the heaters were on for 30 s and then turned

97

off for 30 s. For the higher temperature test the heating cycle was a little different, the heaters were on for 50 s and off for 20.

The placement of the three thermocouples was so that two of them were placed at the side of the clamped bus bar end while the third one was placed at the far end as can be seen in Figure 82. After each experiment, the distance from the shoulder of the bus bar to the two thermocouples on the side was measured. The shoulders of both bus bars are marked on Figure 81 and Figure 82.

It should be noted that in the middle of the lower peak temperature test of Al, see subchapter 7.5.1, thermocouple 1 and 3 broke and thus the temperature data is somewhat limited. It is not of great importance as the data from thermocouple 2 shows a stable temperature cycle and so the temperatures monitored by thermocouples 1 and 3, if not broken, would at least be very close to their final measured temperatures. Due to cooling problems, the temperature in the lower peak temperature test of Cu was very unstable during the first 60 cycles. The force fluctuates with the change in temperature as when the temperature lowers fast so does the bus bar shrink. Later in the test, the temperature cycles reach equilibrium and the force converges back into the anticipated curve and continues to relax normally.

The dimensions of the Al bus bar end used in the high peak temperature test differ somewhat from the one used in the lower peak temperature test. It is a bit longer, wider and thicker. See Table 36.

Table 36 – Differences in the dimensions of the ends of the Al bus bars used

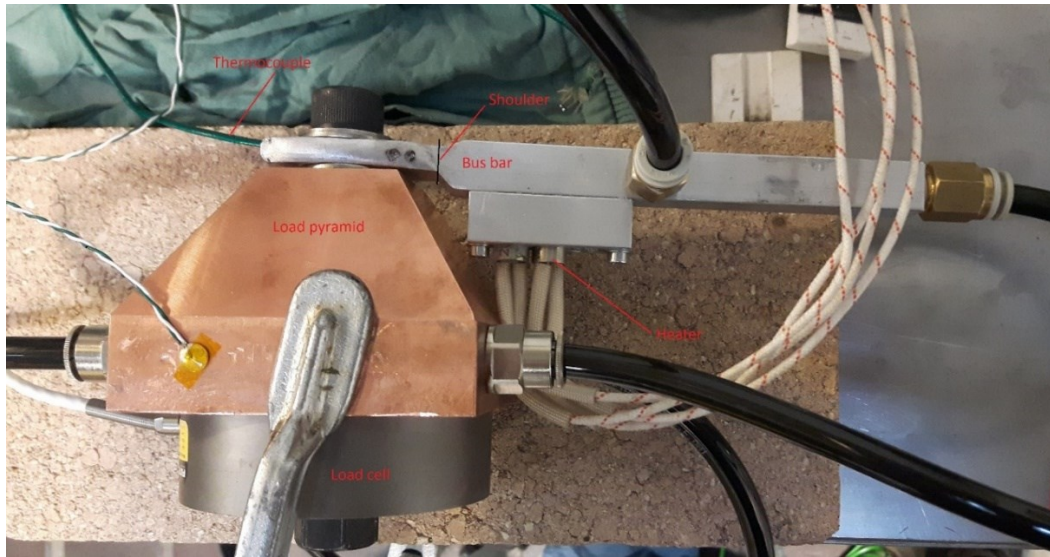| Test	Thickness [mm]	Length [mm]	Width [mm]
Low peak temperature	6.5	42	23.4
High peak temperature	8.2	43.8	26.4

Figure 81 – Experimental setup for Al bus bar
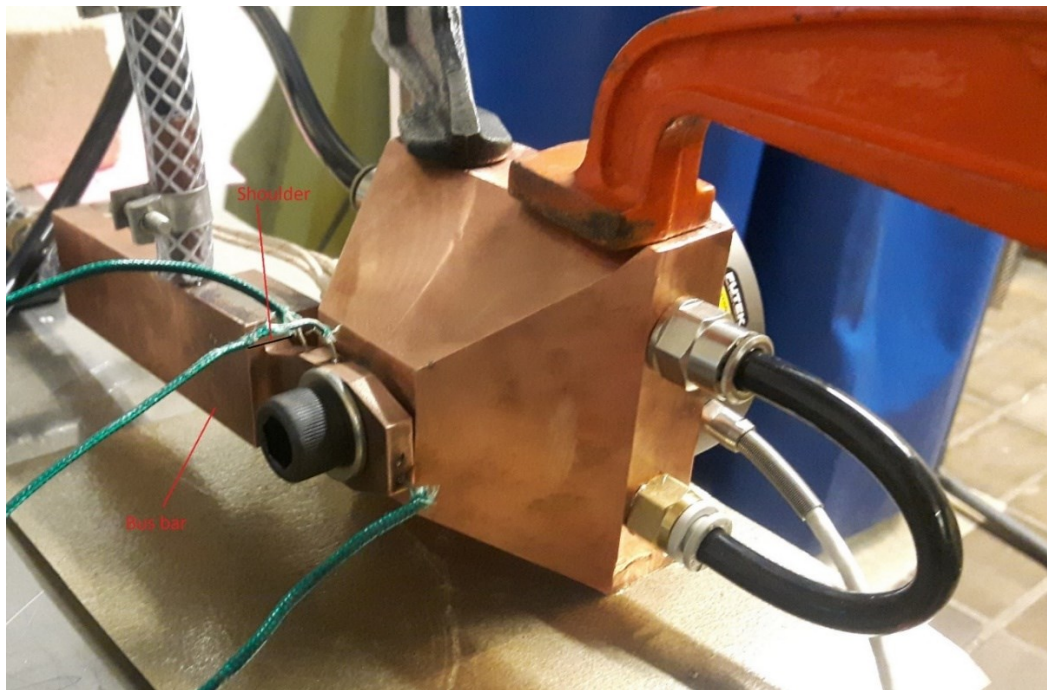
Figure 82 – Experimental setup for Cu bus bar

7.5   Results

The results for each test are presented in the next subchapters. The temperature and force behavior throughout the tests is presented in figures Figure 84, Figure 86, Figure 88 and Figure 90. In these figures, the force presented is the average of the measured force during each cycle and the 6 temperature curves are the maximum and minimum temperatures measured by the thermocouples in each temperature cycle. For each test, the actual position of each thermocouple

is also presented. In the higher peak temperature tests, the x-axis is made logarithmic due to higher amount of cycles.

7.5.1 Lower Peak Temperatures

Figure 83 – Thermocouple positions for Al test at lower peak temperatures

Figure 84 – Force and temperature data for Al test at lower peak temperatures

Figure 85 – Thermocouple positions for Cu test at lower peak temperatures
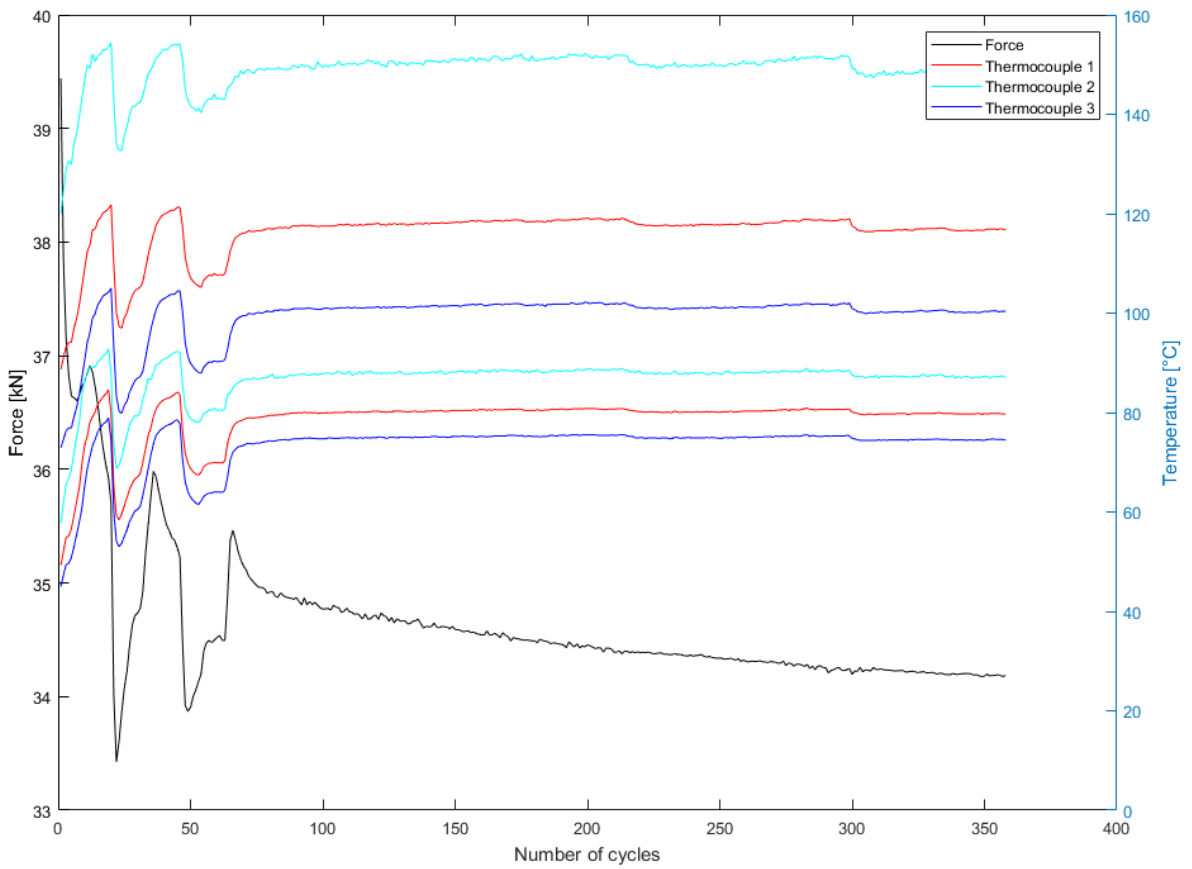
Figure 86 – Force and temperature data for Cu test at lower peak temperatures

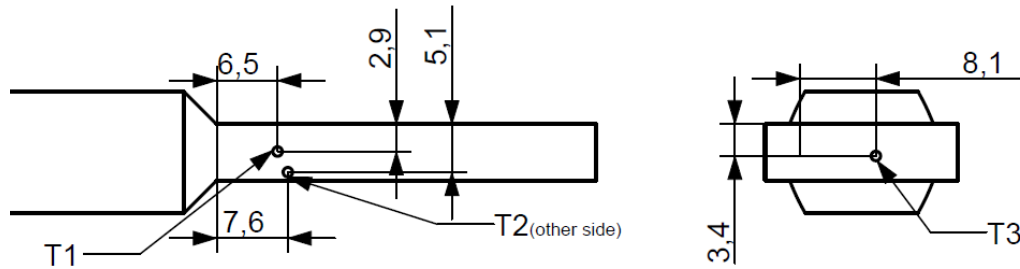## 7.5.2 Higher Peak Temperatures

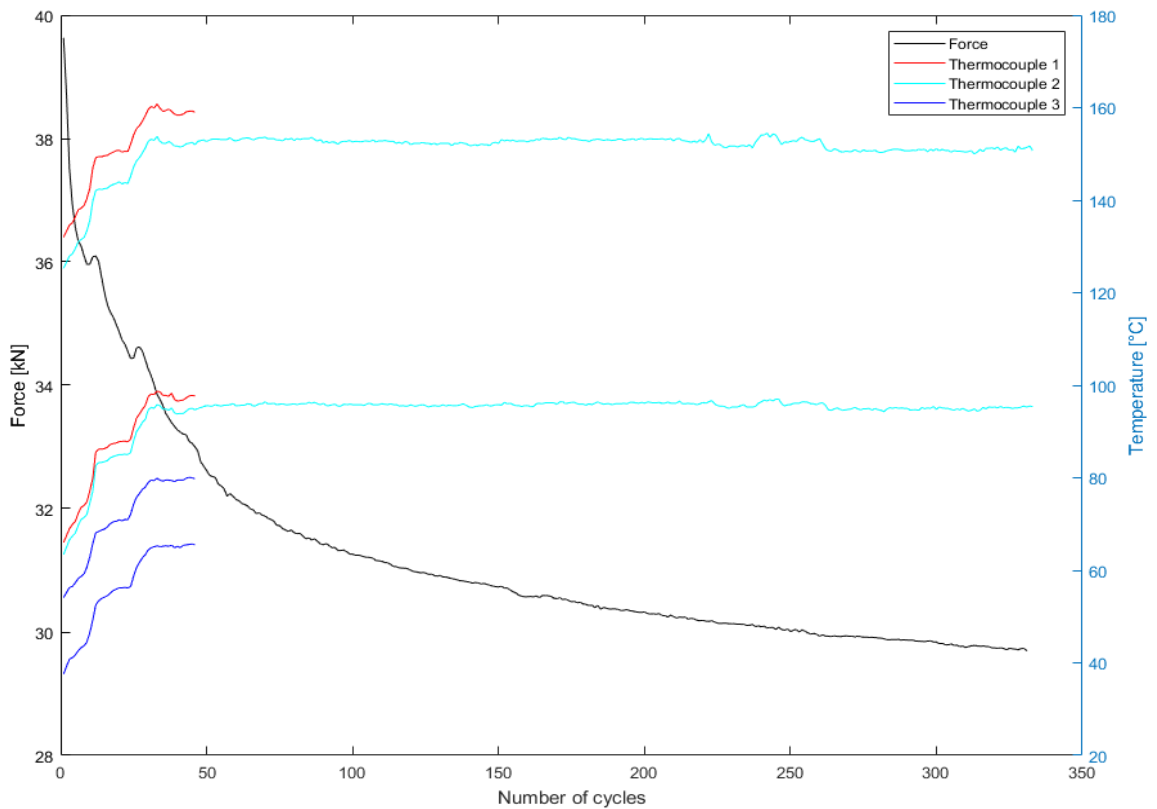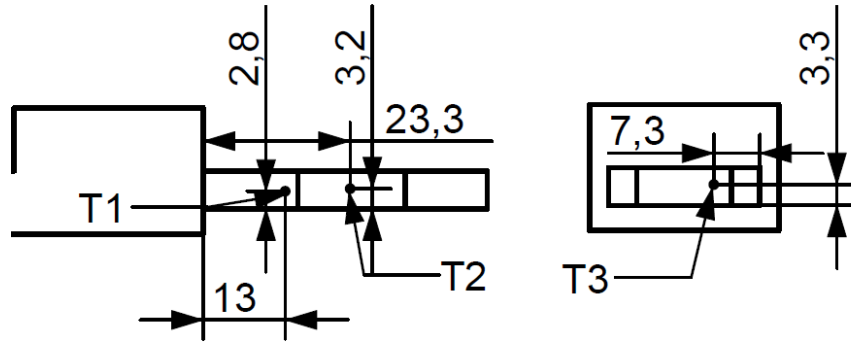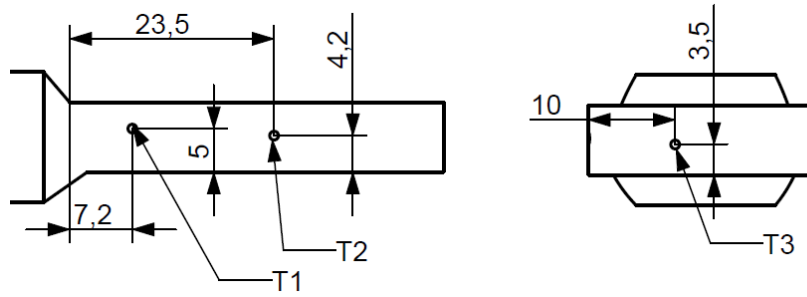Figure 87 - Thermocouple positions for Al test at higher peak temperatures
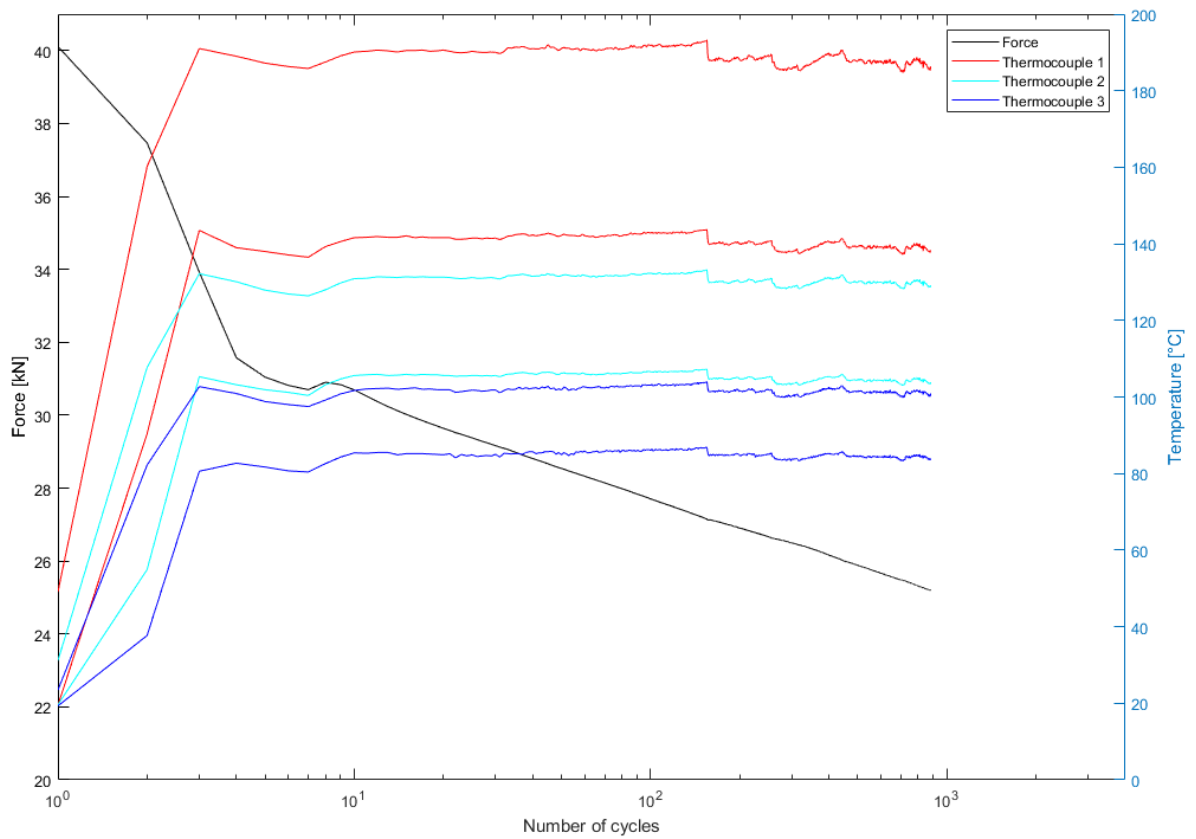
Figure 88 - Force and temperature data for Al test at higher peak temperatures
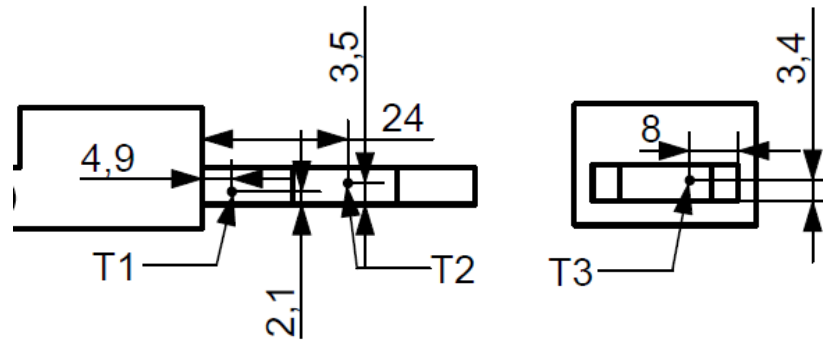
Figure 89 - Thermocouple positions for Cu test at higher peak temperatures
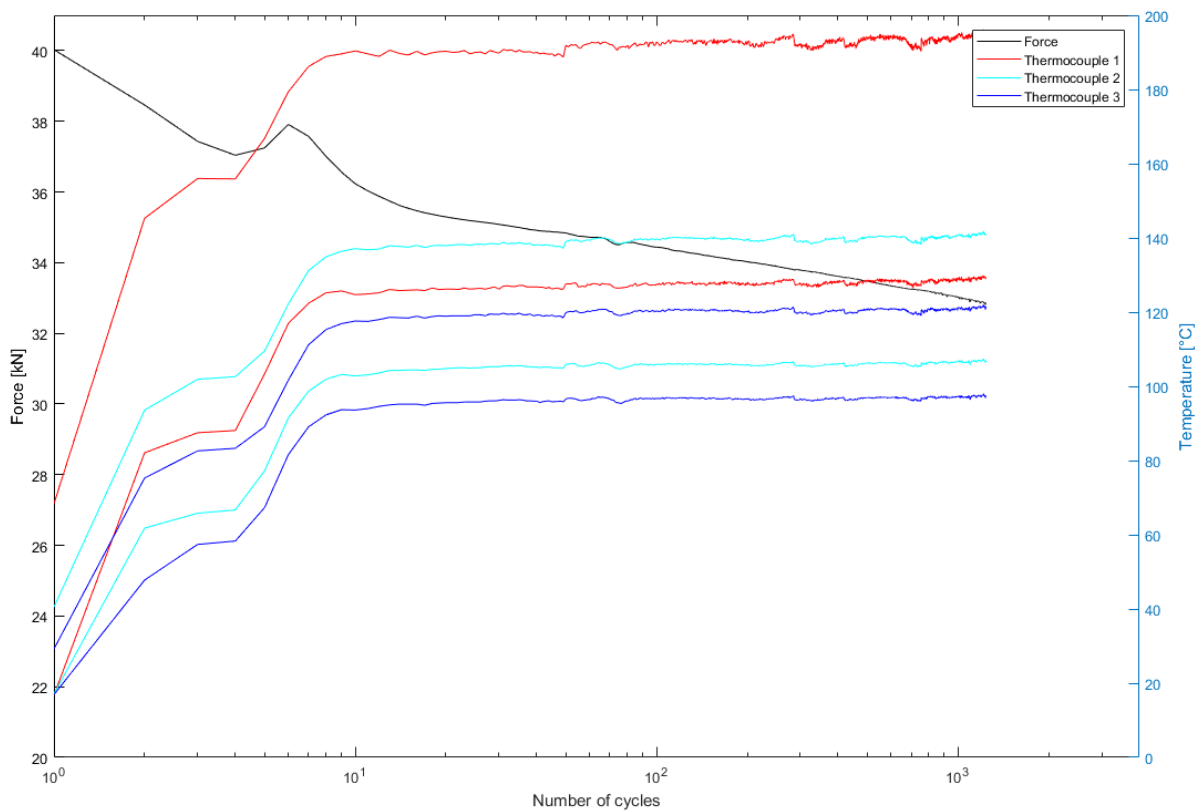
Figure 90 - Force and temperature data for Cu test at higher peak temperatures

7.6   Analysis of the Results

From the results, it can be seen that the force on the Al relaxes much faster than the force on the Cu. The difference in force relaxation becomes clearer with higher peak temperature cycles. There the force on the Al lowers to 25.2 kN after 881 cycles while the force on the Cu lowers to 32.9 kN after 1236 cycles. The difference is less for the lower peak temperatures where the force on the Al lowers to 29.7 kN after 331 cycles while the force on the Cu lowers to 34.2 kN

103

after 358 cycles. Table 37 below details the clamping force in the 4 different tests at 300 and 800 cycles as well as the change in force per cycle between 100 and 200 cycles.

Table 37 – Result comparison between different tests

T_{max}	Material	$F_{@300\ cycles}$	$F_{@800\ cycles}$	$\Delta F/cycle_{@100\text{-}200\ cycles}$
150 °C	Cu-OF-04	34.2 kN	N/A	-3.2 N
	EN-EW-6101-T4	29.8 kN	N/A	- 9.4 N
190 °C	Cu-OF-04	33.8 kN	33.2 kN	- 4.2 N
	EN-EW-6101-T4	26.5 kN	25.3 kN	- 8.1 N

For both materials, the change in clamping force is higher than anticipated and too fast to be caused by creep. It is rather caused by other factors such as thermal expansion and reduced yield strength at elevated temperatures. EN-EW-6101-T4 has a thermal expansion coefficient of $23(10^{-6}/°C)$ [83] compared to $16.8(10^{-6}/°C)$ [84] for Cu-OF. These are the coefficients for temperatures between 20 and 100 °C. Higher thermal expansion rates results in more relaxation as the material seeks to expand in other directions than the one it is being pressed from. The different behavior of yield strength also supports the difference in the relaxation of the clamping force, especially with higher peak temperatures. Cu-OF loses ~40% of its yield strength at 200 degrees Celsius compared to room temperature [85] while EN-EW-6101-T4 loses ~75% of its yield strength at 200 degrees Celsius compared to room temperature [29]. This could explain the increasing difference with higher peak temperatures.

Based on the conducted experiments it can be concluded that Cu-OF-04 bus bar ends would require much less maintenance for the retightening of the clamped end than EN-AW-6101-T4 bus bar ends need. The relaxation rate for EN-EW-6101-T4 is around twice as high compared to Cu-OF-04. Based on the average relaxation of force per cycle the retightening frequency of the Cu bus bar is around 50% compared to the retightening frequency of the Al bus bar.

8 Summary

8.1 General Comments

The Friction Stir Welding (FSW) of Aluminum (Al) and Copper (Cu) was feasible and good quality welds were obtained, considering the typical application requirement in electrical bus bars. The set of optimized conditions has been shown to be quite sensitive to the variation of some parameters. Thus, the quality assurance in a production line will depend on the control and precision of the most critical conditions. Even though the FSW process is not a new process, the application to Al-Cu joints is not extensively investigated and several issues are still pending on further development. A contribution for the development of the state of the art on this issue is given with the present work. The present results promote new possibilities in the manufacturing of high-quality products, supporting various industries in the never-ending search for improved solutions. The aim of this work was to research and develop the process conditions required by Promeco Oy to be able to manufacture bimetallic Al-Cu bus bars for usage in electric industries.

The tool design and matching optimized parameters conceived throughout the conductance of this project should lay the grounds for Promeco Oy's bus bar production. The resulting weld has good mechanical properties as well as excellent electrical performance as the resistance over the joint is negligible, when compared to any type of clamped connection (about $200 \times$ difference, according to experimental measurements). A stationary shoulder friction stir welding tool module was designed and manufactured. This tool module has the potential to produce the same high quality welds with improvement of the top surface finishing. This tool module can be applied not only to dissimilar, but also to similar welds supporting Promeco Oy's FSW based production behind the Al-Cu joints.

A new dedicated test of the relaxation of the bolted joint clamping force, subjected to thermal cycles representing the operational conditions, was designed and conducted for Al and Cu. The relaxation rate results emphasize a relevant operational superiority of bimetallic Al-Cu bus bars over commonly used Al bus bars, which in practice may mean that the Cu ends require only half the amount of maintenance as Al ones.

8.2 Conclusions

Conventional FSW tools were designed and manufactured for the making of 6 mm AA1050-H14/24 – Cu-OF-04 butt joints. Process parameters were optimized for these conditions and the resulting joints characterized:

- Concave shoulder of ØD3 mm gives the best welding results out of the shoulders produced. Its diameter does not cause overly high heat input while still keeping material from escaping the weld.
- ØA mm taper probes are not suitable for manufacturing conditions due to low lifetime

- ØB mm taper probes are able to produce good welds for 6 mm thick base materials and have a long lifetime. Threaded taper and threaded taper probes with scrolls are the most promising probe designs for their intended purpose.
- Optimized parameters for the welding process using N/A mm long, ØB mm threaded taper probe and ØD3 mm concave shoulder are as follows:
    - Rotational speed: 800 RPM
    - Machine tilt: 2°
    - Dwell time: 5 s
    - Acceleration at the start: $1.085 \cdot 10^{-4}$ mm/s^2 (acceleration length: 20 mm)
    - Travel speed: N/A
    - Offset into Al: N/A
    - Weld plunge of the tool in base materials: N/A
- The performance parameters for the weld produced with these parameters are as follows:
    - Global Efficiency to Tensile Strength (GETS), compared to Al: 0.848
    - Global Efficiency to Bending (GEB), compared to Al: 0.408
    - Electrical Conductive Efficiency, compared to an ideal resistless joint: 0.972
- In the stationary domain (near the middle of the weld) the temperature history of points at the same distance from the center of the stirred zone of the base materials differ during welding, with Cu reaching much higher top temperatures. Top temperatures in the middle of weld:
    - Al, 15.8 mm from center of stirred zone: 219.5 °C
    - Cu, 15.8 mm from center of stirred zone: 293.7 °C
- Metallurgical investigation of the optimized joints shows an intense mixture of materials with large amounts of multilayered structures, both Al-matrix composite and intercalated lamae. Occasional voids were observed.
- Intermetallic compounds were found in the weld, both emerging as particles in various mixtures as well as layers. The largest single compound layer identified was measured to be around 3 μm.
- FSW joints produced have negligable electrical resistance compared to the resistance between clamped base materials (200 times lower resistance).

Stationary shoulder FSW module for ESAB Legio FSW machine was designed and manufactured:

- Manufacturing was fully made in-house.
- Design meets the various design specifications.
- The module needs to be tested.

Difference in clamping force behavior between Cu-OF-04 and EN-EW-6106-T4, the Al alloy used in conventional monolithic Al bus bars, during operational conditions was investigated:

- Cu-OF-04 relaxes at a half a rate compared to the Al alloy and therefore would require much less maintenance. Raising the peak temperatures affecting the materials affects the Al alloy more than the Cu.

8.3 Future Work

Various next steps can be taken to further develop the welding conditions for the production of Al-Cu bus bars:

- Develop and optimize welding parameters for different thicknesses such as 8 and 10 mm.
- Optimize the weld force for the current optimized parameters to have fully optimized weld conditions for manufacturing.
- Develop, design and manufacture a clamping system for Promeco Oy's production line which allows for the offset to be set with high precicion.
- Fully investigate the difference between welds produced with threaded taper and threaded taper probes with scrolls.
- Evaluate the life of the tools.

Plenty of further work is needed for the SSFSW module:

- Test the module for various welding conditions, identify weak points in the design and improve it.
- Change the design of the arms so that the module can be attached to Promeco Oy's FSW machine.
- Further modularize the design so that different probe and shoulder geometries can easily be used and changed between welds without the manufacturing of the interchangable parts being too expensive.
- Add various monitoring devices to the shoulder such as load cells and thermocouples.

The work done during this project has paved the way for Promeco Oy's production of dissimilar Al-Cu bus bars as well as the production of other high-value dissimilar components. Additionally it has proved the potential of dissimilar Al-Cu bus bars and their operational advantages over conventional Al bus bars.

9   References

1. I. Galvão, J. Oliveira, A. Loureiro and D. Rodrigues, "Formation and distribution of brittle structures in friction stir welding of aluminium and copper: Influence of shoulder geometry," *Intermetallics*, vol. 22, pp. 122-128 2012.

2. W. Thomas, "Friction stir butt welding," *International Patent Application No.PCT/GB92/0220* 1991.

3. D. Lohwasser and Z. Chen, *Friction stir welding: From basics to applications*, Elsevier, 2009.

4. A. Fehrenbacher, C.B. Smith, N.A. Duffie, N.J. Ferrier, F.E. Pfefferkorn and M.R. Zinn, "Combined temperature and force control for robotic friction stir welding," *Journal of Manufacturing Science and Engineering*, vol. 136, no. 2, pp. 021007 2014.

5. R. Rai, A. De, H. Bhadeshia and T. DebRoy, "Review: Friction stir welding tools," *Science and Technology of welding and Joining*, vol. 16, no. 4, pp. 325-342 2011.

6. M. Mubiayi and E. Akinlabi, "Friction stir welding of dissimilar materials between aluminium alloys and copper, An overview," in *Proceedings of the World Congress on Engineering*, 2013, pp. 3-5.

7. Y. Chen, J. Feng and H. Liu, "Precipitate evolution in friction stir welding of 2219-T6 aluminum alloys," *Mater Charact*, vol. 60, no. 6, pp. 476-481 2009.

8. "Review of tools for friction stir welding and processing," *Can.Metall.Q.*, vol. 51, no. 3, pp. 250-261, 07/01 2012. http://dx.doi.org/10.1179/1879139512Y.0000000015.

9. E. Akinlabi, "Effect of shoulder size on weld properties of dissimilar metal friction stir welds," *Journal of materials engineering and performance*, vol. 21, no. 7, pp. 1514-1519 2012.

10. H. Wu, Y.C. Chen, D. Strong and P. Prangnell, "Assessment of the advantages of static shoulder FSW for joining aluminium aerospace alloys," in *Materials Science Forum*, 2014, pp. 1770-1775.

11. J. Martin, "Stationary shoulder friction stir welding," in *Proceedings of the 1st International Joint Symposium on Joining and Welding: Osaka, Japan, 6-8 November 2013*, 2014, pp. 477.

12. M. Russell, P. Threadgill, M. Thomas and B. Wynne, "Static shoulder friction stir welding of Ti–6Al–4V; process and evaluation," in *Proc. 11th World Conf. on 'Titanium', Kyoto, Japan*, 2007.

13. A. Beckman and M. Sundström, "Development of stationary shoulder for friction stir welding," 2014.

14. ANSI/ASME, "Preferred metric limits and fits," 1978.

15. T. DebRoy and H. Bhadeshia, "Friction stir welding of dissimilar alloys–a perspective," *Science and Technology of Welding and Joining*, vol. 15, no. 4, pp. 266-270 2010.

16. G. Schulze, "Metallphysik (akademie, berlin, 1967; mir, moscow, 1971)," *Google Scholar*.

17. I. Galvao, J. Oliveira, A. Loureiro and D. Rodrigues, "Formation and distribution of brittle structures in friction stir welding of aluminium and copper: Influence of process parameters," *Science and Technology of Welding and Joining*, vol. 16, no. 8, pp. 681-689 2011.

18. C. McHenry, "The new encyclopedia britannica 3 . chicago: Encyclopedia britannica," 1992.

19. F.C. Campbell, *Elements of metallurgy and engineering alloys*, ASM International, 2008.

20. J. Kummer. *29 Cu Copper* [Online]. available: http://images-of-elements.com/copper.php.

21. S. Pappas. *Facts About Copper* [Online]. available: http://www.livescience.com/29377-copper.html.

22. H. Dollwet and J. Sorenson, "Historic uses of copper compounds in medicine," *Trace elements in Medicine*, vol. 2, no. 2, pp. 80-87 1985.

23. R.A. Flinn and P.K. Trojan, "Engineering materials and their applications," *Engineering Materials and Their Applications, 4th Edition, by Richard A.Flinn, Paul K.Trojan, pp.1056.ISBN 0-471-12508-3.Wiley-VCH, December 1994.*, pp. 1056 1994.

24. J.R. Davis, *Copper and copper alloys*, ASM international, 2001.

25. R.C. Weast, M.J. Astle and W.H. Beyer, *CRC handbook of chemistry and physics*.

26. "The price of virtue," *The Economist*, vol. 2017, no. March 7, June 7, 2007 2007.

27. Anonymous *Images of elements* [Online]. available: http://images-of-elements.com/aluminium.php.

28. Anonymous *Industry standards* [Online]. available: http://www.aluminum.org/resources/industry-standards.

29. J.R. Davis and J.R. Davis, *Aluminum and aluminum alloys*, ASM international, 1993.

30. I. Galvao, R. Leal, A. Loureiro and D. Rodrigues, "Material flow in heterogeneous friction stir welding of aluminium and copper thin sheets," *Science and technology of welding and joining*, vol. 15, no. 8, pp. 654-660 2010.

31. P. Carlone, A. Astarita, G.S. Palazzo, V. Paradiso and A. Squillace, "Microstructural aspects in Al–Cu dissimilar joining by FSW," *The International Journal of Advanced Manufacturing Technology*, vol. 79, no. 5-8, pp. 1109-1116 2015.

32. T.K. Bhattacharya, H. Das, S.S. Jana and T.K. Pal, "Numerical and experimental investigation of thermal history, material flow and mechanical properties of friction stir welded aluminium alloy to DHP copper dissimilar joint," *The International Journal of Advanced Manufacturing Technology*, vol. 88, no. 1, pp. 847-861 2017. http://dx.doi.org/10.1007/s00170-016-8820-0.

33. T. Saeid, A. Abdollah-zadeh and B. Sazgari, "Weldability and mechanical properties of dissimilar aluminum–copper lap joints made by friction stir welding," *J.Alloys Compounds*, vol. 490, no. 1–2, pp. 652-655, 2/4 2010.

34. M. Guerra, C. Schmidt, J. McClure, L. Murr and A. Nunes, "Flow patterns during friction stir welding," *Mater Charact*, vol. 49, no. 2, pp. 95-101 2002.

35. I. Galvão, A. Loureiro and D.M. Rodrigues, "Critical review on friction stir welding of aluminium to copper," *Science and Technology of Welding and Joining*, vol. 21, no. 7, pp. 523-546, 10/02 2016. http://dx.doi.org/10.1080/13621718.2015.1118813.

36. M.F.X. Muthu and V. Jayabalan, "Tool travel speed effects on the microstructure of friction stir welded aluminum–copper joints," *J.Mater.Process.Technol.*, vol. 217, pp. 105-113, 3 2015.

37. H. Liu, J. Shen, L. Zhou, Y. Zhao, C. Liu and L. Kuang, "Microstructural characterisation and mechanical properties of friction stir welded joints of aluminium alloy to copper," *Science and Technology of Welding and Joining*, vol. 16, no. 1, pp. 92-98 2011.

38. C.W. Tan, Z.G. Jiang, L.Q. Li, Y.B. Chen and X.Y. Chen, "Microstructural evolution and mechanical properties of dissimilar Al–Cu joints produced by friction stir welding," *Mater Des*, vol. 51, pp. 466-473, 10 2013.

39. H.J. Liu, J.J. Shen, S. Xie, Y.X. Huang, F. Cui, C. Liu and L.Y. Kuang, "Weld appearance and microstructural characteristics of friction stir butt barrier welded joints of aluminium alloy to copper," *Science and Technology of Welding and Joining*, vol. 17, no. 2, pp. 104-110, 02/01 2012. http://dx.doi.org/10.1179/1362171811Y.0000000086.

40. P. Xue, B.L. Xiao, D. Wang and Z.Y. Ma, "Achieving high property friction stir welded aluminium/copper lap joint at low heat input," *Science and Technology of Welding and*

Joining, vol. 16, no. 8, pp. 657-661, 11/01 2011. http://dx.doi.org/10.1179/1362171811Y.0000000018.

41. P. Xue, D.R. Ni, D. Wang, B.L. Xiao and Z.Y. Ma, "Effect of friction stir welding parameters on the microstructure and mechanical properties of the dissimilar Al–Cu joints," *Materials Science and Engineering: A*, vol. 528, no. 13–14, pp. 4683-4689, 5/25 2011.

42. P. Xue, B. Xiao, D. Ni and Z. Ma, "Enhanced mechanical properties of friction stir welded dissimilar Al–Cu joint by intermetallic compounds," *Materials science and engineering: A*, vol. 527, no. 21, pp. 5723-5727 2010.

43. A.O. Al-Roubaiy, S.M. Nabat and A.D. Batako, "Experimental and theoretical analysis of friction stir welding of Al–Cu joints," *The International Journal of Advanced Manufacturing Technology*, vol. 71, no. 9-12, pp. 1631-1642 2014.

44. A. Loureiro, R. Mendes, J. Ribeiro, R. Leal and I. Galvão, "Effect of explosive mixture on quality of explosive welds of copper to aluminium," *Mater Des*, vol. 95, pp. 256-267 2016.

45. H. Barekatain, M. Kazeminezhad and A. Kokabi, "Microstructure and mechanical properties in dissimilar butt friction stir welding of severely plastic deformed aluminum AA 1050 and commercially pure copper sheets," *Journal of Materials Science & Technology*, vol. 30, no. 8, pp. 826-834 2014.

46. B. Lu, K. Chen, W. Meng, A. Karki and R. Jin, "Quantification of thermal resistance of transient-liquid-phase bonded cu/al/cu interfaces for assembly of cu-based microchannel heat exchangers," *Journal of Micro and Nano-Manufacturing*, vol. 1, no. 3, pp. 031001 2013.

47. X. LI, D. ZHANG, Q. Cheng and W. ZHANG, "Microstructure and mechanical properties of dissimilar pure copper/1350 aluminum alloy butt joints by friction stir welding," *Transactions of Nonferrous Metals Society of China*, vol. 22, no. 6, pp. 1298-1306 2012.

48. M. Braunovic and N. Alexandrov, "Intermetallic compounds at aluminum-to-copper electrical interfaces: Effect of temperature and electric current," *IEEE Transactions on Components, Packaging, and Manufacturing Technology: Part A*, vol. 17, no. 1, pp. 78-85 1994.

49. K. Savolainen, J. Mononen, T. Saukkonen and H. Hnninen, "A preliminary study on friction stir welding of dissimilar metal joints of copper and aluminium," in *6th International Friction Stir Welding Symposium*, 2006.

50. M. Avettand-Fenoël, R. Taillard, G. Ji and D. Goran, "Multiscale study of interfacial intermetallic compounds in a dissimilar al 6082-T6/cu friction-stir weld," *Metallurgical and Materials Transactions A*, vol. 43, no. 12, pp. 4655-4666 2012.

51. C. Genevois, M. Girard, B. Huneau, X. Sauvage and G. Racineux, "Interfacial reaction during friction stir welding of al and cu," *Metallurgical and Materials Transactions A*, vol. 42, no. 8, pp. 2290 2011.

52. S. Celik and R. Cakir, "Effect of friction stir welding parameters on the mechanical and microstructure properties of the al-cu butt joint," *Metals*, vol. 6, no. 6, pp. 133 2016.

53. H. Bisadi, A. Tavakoli, M. Tour Sangsaraki and K. Tour Sangsaraki, "The influences of rotational and welding speeds on microstructures and mechanical properties of friction stir welded Al5083 and commercially pure copper sheets lap joints," *Mater Des*, vol. 43, pp. 80-88, 1 2013.

54. M.F.X. MUTHU and V. JAYABALAN, "Effect of pin profile and process parameters on microstructure and mechanical properties of friction stir welded Al–Cu joints," *Transactions of Nonferrous Metals Society of China*, vol. 26, no. 4, pp. 984-993 2016.

55. P.K. Sahu, S. Pal, S.K. Pal and R. Jain, "Influence of plate position, tool offset and tool rotational speed on mechanical properties and microstructures of dissimilar al/cu friction stir welding joints," *J.Mater.Process.Technol.*, vol. 235, pp. 55-67, 9 2016.

56. E.T. Akinlabi, A. Els-Botes and P.J. McGrath, "Effect of travel speed on joint properties of dissimilar metal friction stir welds," in *Proceedings of 2nd international conference on advances in engineering and technology (AET), Uganda. Jan*, 2011.

57. M.H. Tolephih, H.M. Mahmood, A.H. Hashem and E.T. Abdullah, "Effect of tool offset and tilt angle on weld strength of butt joint friction stir welded specimens of AA2024 aluminum alloy welded to commercial pure cupper," 2013.

58. M. Akbari, R. Abdi Behnagh and A. Dadvand, "Effect of materials position on friction stir lap welding of al to cu," *Science and Technology of Welding and Joining*, vol. 17, no. 7, pp. 581-588 2012.

59. I. Galvão, D. Verdera, D. Gesto, A. Loureiro and D. Rodrigues, "Influence of aluminium alloy type on dissimilar friction stir lap welding of aluminium to copper," *J.Mater.Process.Technol.*, vol. 213, no. 11, pp. 1920-1928 2013.

60. J. Feng, X. Songbai and D. Wei, "Reliability studies of cu/al joints brazed with Zn–Al–Ce filler metals," *Mater Des*, vol. 42, pp. 156-163 2012.

61. J. Kerns. *What's the Difference Between Aluminum and Copper in Electrical Applications?* [Online]. available: http://www.machinedesign.com/metals/what-s-difference-between-aluminum-and-copper-electrical-applications.

62. P. Vilaça and W. Thomas, "Friction stir welding technology," in *Structural Connections for Lightweight Metallic Structures,* Anonymous : Springer, 2011, pp. 85-124.

63. Southern Inspection & Testing. *Tensile testing* [Online]. available: http://www.southerninspection.com/PageDisplay.asp?p1=13507.

64. J.F. Shackelford and M.K. Muralidhara, "Introduction to materials science for engineers," 2005.

65. S.C. Sharma. *Lecture 11 - Mechanical properties* [Online]. available: http://www.nptel.ac.in/courses/112107146/lects%20&%20picts/image/lect11/lecture11.htm.

66. D. Kopeliovich. *Flexural strength tests of ceramics* [Online]. available: http://www.substech.com/dokuwiki/doku.php?id=flexural_strength_tests_of_ceramics.

67. R. C. Fries, "Biomaterials--the intersection of biology and materials science (temenoff, J.S. et al.; 2008) [book reviews]," *IEEE Engineering in Medicine and Biology Magazine*, vol. 28, no. 4, pp. 94-94, 100 2009.

68. M.B. Heaney, "Electrical conductivity and resistivity," *Electrical Measurement, Signal Processing, and Displays.*, vol. 7, no. 1 2003.

69. AEIS. *Hardness testing* [Online]. available: http://www.aeisndt.com/mechanical-testing-hardness-testing.html.

70. M.J. Anderson and P.J. Whitcomb, *Design of experiments*, Wiley Online Library, 2000.

71. R.K. Roy, *A primer on the Taguchi method*, Society of Manufacturing Engineers, 2010.

72. P.R. Apte. *Introduction to Taguchi Method (3rd ed.)* [Online]. available: https://www.ee.iitb.ac.in/~apte/CV_PRA_TAGUCHI_INTRO.htm.

73. ProcessPolicy. *The secret of Taguchi methods* [Online]. available: https://processpolicy.com/taguchi-methods.htm.

74. C. Vidal, V. Infante, P. Peças and P. Vilaça, "Application of taguchi method in the optimization of friction stir welding parameters of an aeronautic aluminium alloy," *Advanced Materials Manufacturing & Characterization*, vol. 3, no. 1, pp. 21-26 2013.

75. P.G. Slade, *Electrical contacts: principles and applications*, CRC press, 2013.

76. AZoM. *H13 Tool Steel - Chromium Hot-Work Steels* [Online]. available: https://www.azom.com/article.aspx?ArticleID=9107.

77. J.L. Rosa, A. Robin, M.B. Silva, C.A. Baldan and M.P. Peres, "Electrodeposition of copper on titanium wires: Taguchi experimental design approach," *Journal of Materials Processing Technology*, vol. 209, no. 3, pp. 1181-1188, 1 February 2009 2009.

78. W.H. Yang and Y.S. Tarng, "Design optimization of cutting parameters for turning operations based on the taguchi method," *Journal of Materials Processing Technology*, vol. 84, no. 1, pp. 122-129, 1 December 1998 1998.

79. W.C. Oliver and G.M. Pharr, "An improved technique for determining hardness and elastic modulus using load and displacement sensing indentation experiments," *J.Mater.Res.*, vol. 7, no. 6, pp. 1564-1583 1992.

80. G. Mathers. *Creep and creep testing* [Online]. available: http://www.twi-global.com/technical-knowledge/job-knowledge/creep-and-creep-testing-081/.

81. C. Stocchi, P. Robinson and S.T. Pinho, "Using strain gauges to monitor bolt clamping force and fracture in composite joints during fatigue tests," in *ECCM15 - 15TH EUROPEAN CONFERENCE ON COMPOSITE MATERIALS*, Venice, Italy, 2012.

82. American National Standard Institute Inc., "Testing methods and equipment common to the ANSI C119 family of standards," 2015. https://www.nema.org/Standards/ComplimentaryDocuments/ANSI-C119-0-2015-WATERMARKED.pdf.

83. AzoM. *Aluminium / Aluminum 6101 Alloy (UNS A96101)* [Online]. available: https://www.azom.com/article.aspx?ArticleID=6639.

84. C.D. Hodgman and R. Weast, "Handbook of chemistry and physics, chem," *Rubber Pub.Co., Ohio, USA* 1962.

85. W.S. Loewenthal and D.L. Ellis, "Fabrication of GRCop-84 rocket thrust chambers," 2005.